

https://dspace.org/

Geological study of the Signal Hill Au-As-Sb deposits, Archaean Tati schist belt, Northeast Botswana.

Audet, Marc-Antoine

2016

http://hdl.handle.net/10539/21332

Downloaded from a DSpace repository. https://dspace.org/

Figure 2.9 Undeformed tonalite/granodioritic rock. Northern batholith at Tekwane gold mine (Fig. 1.3, Appendix VII)..... 31

Figure 2.10 Sheared granulitic rock located at the margin of the Bill View pluton, see Appendix VII..... 32

Figure 3.1 Composite sequence of the upper Penhalonga Formation ("F" Zone) constructed from data collected from core boreholes SPD-062, SPD-063 and SPD-064..... 36

Figure 3.2 Very fine-grained carbonated quartz-sericite schist, SPD-063, 69m..... 37

Figure 3.3 Felsic meta-lapilli tuff with sub-rounded ironstone, quartz and volcanic clasts in a fine, sheared, carbonated quartz-sericite matrix, SPD-063, 60m..... .. 37

Figure 3.4 Porphyroblast of epidote being replaced by iron oxide, SPD-063, 58m, 100X..... 38

Figure 3.5 Porphyroblast of chloritoid in a quartz-sericite matrix, SPD-062, 110m, 100X... 38

Figure 3.6 Mapped profile A-A', through the chert and ironstone member, in vicinity of the "F" Zone mineralisation..... 40

Figure 3.7 Basal chert facies of the chert and ironstone member, dip towards the west. For location see Figure 3.6... 41

Figure 3.8 Dark reddish gossan underlying the beige gossan. Both facies are part of the chert and ironstone member. These facies dip towards the west. For location see Figure 3.6..... 41

Figure 3.9 Chert and ironstone breccia showing fragments of angular felsic volcanic material within fine grained ferruginous cherty matrix. For location see Figure 3.6..... 42

Figure 3.10 Figure showing the composite sequence of the Last Hope Formation at Signal Hill Au-As-Sb deposits area. The composite sequence was constructed using data from lithostratigraphic cross-sections, boreholes and trenches along the "A" Zone..... 46

Figure 3.11 Figure showing the composite sequences and surface geology of the "A" Zone. Composite sequences were constructed using data from boreholes and trenches for each section..... 47

LIST OF FIGURES

Figure 1.1 Map illustrating the position of the Archaean Tati schist belt within the Zimbabwe craton..... 3

Figure 1.2 Geological map of the Tati schist belt. Geological information based on Mason (1973), Key (1976) and this study..... 5

Figure 1.3 Location of Selkirk nickel mine and old gold mines and showings, Tati schist belt, modified after Key (1976)..... 8

Figure 2.1 Ironstone member which dominates the Matsiloje Formation. Strong internal deformation with prominent lineations plunging toward the south..... 14

Figure 2.2 North youngging direction indicated by a pillow in a Lady-Mary Formation's matic unit. The unit dips steeply towards the south. The sequence is overturned 17

Figure 2.3 Subdivision into four distinct structural domains of the Penhalonga Formation..... 20

Figure 2.4 Large meta-volcanic block within an agglomerate host, showing a right way-up sequence. The block deformed the underlying sediment while being emplaced, the overlying sediments are not deformed..... 22

Figure 2.5 Rock showing a right way-up sequence within felsic tuff units, Penhalonga Formation North domain. The way-up is indicated by the presence of a rounded clastic fragment (bottom right corner) which created a poorly developed load structure within the underlying unit..... 22

Figure 2.6 Rock succession showing light grey and well banded felsic chert units with felsic meta-tuff. A basal chert unit (1) shows an erosive contact infilled with meta-tuff material (2). The felsic meta-tuff contains the well developed regional schistosity..... 23

Figure 2.7 Highly deformed granitoid rock located at the contact between the New Zealand batholith and the Matsiloje Formation (Appendix VII)..... 29

Figure 2.8 A- Stereoplot showing poles of the foliation and a mineral lineation at the margin of the New Zealand batholith. B- Stereoplot of poles of the regional schistosity observed over the "A" and "F" Zones (Appendices VIII and IX)..... 29

Appendix I	:	Major and trace analysis of rocks from the upper Penhalonga Formation.
Appendix II	:	Specific gravity determination.
Appendix III	:	Major and trace elements analysis of sediments from the Last Hope Formation.
Appendix IV	:	Major and trace elements analysis of the "A" Zone ore samples.
Appendix V	:	"A" Zone surface ore samples collected and assayed by Soltrust Botswana in 1983.
Appendix VI	:	Major and trace elements analysis of rocks from the "E" Zone structure.
Appendix VII	:	Geology of the Tati schist belt, 1: 125,000
Appendix VIII	:	Geology of the southeastern Tati schist belt 1:20,000
Appendix IX	:	Geology of the Signal Hill area, 1: 2,500

5.3.13 Ore paragenesis 117
5.4 Discussion 118

Chapter Six Lithogeochemistry 122

6.1 General Statement 122
6.2 Upper Penhalonga Formation 124
6.2.1 Meta-volcanic unit 126
6.2.2 Quartz-sericite schist units 127
6.2.3 Chert unit 128
6.3 Last Hope Formation 128
6.3.1 Major and trace element behaviour 130
6.4 "A" Zone mineralization 131
6.5 Hydrothermal alteration 136
6.6 "E" Zone structure 142
6.7 Discussion 142

Chapter Seven Discussion 145

7.1 General Statement 145
7.2 Structural deformation affecting the Tati schist belt 145
7.3 Correlation of the Tati schist belt with Archaean greenstone belts within the Zimbabwe craton. 150
7.4 Geology of the Signal Hill area. 153
7.4.1 Sedimentological setting and lithogeochemistry 153
7.4.2 Tectonics 154
7.4.3 Ore chemistry, mineralogy and emplacement 156

Chapter Eight Conclusions. 160

Reference list

3.3 Last Hope Formation 42
3.3.1 Lithostratigraphy of the Signal Hill area 43
Quartz wacke facies 44
Planar laminated quartz wacke facies 49
Trough cross-bedded quartz wacke facies 50
Diamictite facies 52
3.4 Carbonatization 59
3.5 Discussion 60
Proximal alluvial fan 62
Distal alluvial fan interbedded with water-laid sediments 64

Chapter Four Structural deformation affecting the Signal Hill area 66

4.1 General Statement 66
4.2 Previous structural investigations 67
4.3 Structure of the Signal Hill area 71
4.3.1 D1 event 71
4.3.2 Main thrust and associated "E" Zone 75
4.3.3 D2 event 81
4.4 Late structural events 83
4.4.1 Late faults 83
4.4.2 Crenulation cleavage 86
4.5 Discussion 88

Chapter Five Mineralization 90

5.1 General Statement 90
5.2 Mineralization types and distribution 91
5.2.1 "A" Zone mineralization 91
Contact mineralization 91
Footwall mineralization 93
5.2.2 "B" Zone mineralization 98
5.2.3 "C" Zone mineralization 98
5.2.4 "F" Zone mineralization 99
5.3 Mineralogy of the "A" Zone mineralization 100
5.3.1 Stibnite 101
5.3.2 Native Antimony 107
5.3.3 Berthierite 108
5.3.4 Chalcostibite 108
5.3.5 Chalcopyrite 108
5.3.6 Sphalerite 110
5.3.7 Metacinnabarite and/or Tahlorc. 110
5.3.8 Arsenopyrite 113
5.3.9 Pyrrhotite 113
5.3.10 Pyrite 113
5.3.11 Gold 113
5.3.12 Gangue minerals 113

TABLE OF CONTENTS

Abstract		(i)
Acknowledgements		(ii)
Table of Contents		(vi)
List of Figures		(xiv)
List of Tables		
Chapter One	Introduction	1
1.1	General Statement	1
1.2	Geographic setting of the study area	4
	1.2.1 Location	4
	1.2.2 Access	4
1.3	History and mining	6
1.4	Research outline	9
Chapter Two	Geology of the Tati Schist Belt	11
2.1	General Statement	11
2.2	Lithostratigraphy	12
	2.2.1 Matsiloje Formation	13
	2.2.2 Lower Old Tati Formation	14
	2.2.3 Old Tati Formation and Lady Mary Formation	15
	2.2.4 Penhalonga Formation	18
	Structure	18
	2.2.5 Last Hope Formation	24
	2.2.6 Selkirk Formation	26
	2.2.7 Granitoid rocks	27
2.3	Geochronology	32
Chapter Three	Geological setting of the Signal Hill area	33
3.1	General Statement	33
3.2	Penhalonga Formation	34
	3.2.1 Lower members of the Penhalonga overturned sequence	34
	3.2.2 Upper Penhalonga Formation	34
	Meta-volcanic unit	35
	Quartz-sericite schist	35
	Chert and ironstone	39

ACKNOWLEDGEMENTS

The writer would like to express his sincere thanks to Falconbridge Exploration Botswana, Falconbridge Gold Corporation and Mosetse Investments for their financial support.

A word of thanks is due to my supervisors Dr. F.M. Meyer and Dr. G. Charlesworth, for all the help and guidance they gave me. The writer would also like to express his thanks and appreciation for the assistance, encouragement and useful discussions held with geologists of Falconbridge Exploration Botswana, especially Mr. J. Blaine and Mr. C. Byron, and the support given to me by the staff of Falconbridge Exploration Botswana, especially Mr. Moffat Pereko and Mr. and Mrs Legopelo.

Gratitude is also expressed to Mr. L. Neuhoff and to Mr D. Grant for their support.

Thank you, for without you, this would not have been possible.



SIGNAL HILL

assemblage of quartz wackes. Mineralogical study of the Footwall mineralization shows that stibnite and mercury are intimately related and predate the Au-As mineralization. The strong affinity between Sb and Hg suggests fumarolic or hot spring-type of mineralization related to nearby volcanism. It is proposed that the antimony mineralization is related to a syngenetic, and probably endogenous, hydrothermal activity synchronous to the deposition of the Last Hope Formation, while the Contact mineralization is related to a younger, structurally controlled Au-As bearing hydrothermal activity superimposed on the antimony mineralization. The development of a major thrusting event, related to the first stage of tectonic deformation, played a critical role in the mobilisation and the subsequent canalization of the Au-As rich hydrothermal fluid.

ABSTRACT

The Signal Hill Au-As-Sb deposits lie in the uppermost formations of the Archaean Tati schist belt, located in northeast Botswana.

The surface exposures of these potentially economic deposits are confined to three main zones: "A" Zone, "B" Zone and the "F" Zone. The "A" Zone and "B" Zone are found within the sedimentary assemblage of the Last Hope Formation, while the "F" Zone lies within the underlying volcanic Penhalonga Formation.

The Last Hope Formation sediments are characteristic of an alluvial fan which debouched rapidly into a water body. These sediments were deposited synchronously with volcanic activity following an uplift of the underlying formations at the end of the Penhalonga era.

At least four stages of tectonic deformation affected the Signal Hill area. The first stage was the combination of large scale folding and thrusting. The second stage is the development of a regional schistosity. The third and fourth deformational events created normal and reverse faults followed by the development of a crenulation cleavage.

At the "A" Zone, two distinct zones of Au-As-Sb mineralization have been identified; the Contact mineralization and the Footwall mineralization. The Contact mineralization occurs in a sheared contact between a diamictite assemblage and underlying quartz wacke facies. The Footwall mineralization is hosted within lenses of sheared, silicified and sericitized rocks, associated with boudinaged "chert" and/or quartz veins within the silicified footwall

I, **Marc-Antoine Audet,** declare that unless specifically acknowledged, this thesis represents my own unaided work.
This dissertation is being submitted for a Master of Science Degree at the University of the Witwatersrand. It has not been submitted before for any degree or examination, at any other University.

GEOLOGICAL STUDY OF THE SIGNAL HILL Au-As-Sb DEPOSITS, ARCHAEAN TATI SCHIST BELT NORTHEAST BOTSWANA

by

MARC-ANTOINE AUDET

This thesis is submitted to the Faculty of Science, University of the Witwatersrand, for the Degree of Master of Science.

Department of Geolo
University of the Witwat rand
January, 1995

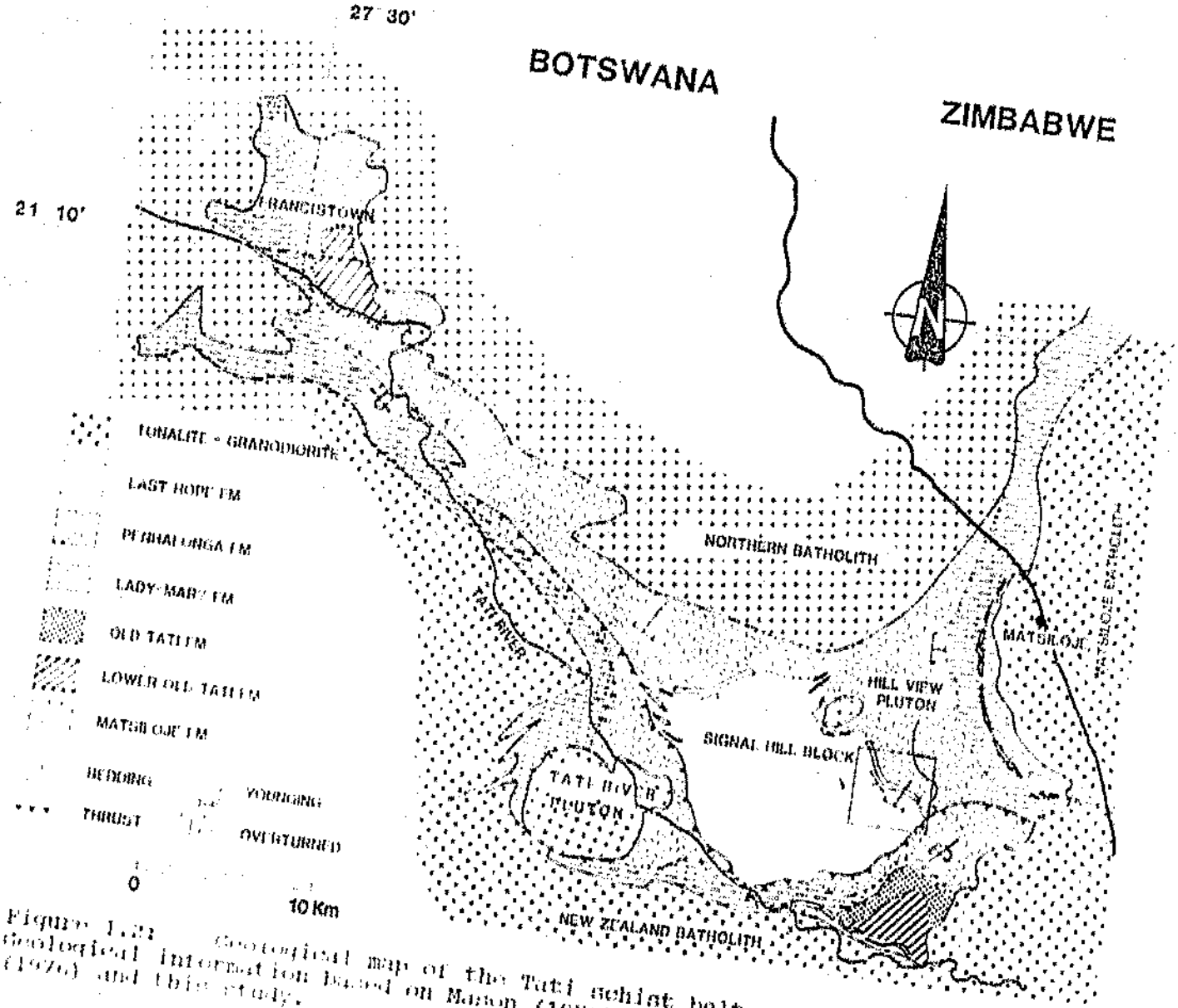


Figure 1.2: Geological map of the Tati schist belt. Geological information based on Mason (1970), Key (1976) and this study.

1.2 GEOGRAPHIC SETTING OF THE STUDY AREA

1.2.1 Location

The Signal Hill Au-As-Sb deposits occur in an area situated at the southeast end of the Tati schist belt in northeastern Botswana (Fig. 1.2), and fall within the latitudes 21° 00' and 21° 25' south and longitude 27° 35' to 27° 60' east.

Falconbridge Explorations Botswana, in joint venture with Mosetse Investments, hold two exploration licences which together cover 35 Km^2, called the Signal Hill block (Fig. 1.2). The Signal Hill Au-As-Sb deposits are located in the southeast corner of this block.

The area lies at an altitude of approximately 950m above sea level and is located between two major eastward flowing ephemeral rivers, namely the Tati and the Ramokwegbana rivers. The area is covered by low mopane trees and thorn scrub except along the rivers where larger trees may be found. The area is mainly used for cattle ranching in the freehold areas and for cattle, goats and subsistence farming in the tribal lands.

1.2.2 Access

The Signal Hill Au-As-Sb deposits are located some 43 Km southeast of Francistown, the second largest town in Botswana. Access to the study area is via an "all-weather" gravel road

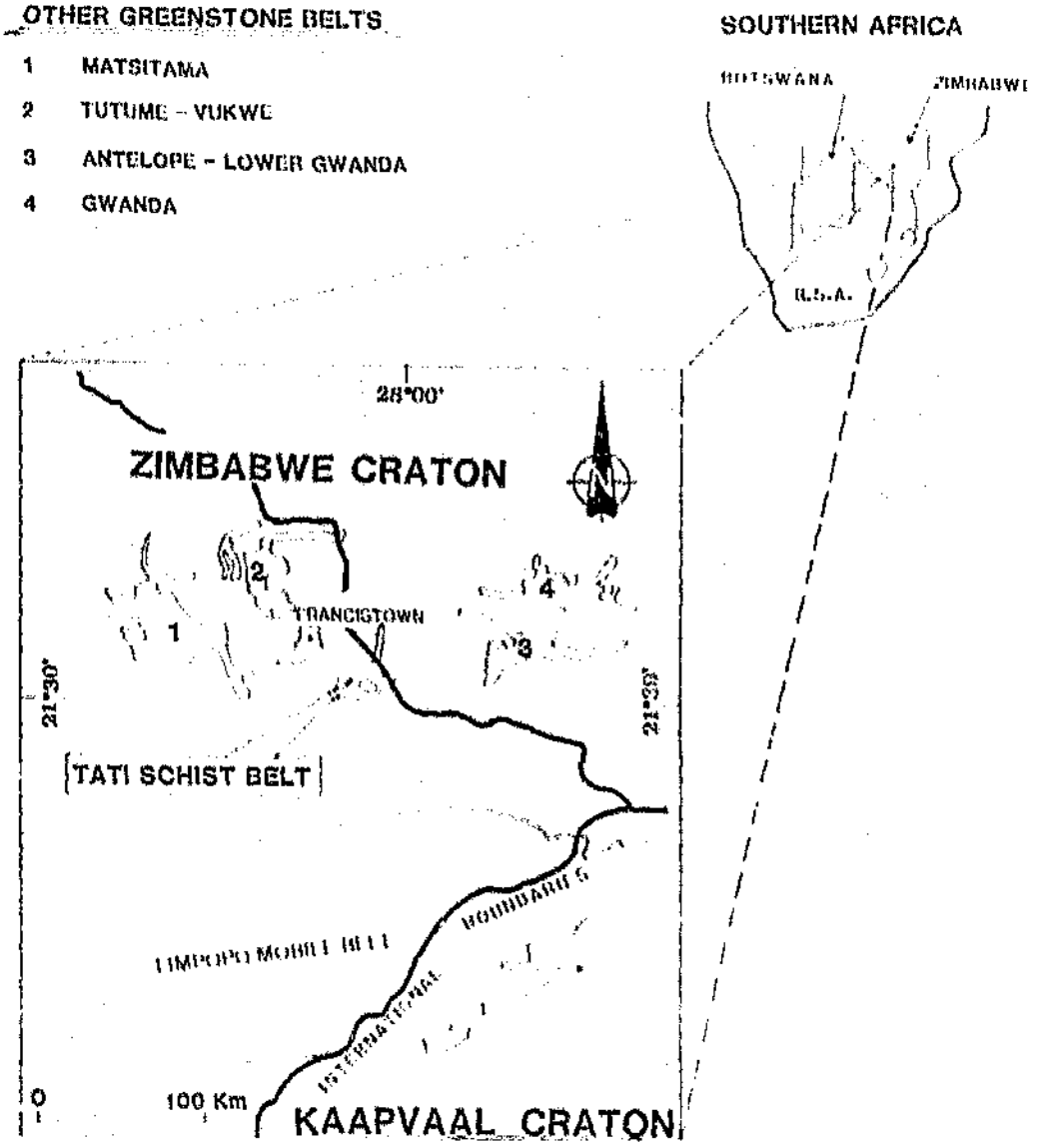


Figure 1.1: Map illustrating the position of the Archaean Tati schist belt within the Zimbabwe craton.

and therefore no model for the origin of the Signal Hill Au-As-Sb deposits has previously been produced.

The main aims of this study are:

A) to establish the local stratigraphy and the sedimentary environment of the Signal Hill area.

B) to establish the nature, distribution and the relative timing of the Signal Hill Au-As-Sb mineralization.

C) to establish the role of structural processes on the location of the ore.

A sedimentological, mineralogical, geochemical and structural study of the Signal Hill Au-As-Sb deposits will provide the framework for establishing a model for the genesis of these complex deposits.

CHAPTER ONE

INTRODUCTION

1.1 General Statement

The Archaean Tati schist belt is situated in the northeast of the Republic of Botswana, and forms part of the Zimbabwe craton (Fig. 1.1). This study is of the Signal Hill Au-As-Sb deposits which lie in the southeastern portion of the Archaean Tati schist belt.

The Tati schist belt consists of various Archaean meta-volcanic and subordinate metasedimentary rocks of low metamorphic grade. The belt covers approximately 570 km^2, and constitutes the main source of gold in Botswana. In 1867, the geologist-explorer Carl Mauch discovered the Monarch reefs in the vicinity of Francistown. A short gold rush followed the discovery, but soon the activities dwindled and finally stopped in 1964. Even after 130 years of gold and other commodity production, the origin of the gold mineralization and the overall geology of the Tati schist belt remain poorly understood.

Exploration work carried out by Falconbridge in the Signal Hill area has outlined several Au-As-Sb mineralized zones within the uppermost formations of the Tati schist belt: the Last Hope Formation and the underlying Penhalonga Formation. Three of these zones called "A" Zone, "B" Zone and the "F" Zone have good economic potential for both oxide and sulphide ore. No detailed geology

LIST OF TABLES

Table 2.1	Stratigraphy of the Tati schist belt after Mason (1970), Molyneux (1971), Key (1976) and this study..	12
Table 4.1	Tectonic events of the Tati schist belt after Mason (1970), Key (1976) and this study.....	69
Table 5.1	Mercury (Hg) content in stibnite core, stibnite rim and within the alteration phase.....	111
Table 6.1	As, Sb, Hg and Au contents of two samples of massive antimony ore from "A" Zone mineralization.....	136
Table 7.1	Zimbabwean Archaean greenstone succession compared to the Tati schist belt stratigraphy (Foster et al (1986) and this study).....	152

Figure 6.12 Variation diagrams for As, Sb and Au versus the K2O/Na2O ratio, samples are listed in Appendix IV..... 141

Figure 7.1 Block diagrams showing the formation of the large scale synform and the subsequent thrusting (along the Main Thrust) of the overturned southern limb over the right way-up northern limb..... 148

Figure 7.2 Block diagrams showing the "split" of the right way-up northern limb by the intrusion of the Northern batholith, together with the thrusting (along the Long gossan structure) of a portion of the overturned southern limb..... 149

Figure 7.3 Cross section through the Lost Hope Formation from the overturned Penhalonga Formation to the right way-up Penhalonga Formation (location of the cross section in Appendix IX)..... 156

Figure 5.25 Precciation due to brittle deformation of the gold bearing second gangue generation (dark colour) and injection of white barren quartz material, SPD-083, sample 10444..... 116

Figure 5.26 Ore paragenesis of the "A" Zone mineralization, Signal Hill area..... 118

Figure 5.27 Paragenetic sequence of mineralization after Harwood (1986). Although gold has been observed and described by Harwood, he did not included gold in the paragenetic sequence..... 119

Figure 5.28 Intersection of "A" Zone mineralization in borehole SPD-083 showing two distinct Ore Zones. The Au, As and Sb distribution is also shown..... 121

Figure 6.1 Schematic stratigraphic profile showing the variation of Na_2O and K_2O and MgO for rocks of the upper Fonhalonga Formation. (Borehole SPD-063)..... 125

Figure 6.2 Zr/TiO_2 - Nb/Y plot showing the classification of the volcanic rocks of the upper Fonhalonga Formation (after Floyd and Winchester, 1978)..... 126

Figure 6.3 Variation of major and trace elements of the Last Hope Formation rocks (borehole SPD-083)..... 129

Figure 6.4 Zr/TiO_2 - Nb/Y plot showing the classification of the quartz wacke facies of the Last Hope Formation and volcanic fragments of diamictite facies (after Floyd and Winchester, 1978)..... 130

Figure 6.5 Variation diagrams of Sb and As vs Au, samples are listed in Appendix IV..... 132

Figure 6.6 Variation diagrams for Zn, Ni and Cu vs Au, samples are listed in Appendix IV..... 133

Figure 6.7 Variation diagrams for Zn, Ni and Cu vs Sb, samples are listed in Appendix IV..... 134

Figure 6.8 Variation diagrams for Hg vs Au, Hg vs As and Hg vs Sb, samples are listed in Appendix V..... 135

Figure 6.9 Variation diagrams for Au with Sr and Rb, samples are listed in Appendix IV..... 138

Figure 6.10 Variation diagrams for As, Sb, Zn, Ni and Cu with Sr, samples are listed in Appendix IV..... 139

Figure 6.11 Variation diagrams for As, Sb, Zn, Ni and Cu with Rb, samples are listed in Appendix IV..... 140

Figure 5.14 Remobilization of early stibnite (Sb) into stibnite stringers, SD-003, 221m, (320 X, reflected light)..... 105

Figure 5.15 Stringers of remobilized stibnite located adjacent to a pyrite crystal, SPD-083, 221m, (320X, reflected light)..... 106

Figure 5.16 Early stibnite (Sb) and berthierite (Be) partially replaced by chalcostibite and/or native antimony and the growth of late pyrite (Py) and arsenopyrite (Apy), SD-003, 55.0om, (320 X, reflected light)..... 107

Figure 5.17 Brecciated early sphalerite (Sp) cut off by a late pyrite crystal (Py). Assemblage occurs within the second gangue generation, SD-107, 126m, (320 X, reflected light)..... 109

Figure 5.18 Early sphalerite (Sp) brecciated by a later tectonic event and associated second gangue generation, within gangue associated to the third hydrothermal event, SPD-067, 85m, (320 X, reflected light)..... 109

Figure 5.19 Brecciated early sphalerite in a quartz-carbonate first generation gangue material, thereafter affected by a later tectonic event and the associated second gangue generation and the growth of arsenopyrite, SD-003, 55m (320 X, reflected light)..... 110

Figure 5.20 Assemblage of euhedral arsenopyrite (Apy) and porous xenomorphic pyrite (Py). Both phases are related to the second hydrothermal event, SD-003, 55m, (320X, reflected light)..... 112

Figure 5.21 Native gold occurring in the second gangue generation, SD-003, 320m, (320 X, reflective light)..... 114

Figure 5.22 Native gold occurring in the second gangue generation, (high reflectivity, top left), SPD-083, 120m, (320 X, reflective light)..... 114

Figure 5.24 Footwall vein with stibnite-berthierite-sphalerite mineralization. The gangue is composed almost exclusively of quartz, SPD-083, 220m, (25 X, + Nic)..... 115

Figure 5.24 First fine-grained, grey quartz gangue tectonically affected by an later event with subsequent replacement by carbonatization and sericitisation, SPD-083, 219m, (25 X, + Nic)..... 115

Figure 5.3 Lenses of Footwall mineralization within the silicified quartz wacke facies, located in the western end of the "A" Zone..... 94

Figure 5.4 Footwall vein plunging 15° towards the southeast. Located near 10040N and 9750E..... 95

Figure 5.5 Detail of the contact between the Footwall vein and the sheared, silicified and mineralised quartz wacke host..... 97

Figure 5.6 Silicified quartz wacke, tectonically brecciated and thereafter affected by the precipitation of pyrite and arsenopyrite by mineralizing fluids, SPD-083, sample 10426..... 97

Figure 5.7 Cross section through the "F" Zone, the section is located along line 11285E..... 99

Figure 5.8 Stibnite (Sb) being replaced firstly by chalcostibite (1) and/or native antimony (1) and thereafter by metacinnabarite and/or lahlore (2), in a second generation gangue, SPD-083, 221.00m, (320 X, reflected light..... 102

Figure 5.9 Stibnite (Sb) with inclusions of native antimony (1) and/or chalcostibite (1) (high reflectance, white, top left), SPD-083, 220m, sample 10430 (320X, reflected light)..... 102

Figure 5.10 Footwall vein with massive and disseminated stibnite partially replaced by stibiconite (Sc). The photo shows a sharp contact between this Footwall vein and the surrounding pyrite and arsenopyrite mineralized zone. Several fine fractures through the Footwall vein has been filled by pyrite and arsenopyrite, SPD-083, sample 10430..... 103

Figure 5.11 Remobilized stibnite as fine stringers, in fractures created by a later tectonic event. Sphalerite (Sp) occurs at the bottom left, SPD-083, 221m, (320 X, reflected light..... 103

Figure 5.12 Stibnite (Sb) and berthierite (Be) (replaced by chalcostibite and/or native antimony) in close relationship with sphalerite (Sp) and chalcopyrite (Cc), SPD-083, 220m, (320 X, reflected light)..... 104

Figure 5.13 Stibnite (Sb) affected by a later tectonic event (fractures infill by the second generation of gangue material) and the growth of late euhedral arsenopyrite (Apy), SD-083, 221m, (320 X, reflected light)..... 104

Figure 4.3 Photo showing the contact between a short section of the "B" Zone foot-wall dipping duplex structure and underlying quartz vein. The contact dips at approximately 60° towards 190°. 77

Figure 4.4 Shear and breccia zones located southwest of the "B" Zone and stacked together to form foot-wall dipping duplex. The "Water" fault crosscut and displaces the whole sequence..... 78

Figure 4.5 Detail of the "F" Zone geology, located west of the "B" Zone..... 79

Figure 4.6 Stockwork of kyanite within the dolomitized and siliceous "F" Zone host rock..... 79

Figure 4.7 Fracture system filled with white quartz and affecting the whole "F" Zone host rock. These fractures dip at an average of 50° towards 010..... 81

Figure 4.8 Figure showing the structural relationship at the "A" Zone, between S0, S2, the normal fault F098 and the cremulation cleavage..... 82

Figure 4.9 Stereoplot showing poles to S2 for "A" Zone and "F" Zone..... 82

Figure 4.10 Exposure of the relationship between the reverse fault system and the normal fault system. The second system has been displaced by the reverse fault system, "A" Zone near 9900E..... 84

Figure 4.11 Stereoplot of the normal and reverse fault systems and the associate stress system. The axis of the maximum compressive stress ($\sigma 1$) plunges 20° towards 072°, the intermediate axis ($\sigma 2$) plunges 64° towards 299° and the minimum principal stress ($\sigma 3$) plunges 20° towards 162°..... 86

Figure 4.12 Cyclographic trace shows the cleavage dipping at 62° towards 046°..... 87

Figure 4.13 Rotational strain ellipse associated with a wrench/strike-slip fault system (McClay 1987)..... 87

Figure 4.14 Summary of the deformation events in the Signal Hill area..... 89

Figure 5.1 Cross-section showing both the Contact mineralization and the Footwall mineralization, along the line 9875 E ("A" Zone grid)..... 92

Figure 5.2 Distribution of gold within the "A" Zone ore body. The ore body is outlined by a cut-off grade of 0.5 Au g/t.. 93

Figure 3.12 Photomicrograph of quartz wacke showing angular quartz fragments in a quartz-sericite matrix. The rock is matrix supported, SPD-081, 94m, 100 X, X nic..... 48

Figure 3.13 Rare twinned plagioclase crystal associated with quartz fragments in a quartz-sericite matrix, SD-077, 64m, 100 X, X nic..... 48

Figure 3.14 Very rare zircon within a quartz wacke, SD-077, 64m, 200 X..... 49

Figure 3.15 Photo showing parallel laminations within the grey purple quartz wacke, west of fault F098..... 51

Figure 3.16 Photo showing the transition zone between the grey purple quartz wacke and the beige trough cross-bedded quartz wacke. This photo also shows a cross section (070° plane) and a longitudinal section (180° plane) of trough cross-beds in quartz wacke..... 51

Figure 3.17 Vertical section of trough cross-beds ... ing concave and tangential forsets. These trough cross-beds indicate a right way-up sequence with younging towards the southwest..... 52

Figure 3.18 Diamictite showing sub-rounded quartz and ironstone clasts and sub-angular to angular and flattened volcanic fragments in a fine carbonated matrix. The sediment is matrix supported, SPD-083, 192m..... 53

Figure 3.19 Carbonated quartz-sericite matrix of a diamictite layer supporting an angular composed quartz fragment, SD-111, 41m, 100X, + nic..... 56

Figure 3.20 Quartz wacke's matrix partially replaced by carbonatisation, SPD-066, 75m..... 58

Figure 3.21 Carbonated quartz wacke unit (reddish-brown) overlying a thin diamictite layer. Unaltered diamictite's matrix filled a small fracture within the overlying carbonated quartz wacke. The younging direction is from the right to the left..... 58

Figure 3.22 Block diagrams showing the possible uplift of the underlying Penhalonga members along a normal fault and the coincident basin subsidence..... 65

Figure 4.1 D1 deformation affecting the chert and ironstone members in the vicinity of the "F" Zone mineralization..... 70

Figure 4.2 Detail of the anticline located approximately 1 Km west of the "A" Zone..... 74

amounts of basalt, banded ironstone and limestone. The Formation is generally not extensively developed, and mainly crops out in the southeastern part of the schist belt (Fig. 1.2, Appendices VII and VIII). Although Molyneux (1971) described ultramafic rocks west of the Matsiloje Hill, the Old Tati Formation is apparently absent in the eastern part of the belt (near the village of Matsiloje).

The Lady Mary Formation is composed of interdigitating mafic and lesser amounts of ultramafic volcanic units, together with minor interbedded meta-sedimentary rocks including banded iron-stone, limestone and quartz schists. The proportion of mafic units increases towards the upper contact. The formation occurs along the southern margins of the schist belt, from Francistown in the northwest to the southeastern extremities of the schist belt, and also in the eastern part of the schist belt (Fig. 1.2, Appendices VII and VIII).

Along the southern margins of the schist belt, all units dip steeply toward the southwest and to the south. Several localities show well-preserved mafic pillowed lava and pillow breccia units. The structural interpretation of the pillowed units show younging directions towards the north, which indicates that at these localities, the sequence is overturned (Fig. 3.2). The contact between Lady Mary Formation and the Old Tati Formation is clearly marked by a structural discordance which has been identified in the field and on the Landsat image of the Tati schist belt (Fig. 1.2,

Old Tati Formation. The eastern part of the Formation was folded and truncated by a granitoid intrusion which could be part of the New Zealand batholith (Fig. 1.2, Appendices VII and VIII). The Lower Old Tati Formation comprises felsic lapilli tuffs and chert units which overlie an assemblage of mafic volcanic and volcanogenic units. This formation has not been previously recognized. According to Dr I.F. Wilson (Pers. Comm., Tati workshop, 1991), the felsic lapilli tuffs and chert units are comparable to the upper members of the Lower Bulawayo sequence in Zimbabwe. The lower Bulawayo sequence contains an extensive development of iron formations interbedded with basaltic and komatiitic flows (Foster et al 1986 (a)).

2.2.3 Old Tati Formation and Lady Mary Formation

The Old Tati Formation was first described by Mason (1970) but was not recognized by later workers. Both Molyneux (1971) and Key (1976), included the Old Tati Formation as a part of the Lady Mary Formation. However, because of the absence of common lithostratigraphic markers in both formations, and the structural nature of the contact between these formations, the writer supports Mason's conclusion that these assemblages represent distinct formations.

The Old Tati Formation is composed of a repetitive sequence of serpentinized ultramafic rocks, which range in composition from dunite through to komatiite and are intercalated with various

70° and 85° to the south, southwest and south-southeast.

A similar mineral lineation, which also plunges towards the south, is present in the ironstone member in the southeastern part of the schist belt (Fig. 2.1).



Figure 2.1: Ironstone member which dominates the Matsiloje Formation. Strong internal deformation with prominent lineations plunging toward the south.

2.2.3 Lower Old Toti Formation

This Formation crops out exclusively in the southeastern portion of the schist belt, where lithological units dip steeply towards the south and to the southwest. This rock succession appears to form a "wedge" between the Matsiloje Formation and the overlying

2.2.1 Matsiloje Formation

Members of the Matsiloje Formation appear in two separate localities, first in the eastern part of the belt near the Matsiloje village, and secondly in the southeastern part of the belt, immediately north of the Tati river (Fig. 1.2, Appendices VII and VIII). This Formation was first recognized by Mason (1970). He described it as a succession of chloritic and siliceous schists and phyllites with thin interbedded limestones. These rocks are considered to represent sheared tuffs and related pyroclastic rocks (Mason 1970). The rock succession is dominated by a thick ironstone member, which varies from less than 3 meters to a maximum of approximately 60 meters. The ironstone formation is composed of alternating thin beds of phyllite and strongly magnetic, black to pale grey chert units (Fig. 3.1).

In the eastern part of the Tati schist belt, in the vicinity of the Matsiloje village (Fig. 1.2), the Formation dips steeply towards the west into the main body of the schist belt. In the southeastern part of the Tati schist belt, the Formation dips steeply towards the south (Appendices VII and VIII).

Mason (1970), observed ripple laminations within ironstone members located in the eastern part of the belt near Matsiloje village. He concluded that the succession at that locality is right way-up.

According to Mason (1970), the ironstone in the eastern part of the schist belt shows a faint mineral lineation plunging between

2.2 Lithostratigraphy

Table 2.1: Stratigraphy of the Tati schist belt after Mason (1970), Molyneux (1971), Key (1976) and this study.

STRATIGRAPHY OF TATI SCHIST BELT			
MASON (1970)	MOLYNEUX (1971)	KEY (1976)	THIS STUDY
SELKIRK		SELKIRK	
LAST HOPE	PENHALONGA		LAST HOPE
		PENHALONGA	
PENHALONGA			PENHALONGA
LADY MARY			LADY MARY
OLD TATI	LADY MARY	LADY MARY	OLD TATI
			LOWER OLD TATI
MATSILOJE			MATSILOJE

The stratigraphy of the belt can be divided into 6 formations, from top to bottom.

Top: Last Hope Formation
Penhalonga Formation
Lady Mary Formation
Old Tati Formation
Lower Old Tati Formation

Bottom: Matsiloje Formation

CHAPTER TWO

GEOLOGY OF THE TATI SCHIST BELT

2.1 General Statement

The Tati schist belt was first described by Mason (1970) as a "typical example of an Archaean greenstone belt which consists of a complex synformal enclave of metavolcanics and metasedimentary schists surrounded and intruded by a sequence of diapiric tonalite-granodiorite plutons".

The stratigraphic subdivisions of the Tati schist belt differ considerably between previous workers and researchers (Table 2.1). In 1970, Mason produced the first geological map of the whole Tati schist belt, which subsequently was modified by T.G. Molyneux in 1971 and R.M. Key in 1976. Key's map of the Tati schist belt was subsequently accepted and published by the Botswana Geological Survey, (Key, 1976). Despite the work done by these previous authors, the lithostratigraphy and the structural deformation affecting the Tati schist belt has largely been unexplained. In this chapter, several modifications to Mason's and Key's interpretations are proposed in order to better explain the stratigraphy and the deformation affecting the Signal Hill area. These modifications are based on the author's research together with an interpretation of the Landsat image of the Tati schist belt.

A number of surface lithostratigraphic cross-sections have been mapped in detail over outcropping areas. Over areas with no surface exposure, mapping was performed using trenches. The outcrop data recorded include: structure, thickness, colour, grain-size, textural characteristics, and bedding features. A modified geological map of the Tati schist belt at a scale of 1:135 000 and compilation maps at scales of 1:20 000 and 1:2500 of the area overlying the ore deposits, have been produced and are presented in Appendices VII, VIII and IX.

An understanding of the geological setting, the mineralogical characteristics of the Signal Hill deposits and the structural controls, will assist in producing a model which in turn would lead to further predictions of ore occurrences, both in and outside the Signal Hill area.

location of all the known gold mines and showings in the Tati schist belt.

1.4 RESEARCH OUTLINE

The current research was aimed at examining the nature and genesis of the Signal Hill Au-As-Sb mineralization, with a view to better understanding the local stratigraphic, structural and lithological controls affecting the location of the ore.

This entailed careful field, and core examination of structure and lithostratigraphy and an investigation of depositional environments.

The first phase of the study was devoted primarily to a field and core examination, during which samples were collected.

From the "A" Zone, "B" Zone and "F" zones, core from 35 boreholes are available. These boreholes have been re-logged with a greater emphasis on the lithostratigraphic descriptions and sulphide mineralization.

A total of 95 thin sections and 65 samples for whole rock major and trace elements analysis were selected from different lithologies. The petrographic and geochemical studies on these samples were made to assess their origins and to interpret the sedimentary environments. A total of 42 polished sections on selected representative ore samples were used to identify the ore constituents and the paragenetic sequence. Geochemical results and specific gravity determination are presented in Appendices I to VI.

location of all the known gold mines and showings in the Tati schist belt.

1.4 RESEARCH OUTLINE

The current research was aimed at examining the nature and genesis of the Signal Hill Au-As-Sb mineralization, with a view to better understanding the local stratigraphic, structural and lithological controls affecting the location of the ore.

This entailed careful field, and core examination of structure and lithostratigraphy and an investigation of depositional environments.

The first phase of the study was devoted primarily to a field and core examination, during which samples were collected.

From the "A" Zone, "B" Zone and "F" zones, core from 35 boreholes are available. These boreholes have been re-logged with a greater emphasis on the lithostratigraphic descriptions and sulphide mineralization.

A total of 95 thin sections and 65 samples for whole rock major and trace elements analysis were selected from different lithologies. The petrographic and geochemical studies on these samples were made to assess their origins and to interpret the sedimentary environments. A total of 42 polished sections on selected representative ore samples were used to identify the ore constituents and the paragenetic sequence. Geochemical results and specific gravity determination are presented in Appendices I to VI.

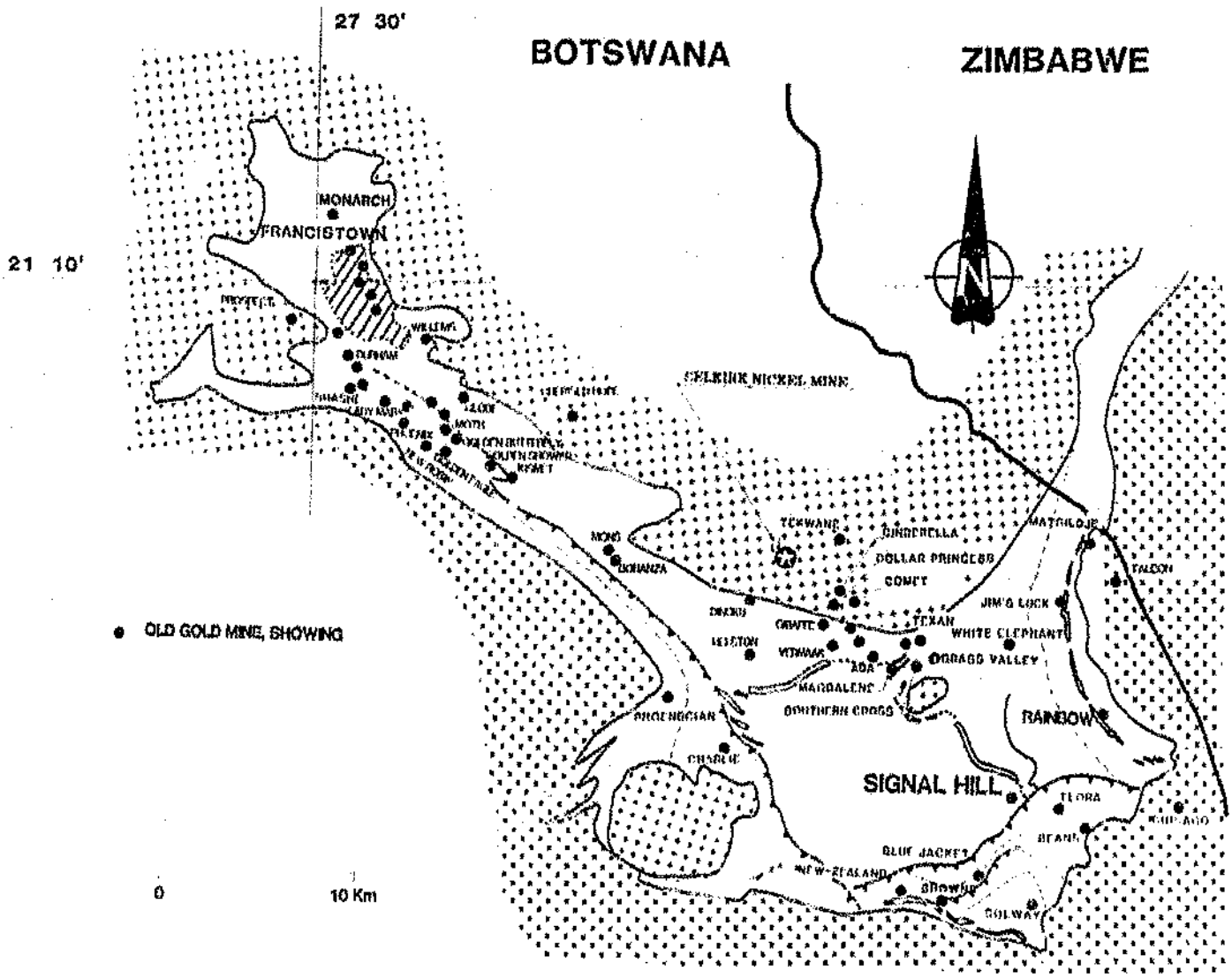


Figure 1.3: Location of Selkirk nickel mine and old gold mines and showings, Tati schist belt, modified after Key (1976).

000 g (200,000 oz) Au from Tati reefs.

In 1867, the geologist-explorer Carl Mauch visited the area of present-day Francistown. He discovered the Monarch reefs which had previously been exploited in several open slots by ancients. The mine resumed production in 1869 and hence is the oldest European-worked gold mine in Southern Africa. A minor gold rush followed, but by the period 1900-1910, the richest parts of the Tati reefs had been exploited and the miners moved on to more lucrative prospects in Rhodesia (now Zimbabwe).

A second period of production in the Tati goldfield occurred during the period 1933 to 1947, since then, activity dwindled and finally stopped in 1964.

During the period 1933-1955, Tati output was 6 265 111 g (201,428 oz) Au and 610 340 g (19,623 oz.) Ag from 944,700 tonnes of ore. The biggest producer was the Monarch mine which yielded 3 357 330 g Au between 19.. and 1949 (Molyneux 1971).

Since 1969, exploration work for gold and other commodities were performed by several exploration and mining companies. Falconbridge has been involved in exploration in the Tati schist belt since 1976. Exploration work by Phelps Dodge and Falconbridge led to a mining operation at Shas ld mine (Fig. 1.3), but unfortunately the mine closed again in 19.. Several other companies have attempted to exploit the smaller reefs. Morex Botswana brought the Rainbow mine back into production in 1988, but was forced to shut down in 1989 and Mineral Holding (Pty) Ltd has been mining at Bonanza reef since 1982. Figure 1.3 shows the

connecting Francistown and the village of Matsiloje on the Botswana-Zimbabwe border. Bush and farm tracks presently connect this road to the Signal Hill Au-As-Sb deposits.

1.3 HISTORY AND MINING

"A mining empire existed in Mashonaland probably from about 600 A.D. to relatively recent times. This empire reached its peak in the sixteenth century when the Zimbabwe edifices probably were built. Prospecting methods employed by the ancients[1] were likely to have been the panning of stream gravels and sampling of anthills. The reefs were broken by fire-setting and as ventilation methods were poor, mining rarely was undertaken at a depth of more than 20m." (Summer 1969).

Ancient prospecting in the Tati goldfield was thorough and as far as is known, only the Rainbow Mine was actually discovered by Europeans (Fig. 1.3). Summer (1969), lists fifty-three ancient mines in the Tati district and three in the Vukwe district (50 km north of Francistown). All the ancient mines were open stopes with the Blue Jacket mine being the deepest, reaching a depth of some 25m (Fig. 1.3).

Summer (1969), concluded that exploitation by ancients of the zone of surface enrichment of reefs in the Tati region was more or less complete. The ancients are likely to have obtained some 6 000

[1] Ancients : Pre-european explorers and miners circa 1100 - 1500 A.D. (Summer 1969)

intrusion has little relationship to the volcano-sedimentary pile of the schist belt. They are represented by massive, sometimes porphyritic, adamellites and granodiorites which in some cases appear to intrude the main tonalitic and granodioritic batholiths, and in other instances appear to grade transitionally into them. (Fig. 1.2, Appendix VII). Only one separate body of granodiorite/adamellite has been mapped by Mason. This body is located north of the schist belt within the Northern batholith (Fig. 1.2, Appendix VII). Its contacts with the surrounding Northern batholith are gradational over a distance of about half a kilometre. The texture developed in these rocks are typically granitoid and the mineral assemblages consist of sodic plagioclase, orthoclase, microcline, quartz, biotite and epidote (Mason (1970)).

The third type consists of a series of small, discrete and circular tonalitic plutons which according to Mason (1970) and Key (1976), represent the youngest granitic intrusions in the area. Hill View and Tati River plutons are considered by Mason (1970) as part of the third type of granitoid intrusion (Fig. 1.2, Appendix VII). These tonalites consist of off-white, granular, medium to coarse-grained, homogeneous rock. The composition is about 20 % quartz, 70 % oligoclase with minor microcline, biotite and epidote

A strong planar foliation has developed along the margins of the tonalitic and granodioritic batholiths which gives them a gneissic appearance (Fig. 2.7), the foliation is highlighted by the

does not represent the top of the volcanic pile of the Tati schist belt. It is proposed that the felsic volcanic units belong to the right way-up members of the Penhalonga Formation (north domain), while the intrusive members belong to the Northern batholith.

2.2.7 Granitoid rocks

Mason (1970) and Crockett (1967) mapped and described all the granitoid batholiths and plutons which surrounded and intruded the Tati schist belt. The following section is a summary of their observations and interpretations.

Three major types of granitic intrusions have been distinguished in the Tati area by Mason (1970). The most common type of granitoid intrusion is represented by a series of tonalitic and granodioritic batholiths which form large arcuate embayments around the schist belt. The Matsiloje, New Zealand and Northern batholiths are part of the most common type of granitoid intrusion (Fig. 1.2).

The batholiths are multicomponent bodies consisting mainly of medium to coarse-grained rock of tonalitic composition, averaging about 20% quartz, 70% oligoclase with minor microcline, biotite and epidote. Associated with these are gabbroic masses and within the "Northern" batholith a few large greenstone relics were recognized by Mason (1970) and Key (1976) (Appendix VII).

According to Mason (1970), the second type of granitoid

Penhalonga Formation has been identified in the Signal Hill area (Fig. 2.3). Detailed lithostratigraphic investigations of the Last Hope sediments in the Signal Hill area shows a right way-up sequence with a younging direction towards the south (Chapter 3).

2.2.6 Selkirk Formation

Mason (1970) and Key (1976), described the Selkirk Formation (Table 2.1) as a thick overturned succession of dacitic and rhyolitic lavas and associated pyroclastic rocks, which occurred at the top of the volcanic pile. According to them the Selkirk Formation crops out along the northern part of the schist belt in contact with the Northern batholith, extending from Francistown to the Zimbabwean border. Molyneux (1971) considered the Selkirk Formation to be younger than the other greenstone formations of the Tati schist belt, and composed largely of an intrusive basic complex together with lesser amounts of dacitic lavas. Work done by Thatcher (1990) and Siegfried (1990) has indicated that the Selkirk Formation referred to by Mason (1970) and Key (1976), is composed mainly of intrusive rocks (granodiorite, tonalite, diorite and gabbro) in contact with intermediate and felsic meta-volcanic rocks, therefore supporting Molyneux (1971) observations. The present study has indicated that the intermediate and felsic meta-volcanic assemblage shows a right way-up succession (see Penhalonga Formation, North domain) instead of an overturned succession as proposed by Mason (1970) and Key (1976). Therefore, this succession

mapped the same area and included the Last Hope lithologies as a conformable assemblage within the Penhalonga Formation (Table 2.1).

The Last Hope Formation consists of various metasedimentary rocks which form a discrete basin in the central part of the Tati schist belt (Macon, 1970) (Fig. 1.2). The bulk of the metasedimentary rocks are of clastic, volcaniclastic or volcanogenic origin. In the central, north and northwest areas of the basin, clastic sediments, shale, volcanic and volcanogenic units were identified. In the southern sector of the Last Hope Formation, the rock assemblage is mainly composed of volcaniclastic and volcanogenic units (Appendix VII).

Work carried out in the southeastern side of the basin (vicinity of Signal Hill Au-As-Sb deposits), has identified a sequence of mainly quartz wacke sediments interbedded with diamictite units.

On the west side of the basin, the Last Hope Formation and the Penhalonga Formation are separated by the Long Gonuan structure (Fig. 2.4). In the north, northeast and east sides of the basin, members of the Last Hope Formation strike and dip sub-parallel to the underlying chert and ironstone units (Penhalonga Formation, East and North domains, Fig. 2.4). In the north, northeast and east of the basin, Key (1976) identified a conformable contact between the Penhalonga Formation and the Last Hope Formation.

In the south and southwest sides of the basin, an unconformable contact between the Last Hope Formation and the underlying

4) South domain

Within this domain all lithologies dip steeply toward the south and southeast. The rocks possess a well-developed schistosity and a late crenulation cleavage. A well-developed stretching lineation which plunges towards the south is frequently observed. In the vicinity of Signal Hill area, the rock assemblage overlies the Lady Mary Formation and terminates at the "Main Thrust Front" structure (Fig. 2.3). The "Main Thrust Front" is a structure of approximately 15 km length, which forms a large-scale arc. This structure separates the structural South domain from the structural East domain. It is suggested that this structure is related to a major thrusting event (Chapter 4). However, it is not clear whether or not the Long gossan structure (Southwest domain) and the Main Thrust Front structure represent the extension of the same structure or if they are two independent structures. The Landsat image interpretation suggests that the Long gossan structure cross-cuts the Main Thrust Front structure (Fig. 2.3). This relationship has not been confirmed by field evidence (the converging area of these structures being an area of poor outcrops).

2.2.5 Last Hope Formation

The Last Hope Formation was first described by Mason (1970). He established that the contact with the underlying Penhalonga Formation was marked by an unconformity. In contrast, Key (1976),



Figure 2.6: Rock succession showing light-grey and well-banded chert units with felsic meta-tuff. A basal chert unit (1) shows an erosive contact infilled with meta-tuff material (2). The felsic meta-tuff contains the well-developed regional schistosity.

tuff units. The right way-up is indicated by the presence of a rounded clastic fragment which created a poorly developed load structure within the underlying unit.

3) East domain

In the East domain the Penhalonga Formation dips towards the west and overlies the right way-up Lady Mary Formation. Chert units interbedded with felsic aphanitic [illegible] the Signal Hill ironstone also indicate a right way-up sequence (Fig. 2.6). This sequence shows a repetitive succession of light grey, well-banded chert units with felsic meta-tuff units. The unit dips at 62° towards the southwest. A chert unit has been eroded prior the deposition of an overlying felsic meta-tuff.



Figure 2.4: Large meta-volcanic block within an agglomerate host, showing a right way-up sequence. The block deformed the underlying sediment while being emplaced, the overlying sediments are not deformed.

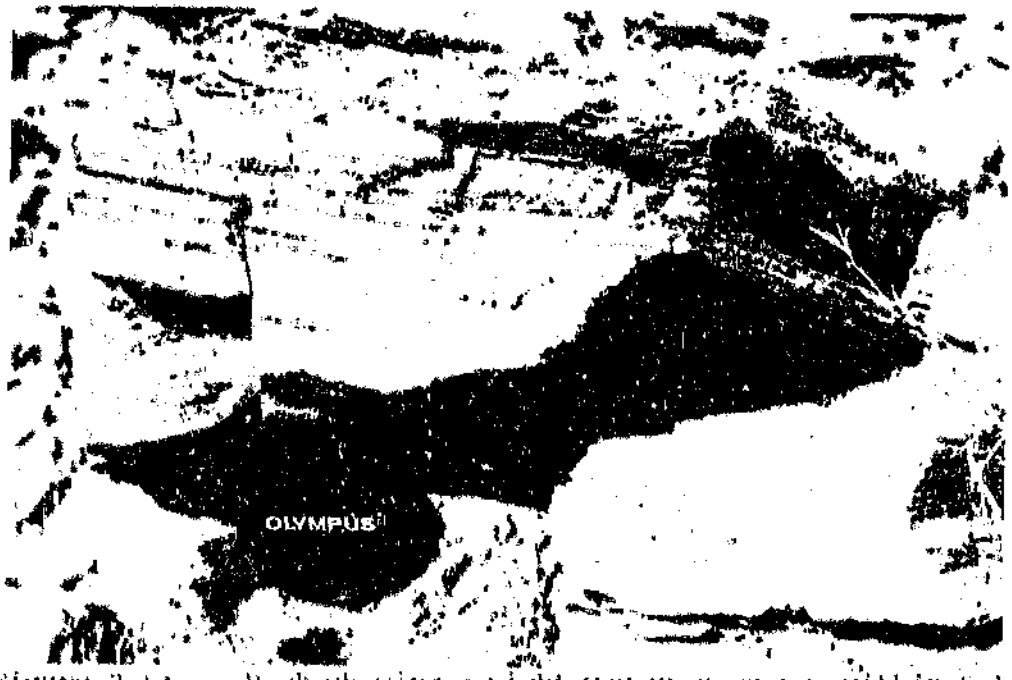


Figure 2.5: Rock showing a right way-up sequence within felsic tuff units, Penhalenna Formation North domain. The way-up is indicated by the presence of a rounded clastic fragment (bottom right corner) which created a poorly developed load structure within the underlying unit.

on Landsat image, from south of Francistown to the Sikukwe river and then south to the Tati river (Fig. 2.3).

2) North domain

Units of the north domain dip towards the southwest (near Francistown), south and southeast (near Texan gold mine). The rocks possess a well-developed schistosity and a well-developed late crenulation cleavage. A relatively well-developed stretching lineation which plunges towards the south is also frequently observed throughout the north domain.

South of the Texan gold mine, chert and ironstone members underlying the right way-up Last Hope Formation dip at 35-40° towards the southeast (Appendix VII).

The prominent alumina-rich horizon, which forms part of the Penhalonga Formation described earlier, belongs to this structural domain. According to Mason (1970), this horizon is a succession of salic tuffs and agglomerates in which bedding, cross-bedding, scour structures and pyroclastic "bombs" can be recognized. Figure 2.4, shows a large meta-volcanic block within an agglomerate host. The block deformed the underlying sediment while being emplaced, the overlying sediments are not deformed. This evidence indicates a right way-up sequence. Other evidences for the right way-up succession of the north domain was given by Cain (1980). He found right way-up structures in felsic tuffs east of Penhalonga mine. Figure 2.5, shows the right way-up sequence within these felsic

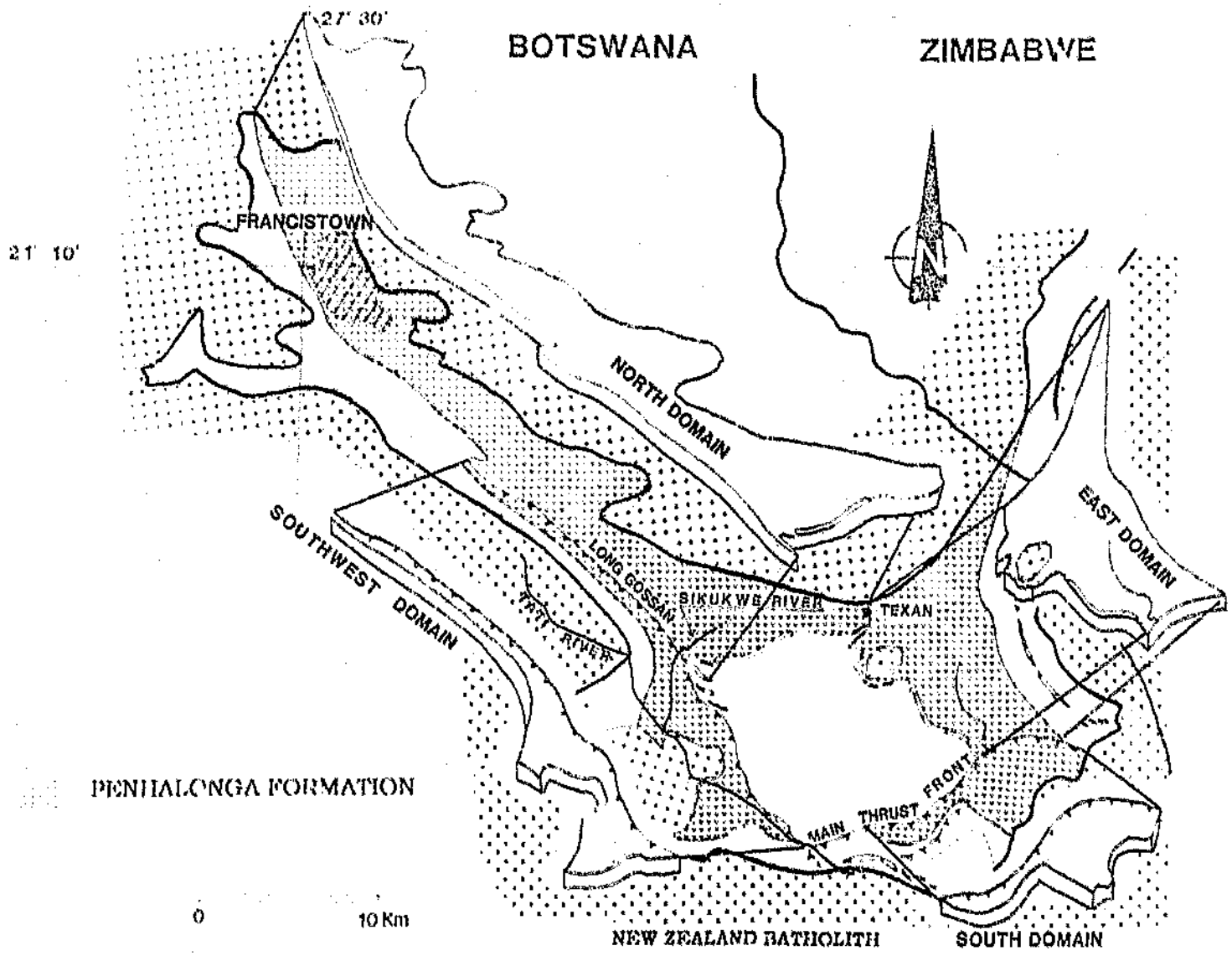


Figure 2.3 : Subdivision into four distinct structural domains of the Penhalonga Formation.

distinct structural domains (Fig. 2.3);

1) a southwest domain which occurs in the area south of Francistown to the Sikukwe river and then extends southeast from the Sikukwe river to the New Zealand batholith.
2) a north domain which covers the area from Francistown to the Texan gold prospect.
3) an east domain which extends from the Signal Hill area to the Texan gold prospect.
4) a south domain is located in the southernmost portion of the Tati schist belt. It extends from the intersection of the Long Gossan structure with the Main Thrust Front structure to the Signal Hill area (Fig. 2.3).

1) Southwest domain

Within this domain all lithologies dip steeply towards the southwest. The rocks possess a well-developed schistosity and a late crenulation cleavage. A relatively well-developed stretching lineation which plunges towards the south is frequently observed throughout the domain. All members are overturned and show younging directions towards the north, the northern boundary is defined by the "Long gossan" structure (Fig. 2.3). The "Long gossan" structure at surface is a ferruginous siliceous and occasionally sulphidic rock. No detailed study has been done along this structure, however, it can be traced in the field as well as

2.2.4 Penhalonga Formation

"Perhaps the most varied and interesting formation in the schist belt, the Penhalonga Formation, consists of a series of calc-schists (carbonated schist), limestones, quartz-schists, chert and meta-volcanic (andesitic) rocks" (Mason 1970). Pyroclastic rocks are commonly found interbedded with volcanic and sedimentary units. A prominent alumina-rich schist horizon containing kyanite, chloritoid and pyrophyllite occurs together with quartz-sericite and chlorite schists. This horizon can be traced from near Francistown in the northwest, to beyond the Texan gold showing in the southeast over a strike distance of approximately 13 km (Fig. 2.3, Appendices VII and VIII). The thickness of this horizon varies from 15m to up to 300m.

A sulphidic and occasionally siliceous ironstone formation forms the lower contact between the Lady Mary Formation and the Penhalonga Formation. The contact between the Penhalonga Formation and the overlying Last Hope Formation is delineated by another major chert and ironstone member, namely the Signal Hill ironstone. The composition of the ironstone is dominated by siliceous non-magnetic chert occasionally interbedded with local massive bands of magnetite.

Structure

Members of this Formation can be subdivided into four

Appendices VII and VIII). In the field, this structural contact is indicated by a zone comprising highly sheared, folded and deformed ultramafic units.

However, within the old Pati Formation, it is not clear if the repetitive sequence of intercalated ultramafic and basaltic units is the product of duplication by thrusting or if the sequence represents the original lithostratigraphy.

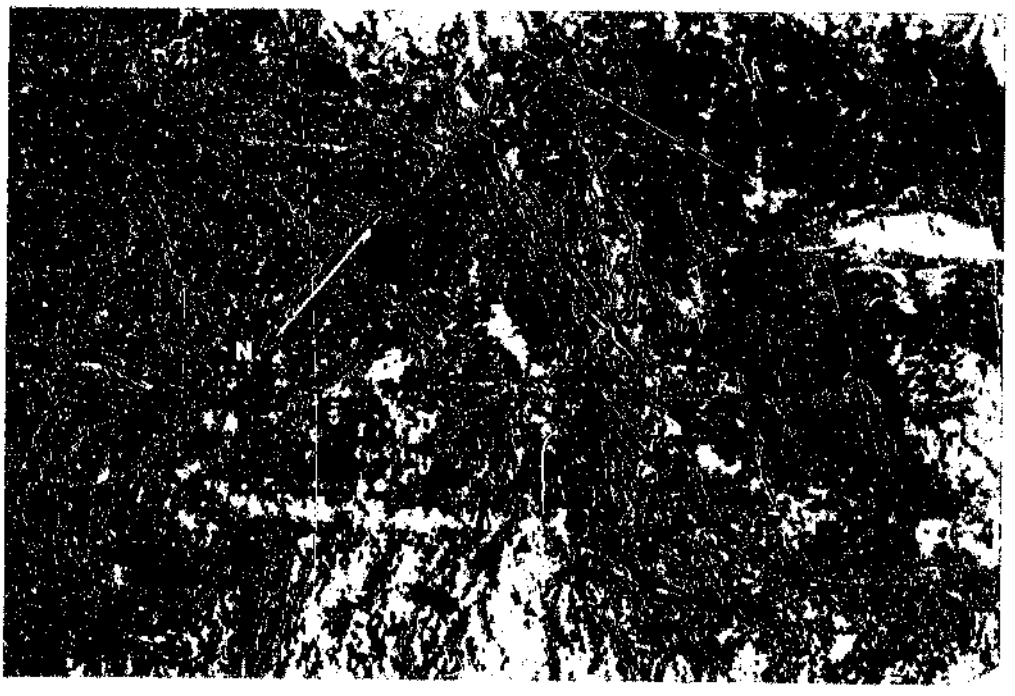


Figure 2.2: North younging direction indicated by a pillow in a Lady Mary Formation's matic unit. The unit dips steeply towards the south. The sequence is overturned.

In the eastern part of the schist belt (Fig. 1.2), the Lady Mary Formation overlies the Matsiloje Formation and dips steeply towards the west. At this locality, the Lady Mary Formation is right way-up.

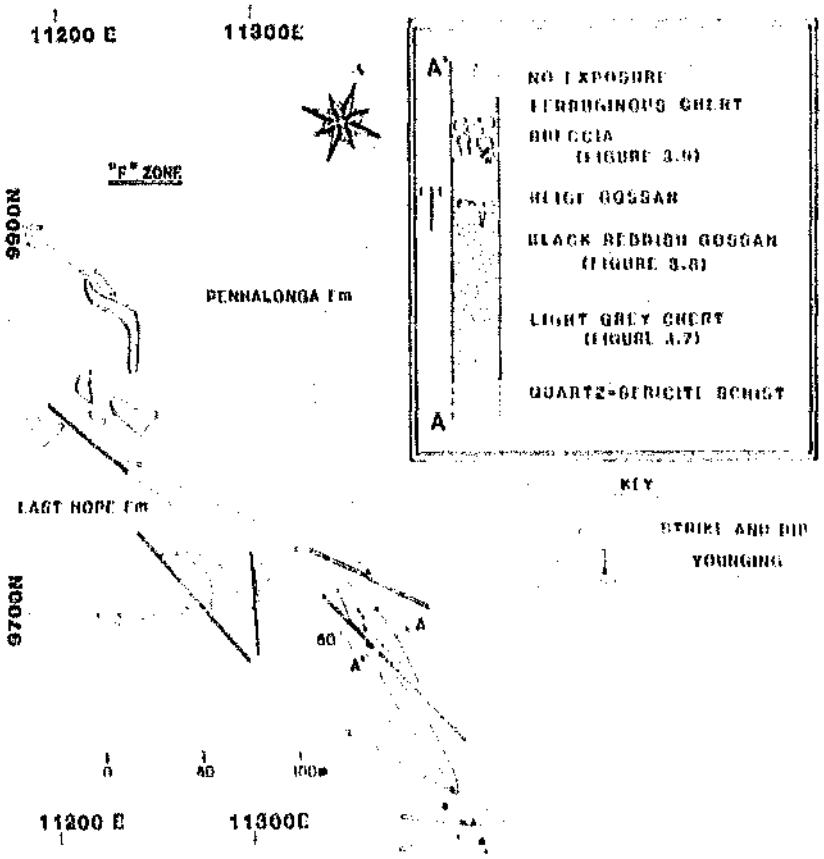


Figure 3.5 : Magnet profile A-A", through the chert and ironstone member, in vicinity of the "F" zone mineralisation.

Successive periods of deformation as well as intense hydrothermal alteration has changed the original mineralogy into a quartz-sericite schist. Figures 3.4 and 3.5, show the growth of metamorphic chloritoid and epidote crystals in quartz-sericite matrix.

Chert and ironstone

A detailed cross-section mapped immediately south of the "P" Zone, shows that at least five distinct litholoqical units form this member (Fig. 3.6). A light grey chert (Fig. 3.7) is overlain by a dark-reddish ferruginous gossan (Fig. 3.8). A beige gossan (slightly more siliceous than the reddish ferruginous gossan) overlies the reddish gossan. A "breccia" composed of angular fragments of felsic material in a fine siliceous and ferruginous matrix (Fig. 3.9) overlies the beige gossan. At the top of the succession is a well bedded, slightly ferruginous chert, which is overlain in places by another light grey chert. With the exception of the light grey chert at the base, all of these facies are generally not laterally extensive, but can be used locally as marker horizons.

The basal light grey chert is locally interbedded with thin members of aphanitic, felsic meta-tuff (Fig. 3.6). The portion of tuffaceous bands within this unit decreases sharply towards the top of this facies.

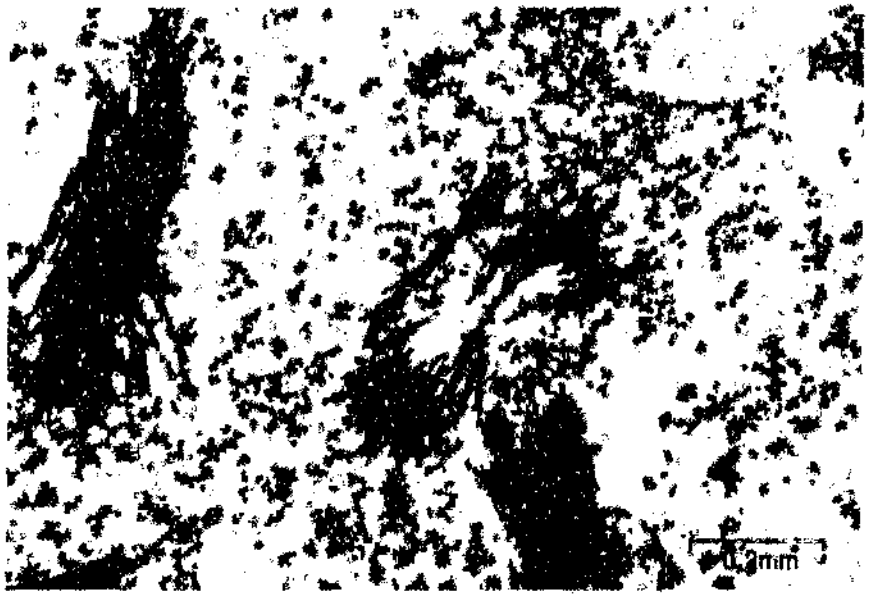


Figure 3.4: Porphyroblast of epidote being replaced by iron oxide, [illegible], 58m, 100 X.

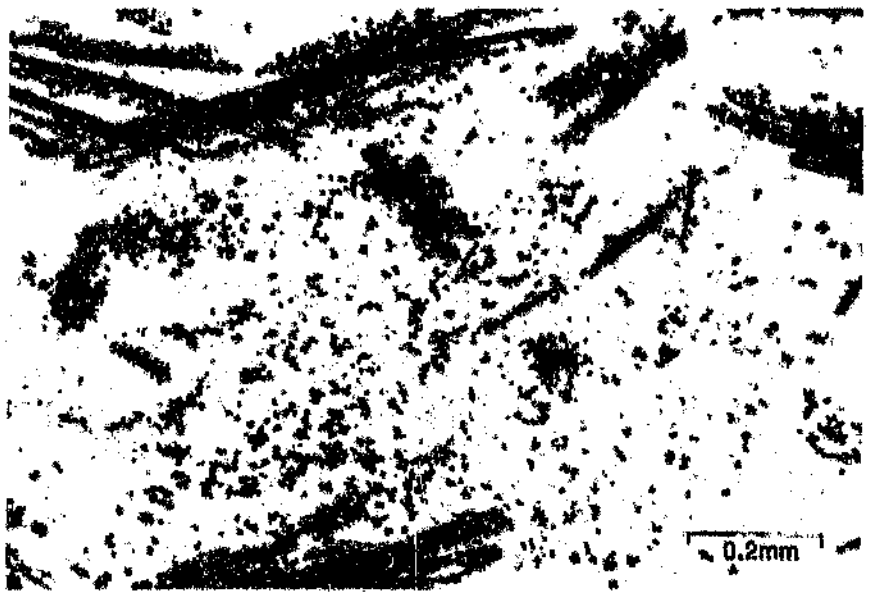


Figure 3.5: Porphyroblast of chloritoid in a quartz-sericite matrix, [illegible], 11m, 100 X.



Figure 4.3: Very fine-grained carbonated quartz-sericite schist, HPD-063, 60m



Figure 4.4: Felsic meta lapilli tuff with sub-rounded ironstone, quartz and volcanic clasts in a fine, sheared, carbonated quartz-sericite matrix, HPD-063, 60m.

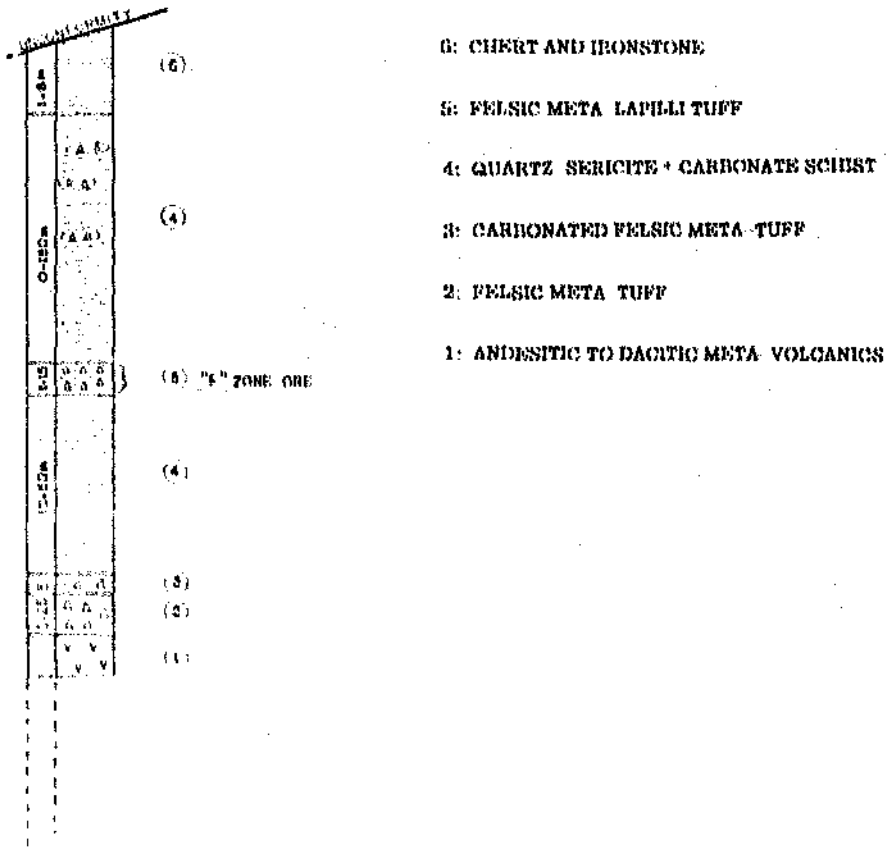


Figure 3.1: Composite sequence of the upper Penhalonga Formation ("F" Zone) constructed from data collected from core boreholes SPD=002, SPD=003 and SPD=004.

forms part of the right way-up succession. It consists of a basal meta-volcanic unit, followed by a succession of quartz-sericite schists interbedded with felsic meta-lapilli tuffs and overlain by the Signal Hill chert and ironstone (Fig. 3.1).

Meta-volcanic unit

A dark green, aphanitic, intermediate to mafic volcanic unit has been observed only in borehole SPD-063 (Fig. 3.1, Appendix IX). The original mineral assemblage has been completely metamorphosed to a chloritoid - chlorite ± carbonate schist.

Quartz-sericite schist

This assemblage has been intensely altered and deformed by several deformation events. These rocks are highly sheared, silicified, sericitized and, to variable degrees, dolomitized (Fig. 3.2). Within this quartz-sericite schist assemblage, several sub-units show concentrations of rounded fragments of quartz and ironstone, as well as sub-angular to angular fragments of carbonated quartz-sericite schist of the same composition as the matrix, (Fig. 3.3). It is proposed that these sub-units are felsic meta-lapilli tuffs interbedded within the quartz-sericite schists. The "P" Zone mineralization is intimately associated with one of these felsic carbonated meta-lapilli tuff sub-units (Fig. 3.1).

3.2 Penhalonga Formation

According to Mason (1970), Key (1976) and the exploration work done by Falconbridge geologists south of the Signal Hill block (Fig. 1.2), the Penhalonga Formation is overturned with a younging direction towards the north. In the east and northeast of the Signal Hill block, the Penhalonga Formation shows a right way-up succession.

Due to the lack of outcrops, the overturned sequence of the Penhalonga Formation is exposed only in six small trenches (LAR-01 to 06, LAR-03 as indicated in Appendix VIII), whereas in the vicinity of the "F" Zone, numerous trenches and 3 core boreholes show a right way-up sequence of the upper members of the Penhalonga Formation (Appendix IX).

3.2.1 Lower members of the Penhalonga overturned sequence

The lower members of the Penhalonga Formation, constitute a sequence of intermediate meta-volcanic units intercalated with well bedded aphanitic volcanogenic units, shale and a prominent carbonated ironstone.

3.2.2 Upper Penhalonga Formation

The uppermost sequence of the Penhalonga Formation, is exposed only in the vicinity of the "F" Zone (Appendices VIII and IX), and

CHAPTER THREE

GEOLOGICAL SETTING OF THE SIGNAL HILL AREA

3.1 General Statement

Despite work done by Mason (1970) and Key (1976), very little work has been carried out previously on the sedimentary aspect of the Signal Hill area.

The Last Hope Formation underlies approximately 80% of the Signal Hill block, while the Penhalonga Formation is present only in the southeast, east and northeast of the block (Fig. 1.2).

Interpretation of the sedimentary aspect of the Last Hope Formation was done by examining vertical and lateral sedimentary successions from several boreholes, outcrops and trench exposures. The interpretation of the volcanic rocks of the Penhalonga Formation was done using boreholes and trench exposures. Classification of the Last Hope Formation sedimentary rocks and the Penhalonga Formation constituents was previously in a state of disarray. The purpose of this chapter is firstly, to provide a classification for these rocks, and secondly, to use vertical and lateral associations of sediment assemblages to define lithofacies and possible changes in the depositional environment through time.

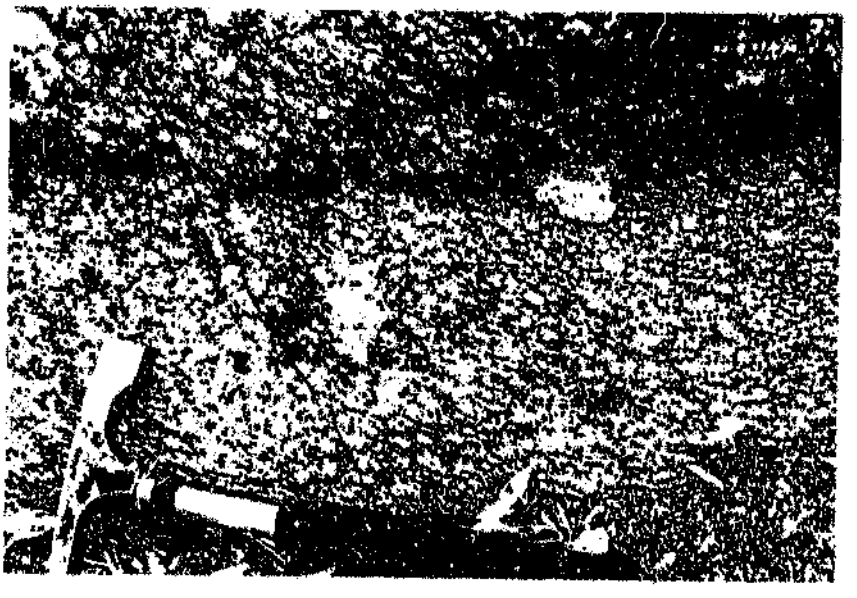


Figure 2.10: Sheared granodiorite rock located at the margin of the Hill View pluton, see Appendix VII.

2.3 Geochronology

No detail geochronological work has been done on the Tati schist belt. However, Dr J. Wilson, from the Department of Geology, University of Zimbabwe, as a guest speaker at the Tati workshop (March 1991) identified several similarities between the Old Tati Formation and Upper Bulawayan series in Zimbabwe, which is dated between 2,7 to 2,8 Ga years.

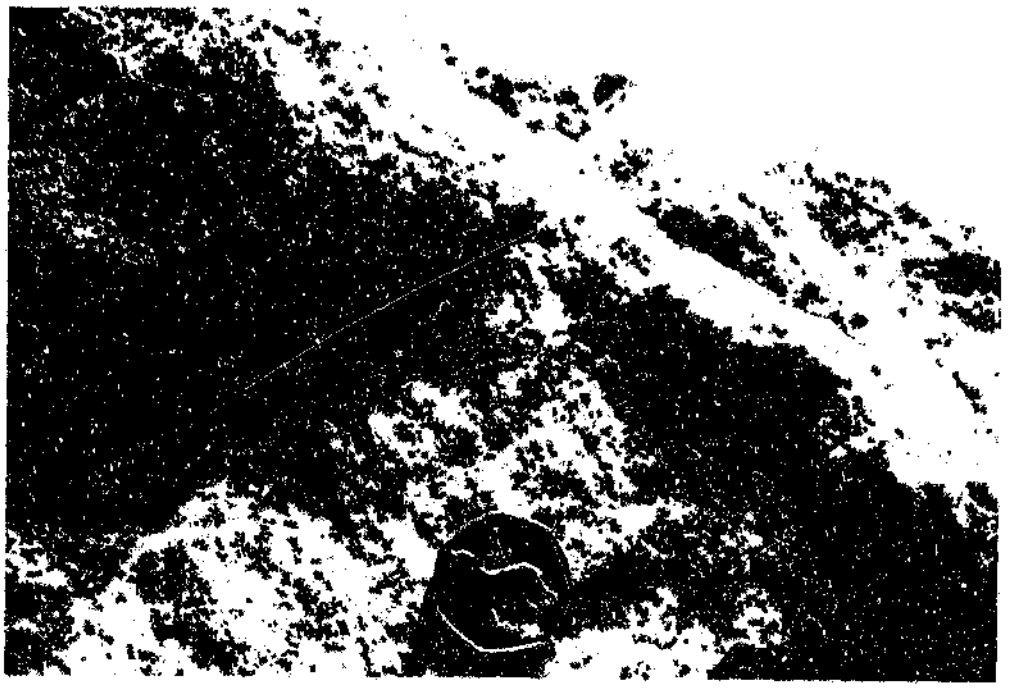


Figure 2.9: Undeformed tonalitic-granodioritic rock. Northern batholith at Tokwane gold mine (Fig. 1.3, Appendix VII)

possible that the intrusion of these batholiths and the Hill View tonalite were contemporaneous and that their final consolidation predates the development of the regional foliation (S_2).

According to Mason (1970), the evolution of the Tati schist belt is thought to have been largely controlled by vertical tectonic forces related to the intrusion of tonalitic and granodioritic batholiths and the sympathetic collapse of the volcano-sedimentary formations. However, Litherland (1976), identified tectonic fabrics which predate Mason's first phase of deformation (Chapter 4.3) in the Zimbabwe craton, which suggested that large nappe-type structures have been formed during an early episode.

alignment of quartz and feldspar crystals in poorly developed thin bands (1 to 2 mm thick) together with the development of sub-parallel cleavages (Key 1976). The writer observed that the foliation at the contact between the New Zealand batholith and the Old Tati Formation is parallel to the contacts of the intrusions, and similar in strike and plunges with the regional schistosity observed over Signal Hill's "A" and "F" Zones (Fig. 2.8 A and B).

Mineral stretching lineations, defined by elongated quartz and feldspar grains are developed on the foliation surfaces and plunge at approximately 50° to the south (Fig. 2.8 A). In the centre of these tonalitic plutons, the foliation is weaker and frequently absent. Selkirk mine and Tekwane gold mine (Fig. 1.3) are good localities where exposures of mostly undeformed tonalite can be seen (Fig. 2.9).

The Hill View tonalite has identical composition and structural deformation as the New Zealand batholith or the tonalitic facies of the Northern batholith at Tekwane gold mine. Key (1976) mentioned that the Hill View tonalite was a "homogeneous rock with no tectonic or compositional fabric" and therefore represents a much younger event than the other tonalitic intrusions. Figure 2.10 demonstrates that like the Northern and New Zealand batholiths the Hill View tonalite is also affected by planar foliation at the margins, while in the centre the foliation is weaker and frequently absent. Therefore, it is not clear whether the Hill View tonalite represents a younger intrusion than the New Zealand or the Northern batholiths, as proposed by Mason (1970) and Key (1976). It is

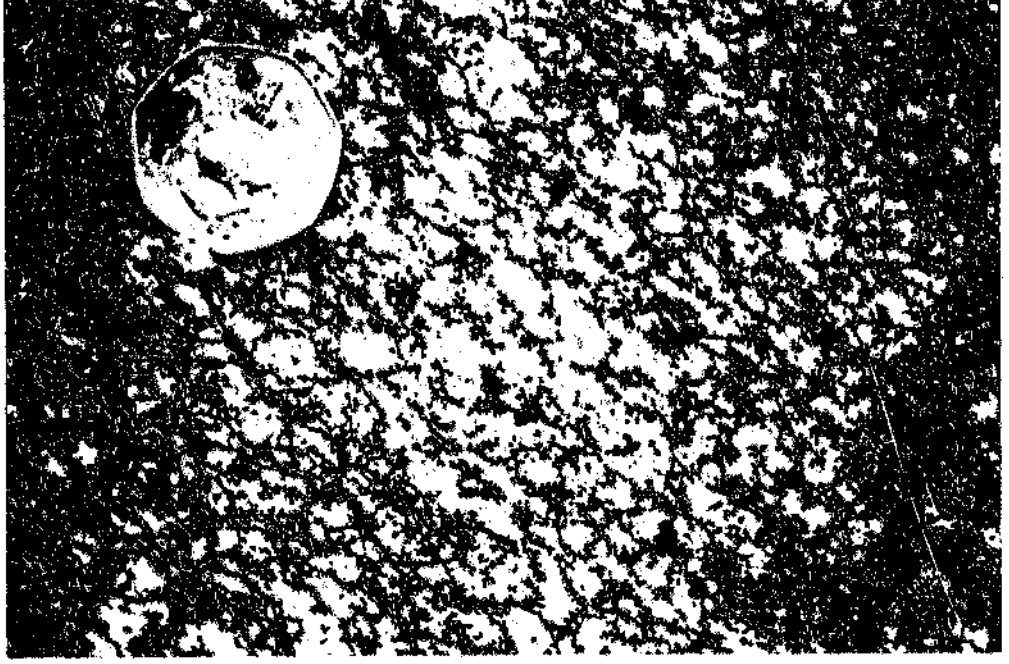


Figure 2.7: Highly deformed granitoid rock located at the contact between the New Zealand batholith and the Matsiloje Formation (Appendix VII).

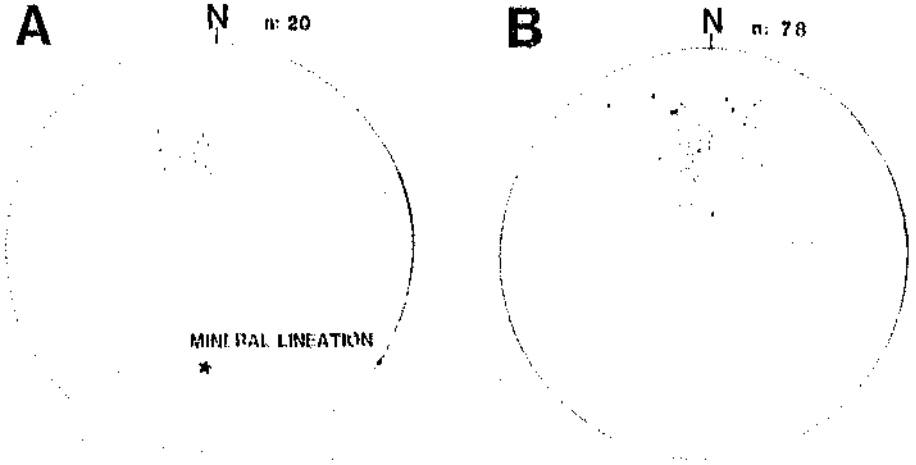


Figure 2.8: A- Stereoplot showing poles of the foliation and a mineral lineation at the margin of the New Zealand batholith. B- Stereoplot of poles of the regional schistosity observed over the "A" and "F" Zones (Appendices VIII and IX).

Northern package

This package is exposed in trenches mainly in the vicinity of the "C" Zone. Narrow intersections of the Northern package were encountered in two core boreholes drilled from the "A" Zone. This package was not studied in detail. Nevertheless, surface mapping shows interbedded diamictite with numerous thin layers of quartz wacke. The major characteristic of the Northern package is the broad transition from diamictite with a fine quartz-sericite matrix to diamictite with a quartz wacke matrix. The "C" Zone mineralization appears to be located within this transition zone.

Fat Boy package

Within the Fat Boy package, host of the "A" Zone mineralization, numerous individual diamictite layers have been observed (up to 10 individual layers in BPD-083 core borehole intersection). The thickness of these individual layers vary from less than 1 meters up to 10 meters. These diamictite layers have varying amounts of clasts ranging from less than 5% up to 90%. They are matrix supported and unsorted.

Two specific layers show distinctive characteristics. At the base of the package a blocky meta-tuff unit is overlain by a pink diamictite. The blocky meta-tuff unit consists of a sheared, fine grained, quartz-sericite matrix (absence of detrital quartz fragments) with less than 5% of subrounded fragments of ironstone

vein fragments and granitoid fragments when present, do not exceed 5% and 1% respectively. The diamictites are matrix supported and show no sign of reworking after deposition (Fig 3.18).

Three major sequences of diamictite facies have been identified, namely the Northern, the Fat Boy and the "B" Zone packages. Several individual lenses of diamictite are also observed within the quartz wacke facies (Fig. 3.10). Each of the three packages consists of alternating diamictite layers with thin, pebbly, very coarse grained, assorted, and immature quartz wackes. With the exception of a broad upward fining sequence within each package, the individual diamictite layers lack any sedimentary structures.

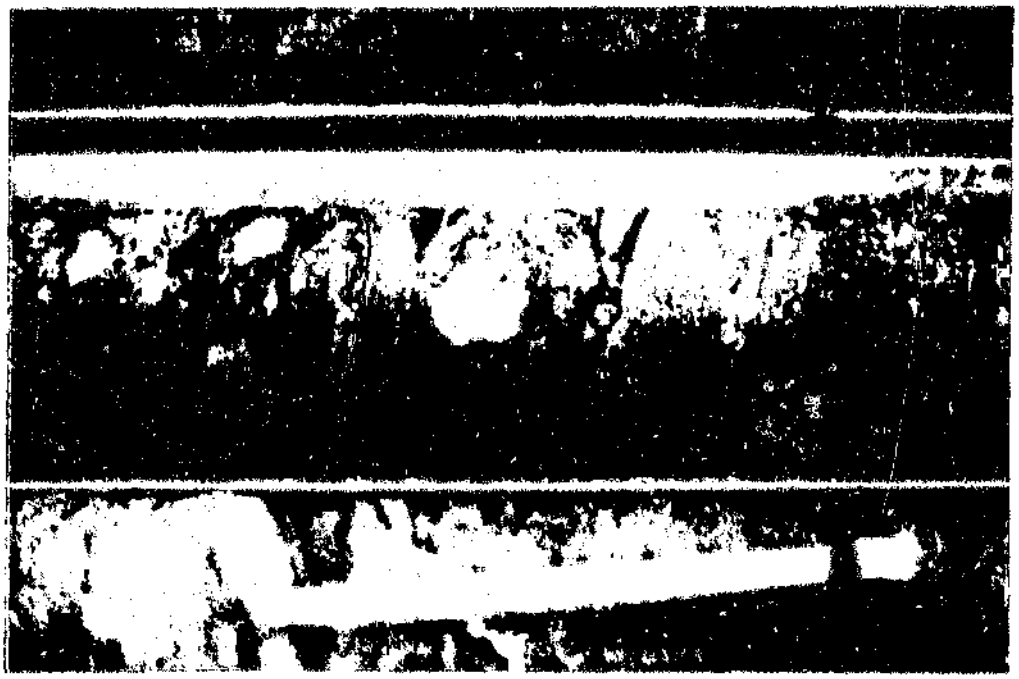


Figure 3.18: Diamictites showing sub-rounded quartz and iron-stone clasts and sub-angular to angular and flattened volcanic fragments in a fine carbonated matrix. The sediment is matrix supported, SP3-083, 100m.



Figure 3.17: Vertical section of trough cross-beds showing concave and tangential foresets. These trough cross-beds indicate a right way-up sequence with younging towards the southwest.

Diamictite facies

The diamictite facies consists of volcanic material, banded ironstone chert, quartz and granitoid fragments, within a matrix of fine to coarse grained quartz wacke mixed to various degrees with fine quartz-sericite material. Volcanic clasts represent the most abundant fragments, averaging 60% to 100% of the clast population. The chert and ironstone clasts represent locally up to 40% of the clasts present, but average approximately 15%, whereas the quartz



Figure 3.15: Photo showing parallel laminations within the grey purple quartz wacke, west of fault F098.

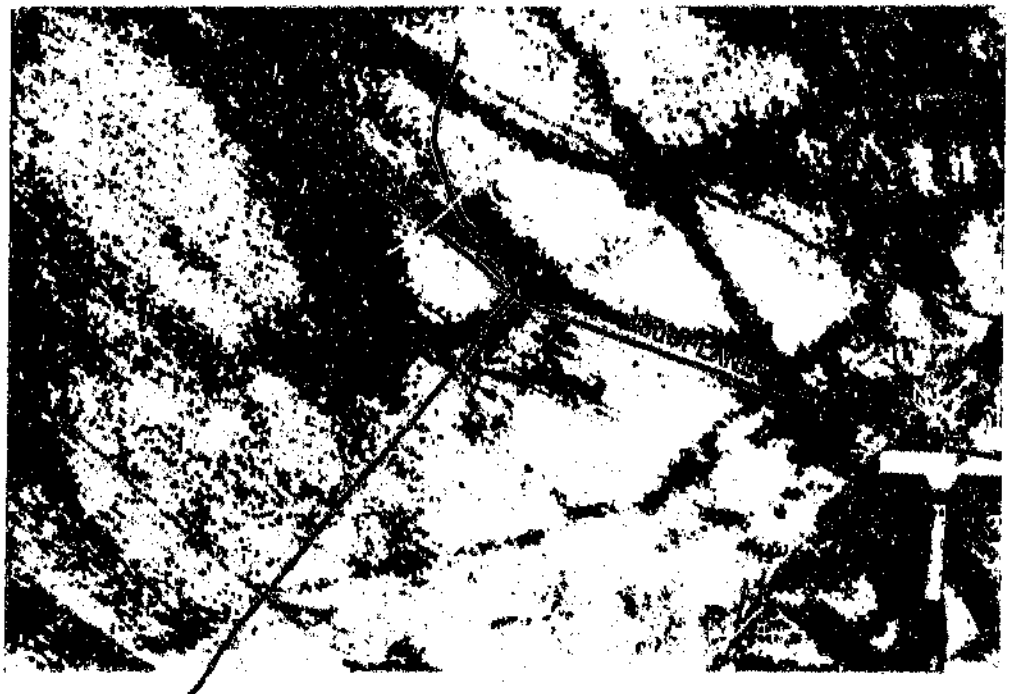


Figure 3.16: Photo showing the transition zone between the grey purple quartz wacke and the bedded green-weathering quartz wacke. This photo also shows a cross-cutting dyke (dolerite) and a tonalitoid (not too clear) on the left of the photo. Scale is 30 cm long.

serves as a good marker horizon.

Trough cross-bedded quartz wacke facies

At the southwestern end of the "A" Zone, a facies of beige, occasionally slightly silicified, trough cross-bedded quartz wacke overlies the planar laminated quartz wacke (Fig. 3.11, Appendix IX). Compositionally the rock is similar to that of the planar laminated quartz wacke. The sediment is coarse grained, poorly sorted and texturally immature. Individual beds vary from 3 cm to 20 cm in thickness. Each bed is composed of a multitude of fine laminations which form either tangential or concave forsets (Figs. 3.16 and 3.17). Cross-beds observed in this facies, show that the rock assemblage is the right way-up (Fig. 3.17). The transition from planar laminated quartz wacke to trough cross-bedded quartz wacke, although sharp in a few localities, is generally gradational.

Three-dimensional exposures of trough cross-beds in two specific localities (Appendix IX) were used to collect reliable palaeocurrent measurements. Results indicate that in both localities the palaeocurrent pattern is unimodal. In the locality A, the average current direction is plunging 50° towards 190° (Appendix IX). In the locality B, the average current direction is plunging 35° towards 220° (Appendix IX).

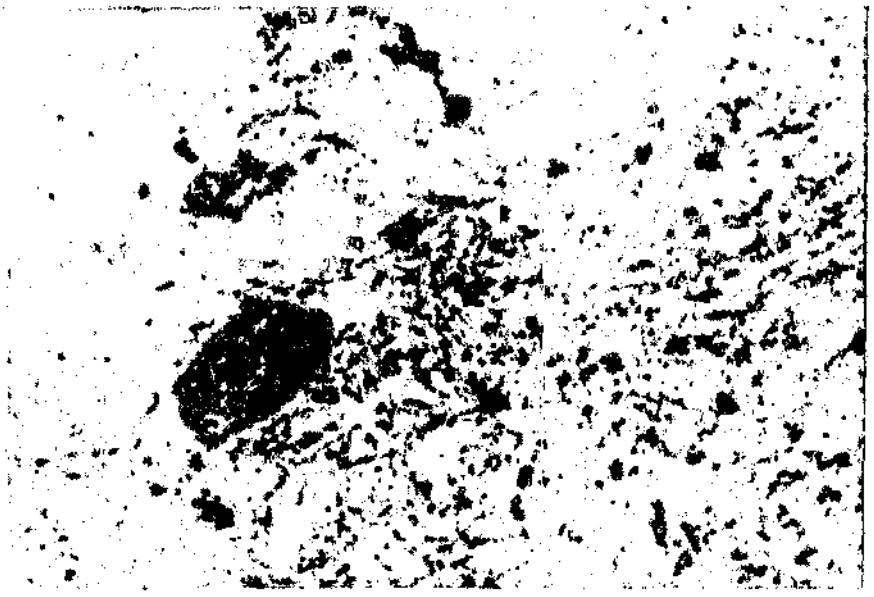


Figure 3.14: Very rare zircon within a quartz wacke, SD-077, 64m, 300 X.

Planar laminated quartz wacke facies

West of the fault F098, a planar laminated grey to purple quartz wacke underlies thin lenses of diamictite belonging to the "Fat Boy" package (Fig. 3.11 and 3.15). Like the quartz wacke facies described above, this facies is composed of sub-rounded to angular detrital quartz grains in a quartz-sericite matrix. The rock is matrix supported, poorly sorted and texturally immature. Grain size of the detrital fraction varies from 0.1mm to 3.0mm. This facies increases in thickness towards the west, from less than one meter (immediately west of fault F098) to more than 6 meters (western end of the "X" zone). This planar laminated quartz wacke

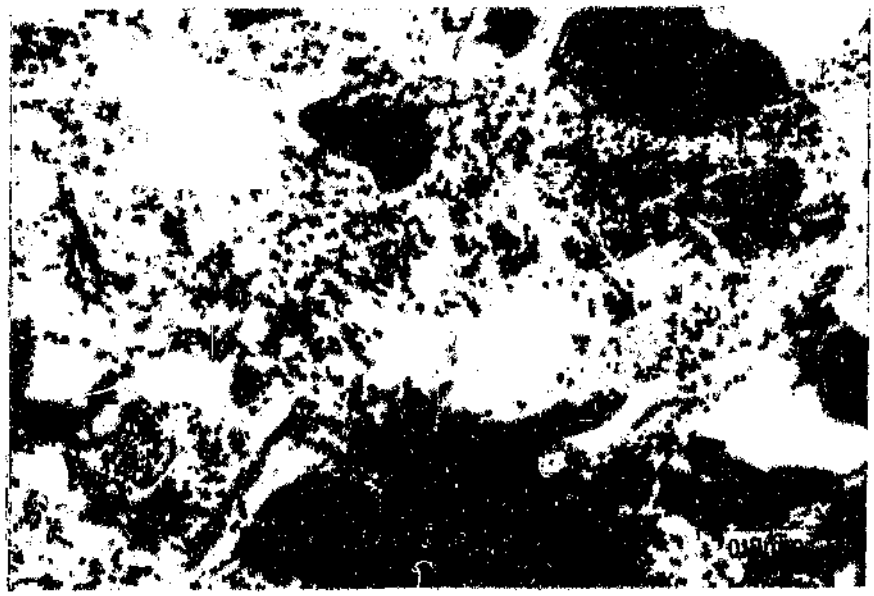


Figure 3.12: Photomicrograph of quartz wacke showing angular quartz fragments in a quartz-sericite matrix. The rock is matrix supported, SPD-081, 94m, 100 X, X nic.

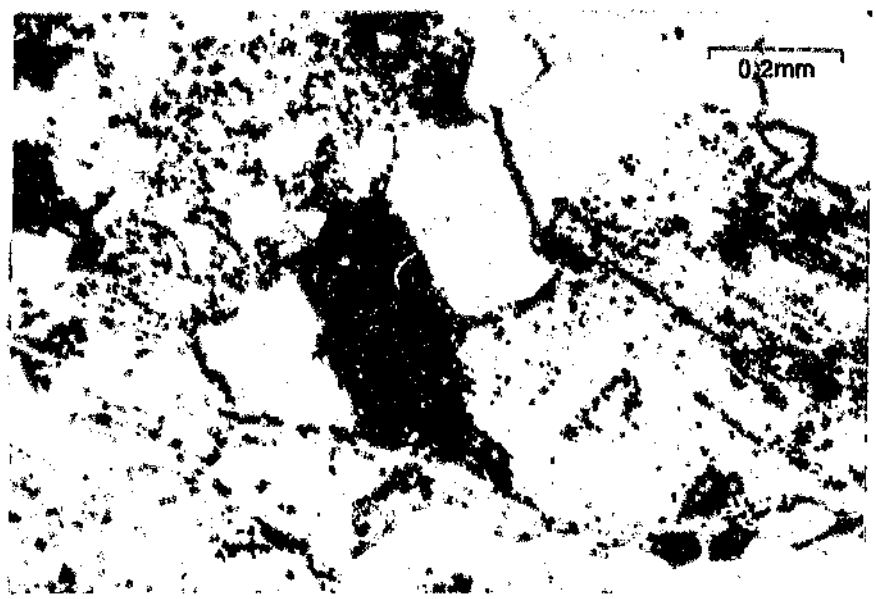
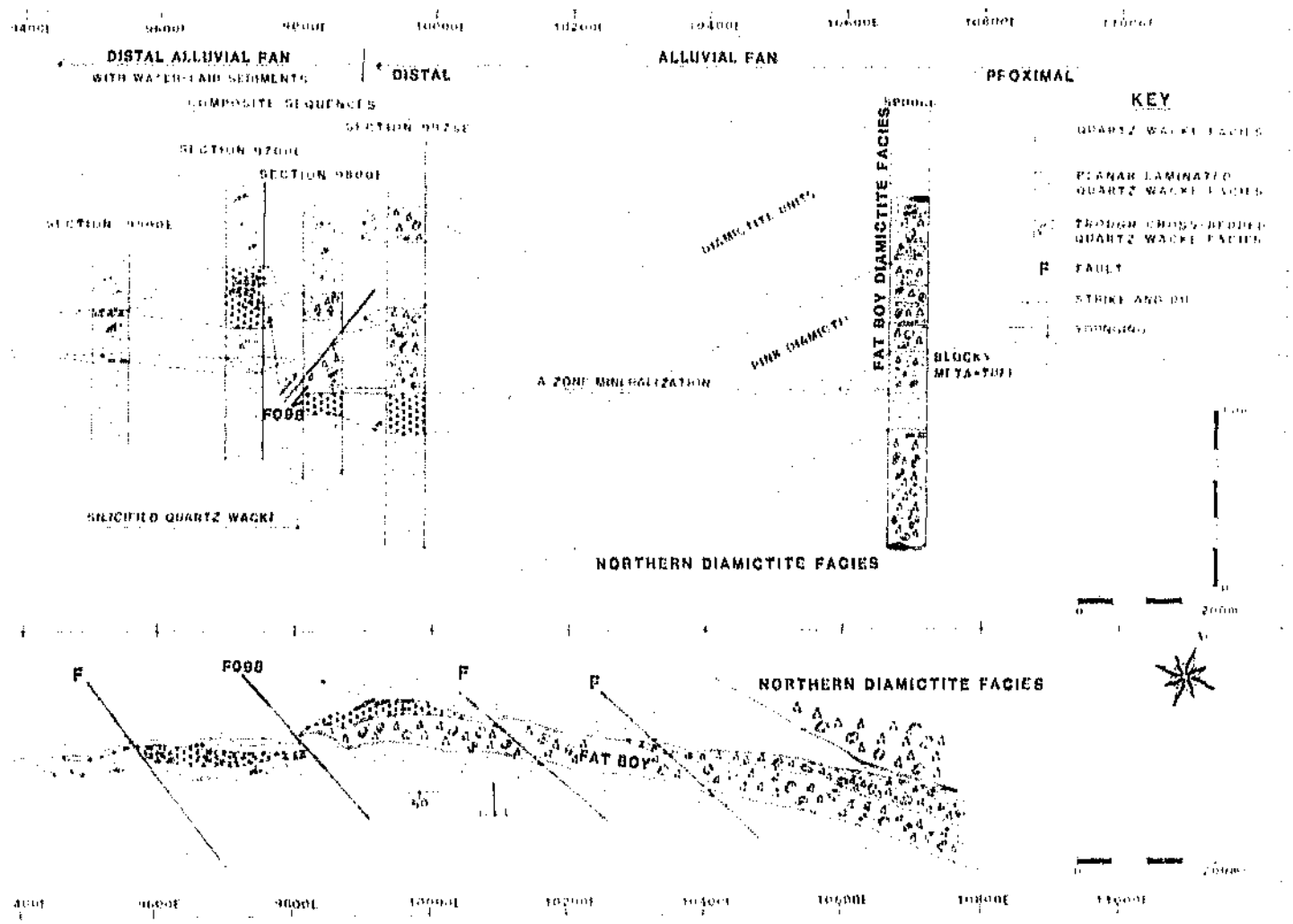


Figure 3.13: Rare twinned plagioclase crystal associated with quartz fragments in a quartz-sericite matrix, SPD-077, 60m, 100 X, X nic.



ure 3.11: Figure showing the composite sequences and surface logy of the "A" Zone. Composite sequences were constructed ng data from boreholes and trenches along each sections.

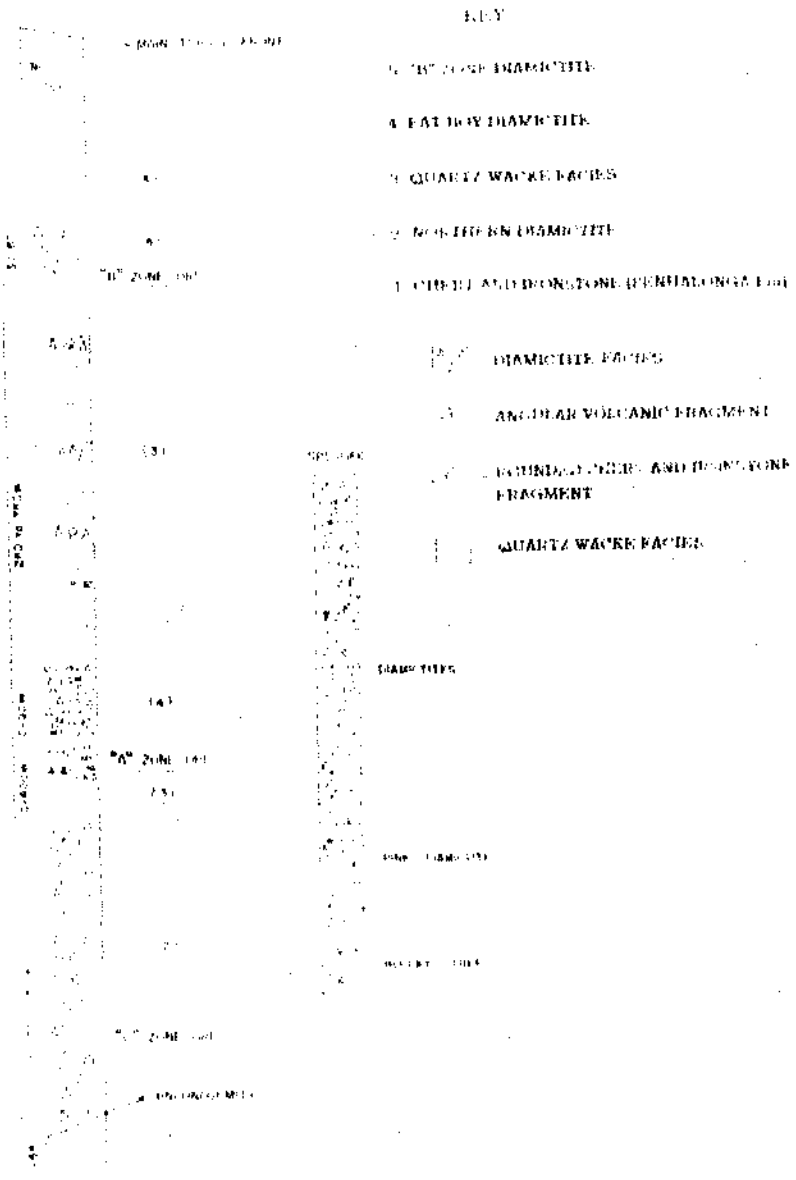


Figure 4.10: Figure showing the composite sequence of the Last Hope Formation at Signal Hill Au-Ag-Sb deposits area. The composite sequence was constructed using data from lithostratigraphic measurements, boreholes and trenches along the "A" zone.

ments are relatively easily transported in debris flows because they are supported in part by high buoyancy forces due to the high density of the mud in which they are submerged. They also mention that subaqueous rapid mass flows have never been directly observed and even the location and characteristics of modern examples are in doubt.

A conglomerate is a coarse-grained clastic sedimentary rock, deposited in a range of aqueous environments (Bates and Jackson 1984), whereas an agglomerate is a volcanic breccia formed by disruption of a solidified crust or hardened plug of lava (Bates and Jackson 1984).

The terms debris flow, conglomerate and agglomerate, due to their genetic connotation are not appropriate for descriptive purposes of these sedimentary facies. The term diamictite will be used hereafter to classify these facies. Diamictite is a comprehensive, nongenetic term proposed by Flint et al (1960) for a nonsorted or poorly sorted, noncalcareous, terrigenous sedimentary rock that contains a wide range of particle sizes, such as a rock with sand and/or larger particles in a muddy matrix.

3.3.1 Lithostratigraphy of the Signal Hill area

Four lithological facies have been identified over the Signal Hill area: quartz wacke, planar laminated quartz wacke, trough cross-bedded quartz wacke and diamictite facies.

A sequence of quartz wackes interbedded with several dia-



Figure 3.9: Chert and ironstone breccia showing fragments of angular felsic volcanic material within fine grained, ferruginous cherty matrix. For location see Figure 3.6.

3.3 Last Hope Formation

A sequence of quartz wackes interbedded with diamictites, parallel laminated quartz wackes and trough cross-bedded quartz wackes, characterizes the Last Hope Formation in the vicinity of the Signal Hill Au-As-Sb deposits. The terms "conglomerate, agglomerate and debris flow" have been extensively used as a descriptive classification for these diamictite facies in previous Falconbridge internal reports. Blatt et al (1972), describe a debris flow as a subaerial deposit, poorly sorted and bimodal with cobbles and boulders imbedded in a finer matrix. Beds deposited by individual flows lack internal stratification. The larger frag-



Figure 3.7: Basal chert facies of the chert and ironstone member, dip towards the west. For location see Figure 3.6.

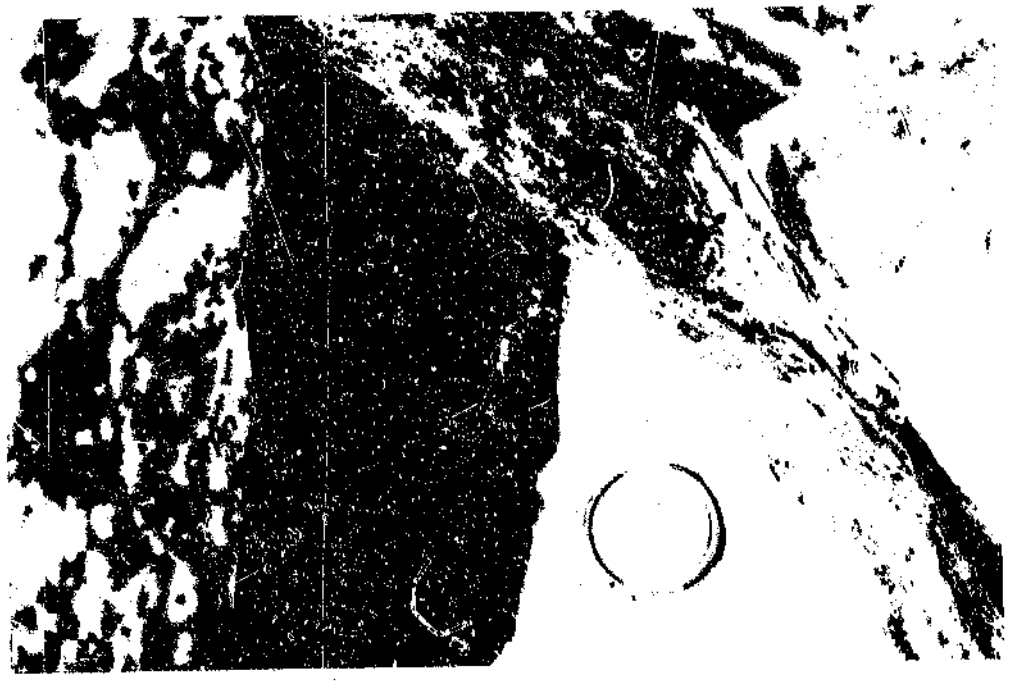


Figure 3.8: Dark reddish gossan underlying the beige gossan. Both facies are part of the chert and ironstone member. These facies dip towards the west. For location see Figure 3.6.

CHAPTER FOUR

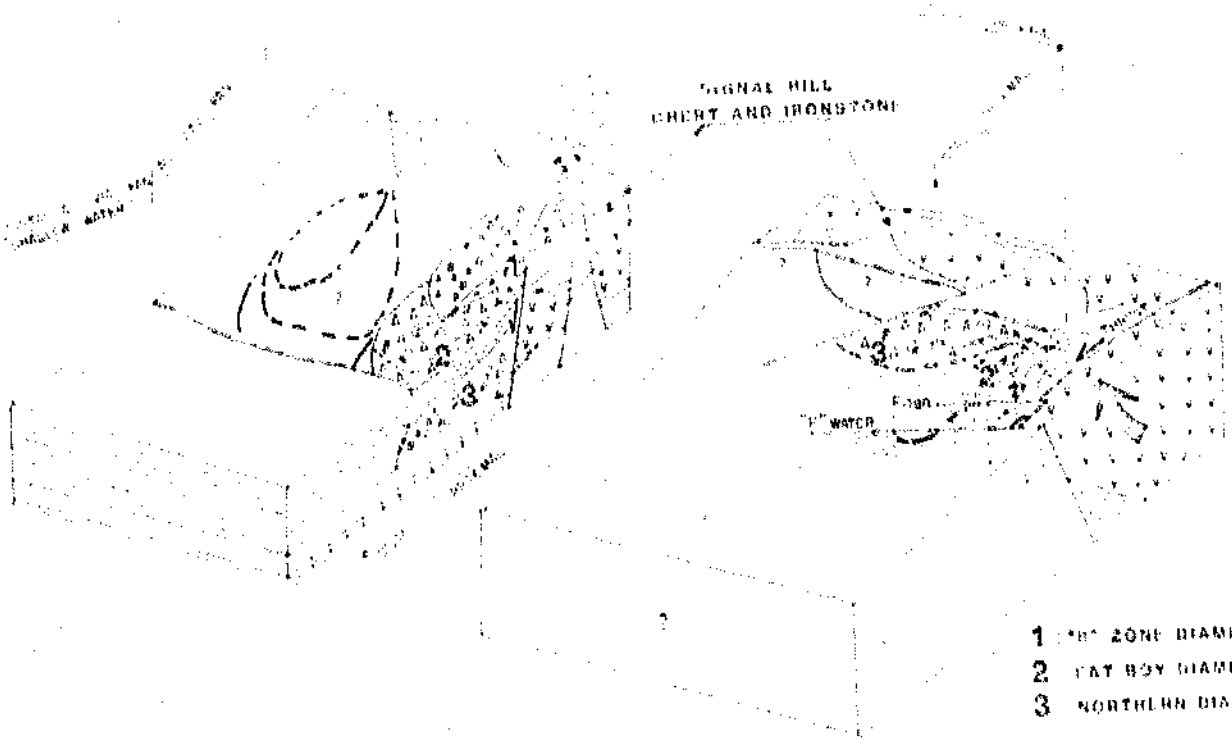
STRUCTURAL DEFORMATION AFFECTING THE SIGNAL HILL AREA

4.1 General Statement

The purpose of this chapter is to describe the successive structural events which affected the Signal Hill area and post-dated the deposition of the Last Hope Formation. A review of previous structural investigations is first presented followed by a detailed investigation carried out in the present study.

Most geological units within the Signal Hill block are south dipping. Bedding and cross-laminations in the Last Hope sediments indicate a right way-up sequence which youngs towards the south and southwest. South of the Signal Hill block, the Penhalonga Formation is overturned and youngs towards the north, whilst in the east and northeast of the Signal Hill block, the Penhalonga Formation is right way-up.

Evidence of early phases of deformation in the Signal Hill area, have been outlined in chapter 3. These early phases are related in the first instance to the deformation and alteration (quartz stockwork and pervasive carbonatization observed on volcanic clasts of diamictite layers) which affected the area before the deposition of the Last Hope sediments, and thereafter by an uplift at the end of the Penhalonga era which led to the deposition of the Last Hope Formation.



ORIGINAL BASIN

TILTED BASIN
(ACTUAL DISPOSITION)

Figure 1.2.2: Block diagrams showing the possible uplift of the underlying Penhalonga members along a normal fault and the coincident basin subsidence.

Distal alluvial fan interbedded with water-laid sediments

The first appearance of parallel and trough cross-bedded quartz wackes (west of fault F098, Fig. 3.11), together with the thinning of the diamictite layers, suggests a distal alluvial fan environment interbedded with a braided channel environment. The interpretation of the shape of the trough cross-bed quartz wackes, suggest that the palaeocurrent direction at these localities was roughly perpendicular to the main axis, oriented east-west of the alluvial fan lobes. It is also suggested that the hydrodynamic conditions had changed from higher velocity current and/or shallower water environment to a lower velocity current and/or deeper water environment.

Block diagrams presented in the Figure 3.22, summarize the proposed model of an uplift along a normal fault to explain the configuration of the Last Hope Formation and the local unconformity in the vicinity of the Signal Hill.

Reineck and Singh (1982), favourable conditions for the deposition and preservation of alluvial fan deposits exist where several alluvial fans are juxtaposed in a tectonically active area (subsiding basins).

The writer suggests that an uplift of the underlying formations along a normal fault, occurred at the end of the Penhalonga era. This uplift together with synchronous volcanic activity could have been responsible for the unconformity between the Penhalonga Formation and the Last Hope Formation, and for the deposition of alternating quartz wackes and diamictite packages of the Last Hope Formation.

Evidence for the normal fault can be seen in trenches STC-011 and STA-007 (Appendix IX), where in both trenches a sub-vertical contact separates the quartz-sericite schist assemblage (Penhalonga Formation) from the Northern and the Fat Boy diamictite packages. Furthermore, in trench STA-007, the fault is characterized by a zone of intense carbonatization and formation of a thick layer of calcrete at surface at the interface between the Last Hope units and the Penhalonga quartz-sericite schist. Geological mapping has also indicated that an abrupt transition between quartz-sericite units and Last Hope rocks occur along a plane striking 130° passing through both trenches STC-011 and STA-007.

The uplift combined with rapid basin subsidence could perhaps explain the suggested frequent alternation from subaerial (diamictite facies) to subaqueous environments (quartz wacke facies).

hydrodynamic environment and/or in shallower water than trough beds with tangential foresets. It is interpreted that from the base of the planar laminated quartz wacke to the top of the trough bedded quartz wacke, the hydrodynamic conditions of deposition changed from a higher velocity and/or shallower water environment to a lower velocity and/or deeper water environment.

Palaeocurrent measurements taken west of the "A" Zone indicate that the palaeocurrent direction at this specific locality, was roughly perpendicular to the long axis, oriented east-west, of the Fat Boy diamictite package.

Sedimentation in the Last Hope basin, in the vicinity of the Signal Hill area, occurred in two distinct environments:

A) in a proximal alluvial fan, and a
B) distal alluvial fan interbedded with water-laid sediments

Proximal alluvial fan

Blatt et al (1972) describe an alluvial fan as "deposits with great thickness, rapid lateral facies changes, and the preponderance of conglomerates and sandstones with not so abundant shale."

According to Bull (1972), diamictite and debris flow, might be part of an alluvial fan. An alluvial fan can be subaerial and/or subaqueous. The alternating quartz wackes and diamictite layers, presently seen at the "A" Zone, eastward from fault F092 to the contact with the Penhalewca Formation Signal Hill ironstone, are characteristic of an alluvial fan. According to

sub-aqueous and sub-aerial environments are envisaged to explain the present assemblage of diamictite and quartz wacke.

The first appearance of quartz wacke with internal sedimentary structures, (planar laminated and trough cross-bedded quartz wacke facies), occurs west of fault F098 (Fig. 3.11). These quartz wackes are interbedded with thin layers of diamictite of the Fat Boy package, as well as several immature quartz wackes. It has been observed that the thickness of quartz wacke units with internal sedimentary structures increases rapidly from east to west. According to Tucker (1989), planar lamination is most commonly produced in two ways: either by deposition from strong currents, or by deposition from suspension (low-density turbidity currents or from weak traction currents). It has been observed that the planar laminated quartz wacke facies are texturally immature, coarse grained and poorly sorted, which suggests that they were formed by deposition from strong currents.

According to Reineck and Singh (1982), large-scale cross-bedding, including trough cross-beds thicker than 5 cm, are of varied origin and they acquire different shapes (from angular to tangential to concave to sigmoidal) depending on the hydrodynamic factors existing at the time of deposition. Field observations show that the Signal Hill trough cross-bedded facies progress from concave at the bottom, to concave and tangential towards the top of the sequence. Reineck and Singh (1982), concluded that trough cross-beds with concave foresets are either deposited in a higher

The filling material is similar in composition to the matrix of the underlying diamictite layer. This features suggests that the carbonatization took place within the quartz wacke prior to the consolidation of the underlying diamictite member.

3.5 Discussion

It is interpreted that the quartz wackes originate from a mixture of fine tuffaceous and argillaceous material with highly variable amounts of detrital material. The diamictite packages are mainly composed of volcanic derived sediments with variable proportions of reworked clastic sediments (rounded to sub-rounded chert, ironstone and granitoid blocks). To produce the concentration of volcanic clasts present within these diamictite members, a significant amount of volcanic activity must have been synchronous with the deposition of the Last Hope sediments. Each individual bed of these diamictite packages represents a single depositional event.

Individual diamictite layers do not show signs of reworking after deposition. It is suggested that these sediments were deposited in a sub-aerial rather than a sub-aqueous environment. However, the quartz wackes underlying the Fat Boy package have broad sub-parallel beds with no internal sedimentary structures. Beds lacking lamination are formed either by very rapid deposition from suspension or by deposition from very highly concentrated sediment dispersions (Blatt et al, 1972). Therefore, alternating

strong internal deformation. These fragments are sub-rounded to rounded in shape and their sizes varies from 1.5 to 5.0 cm.

"B" Zone package

This package is exposed in trenches at the "B" Zone located roughly 600m south of the "A" Zone (Appendix IX). Like the Northern package the "B" Zone package was not studied in detail. However, the surface mapping indicates that the "B" Zone package is similar in composition to the Fat Boy package. The "B" Zone mineralization is located at the basal contact between the "B" Zone diamictite package and an underlying quartz wacke facies.

3.4 Carbonatization

Carbonatization is present, with varying intensities, in all sedimentary facies of the Last Hope Formation. In most units the alteration had partially replaced the matrix of the host unit (Fig. 3.20) and less frequently almost completely replaced the matrix of the host unit (Fig. 3.21). Figure 3.21, shows unaltered diamictite matrix filling a small fracture within the overlying carbonated quartz wacke. This feature can be compared to a clastic dyke, where an injection of water soaked matrix of diamicton took place into overlying semi-consolidated quartz wacke unit. The petrography of the filling material indicates a composition of fine quartz-sericitic matrix with small fragments of detrital quartz.

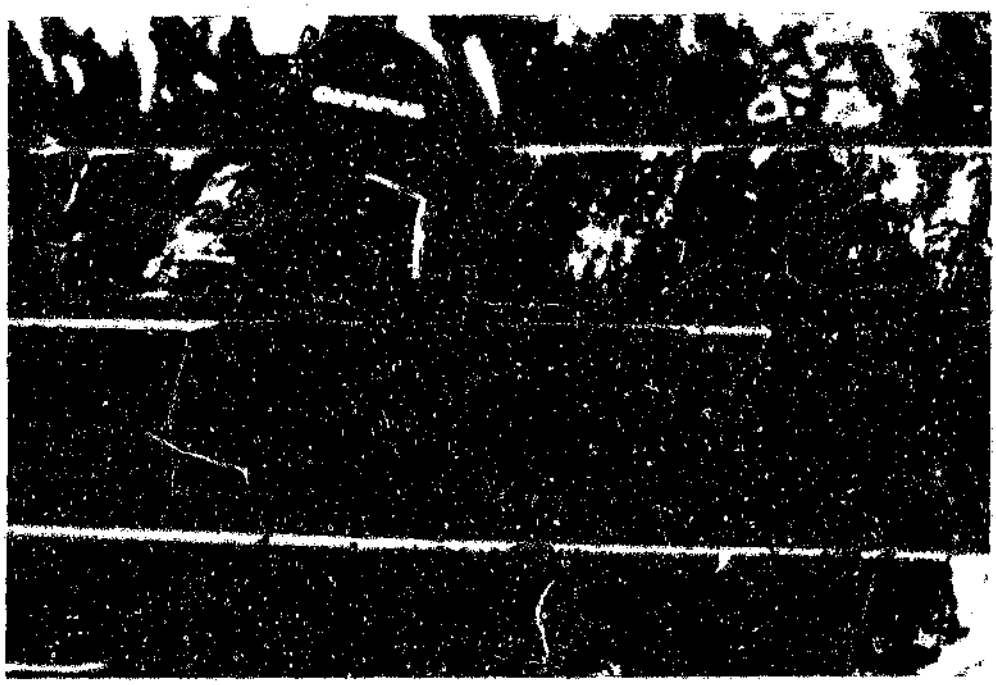


Figure 4.20: Quartz wacke's matrix partially replaced by carbonatization, SPD-066, 75m.



Figure 4.21: Carbonated quartz wacke (reddish-brown) overlying a thin diamictite layer. Unaltered diamictite's matrix filled a small fracture within the overlying carbonated quartz wacke. The younging direction is from the right to the left.

dark green material. In addition, minor amounts of aphanitic to finely grained fuchsitic and siliceous clasts, pale beige to greyish clasts with an intense quartz stockwork and dark-brownish intensively carbonated material have been observed. These latter three types suggest that the source rock was altered prior to it erosion and incorporation in the diamictite layers. The petrographic work carried out on volcanic clasts has identified an assemblage of quartz-sericite ± carbonate ± chloritoid. This assemblage shows strong similarity to the quartz-sericite schist assemblage of the upper Penhalonga Formation.

The chert and ironstone fragments are composed of aphanitic siliceous material. Within the clasts, laminations vary from well to poorly banded, and in some cases the laminae and bands are deformed, possibly by slumping. Few clasts are brecciated by later quartz stockwork. They are generally rounded to sub-rounded and occasionally sub-angular in shape. Their sizes vary from 1 cm to 20 cm in diameter.

The quartz vein clasts are generally white to light grey and aphanitic. They are usually rounded to sub-rounded with sizes varying from less than 1 cm to 5 cm in diameter.

The granitoid fragments are composed of coarse grained material averaging 25-30% quartz and 70-75% feldspar. No mafic material has been observed. All crystals are anhedral and show

Petrographic studies of the diamictites of the Fat Boy package, show that the matrix consists of fine to coarse quartz-sericite ± epidote ± carbonate material with varying amounts of angular fragments comprising polygranular aggregates of detrital quartz, and polygranular aggregates of quartz of a chemical sedimentary origin (chert and ironstone) (Fig. 3.19). The composition of the matrix is generally similar to that of the quartz wacke facies described above.

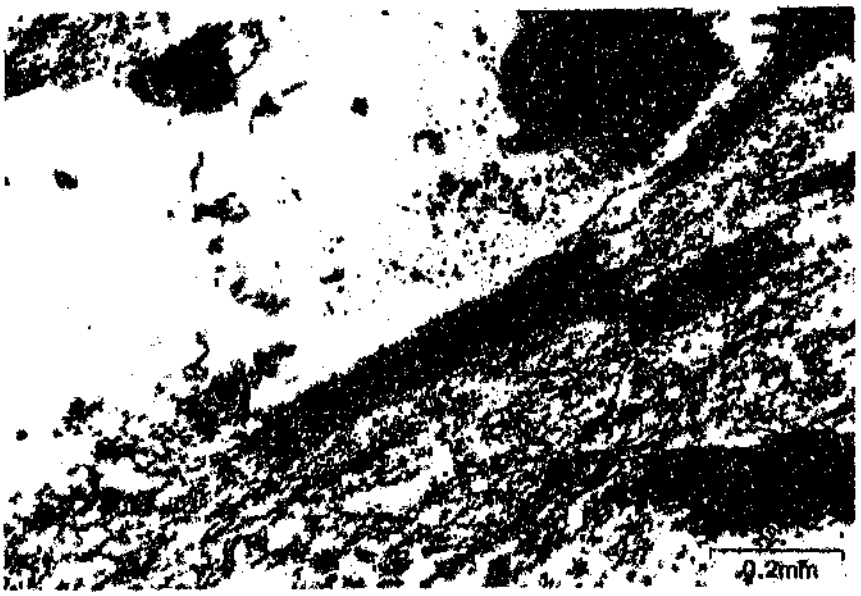


Figure 3.19: Carbonated quartz-sericite matrix of a diamictite layer supporting an angular composed quartz fragment, SD-111, 41m, 100 X, + nic.

Three types of volcanic fragments represent the bulk of the volcanic clasts. They are composed of aphanitic pale beige material, pale green slightly sericitic material, and unaltered

and angular blocks of quartz sericite material (similar to the "F" Zone's quartz-sericite rock). The size of fragments varies from 1cm to 15 cm. The size and concentration of fragments decreases from bottom to top (i.e upward fining). The blocky meta-tuff unit extends laterally for approximately 150 meters before pinching out (Fig. 3.11).

The pink diamictite is characterised by 80-90% angular quartz -sericite ± carbonate fragments (few fragments are up to 35 cm in diameter) and a lesser amount of rounded ironstone blocks in a sheared quartz-sericite ± carbonate matrix. Qua sericite ± carbonate fragments are interpreted to be of felsic volcanic origin. Despite the high proportion of clasts, the pink diamictite is matrix supported.

The overlying diamictite layers of the Fat Boy package expose a sequence of more than 200 meters thick in the eastern portion of the "A" Zone. However, the thickness decreases rapidly towards the west (Fig. 3.11). Detailed mapping indicated that the lateral extent of individual diamictite layers is limited. It is difficult to trace a specific layer for more than 150 meters, they pinch out rapidly or are abruptly terminated by other layers. West of the fault "F098", the surface expression of the Fat Boy package is limited to few thin sheared diamictite horizons interbedded with pebbly quartz wacke facies (Fig. 3.11). However, boreholes (SPD-083 and SID-098) drilled west of the fault F098, intersected a thick sequence of the package, which indicates that the main body of the package plunges to the west.

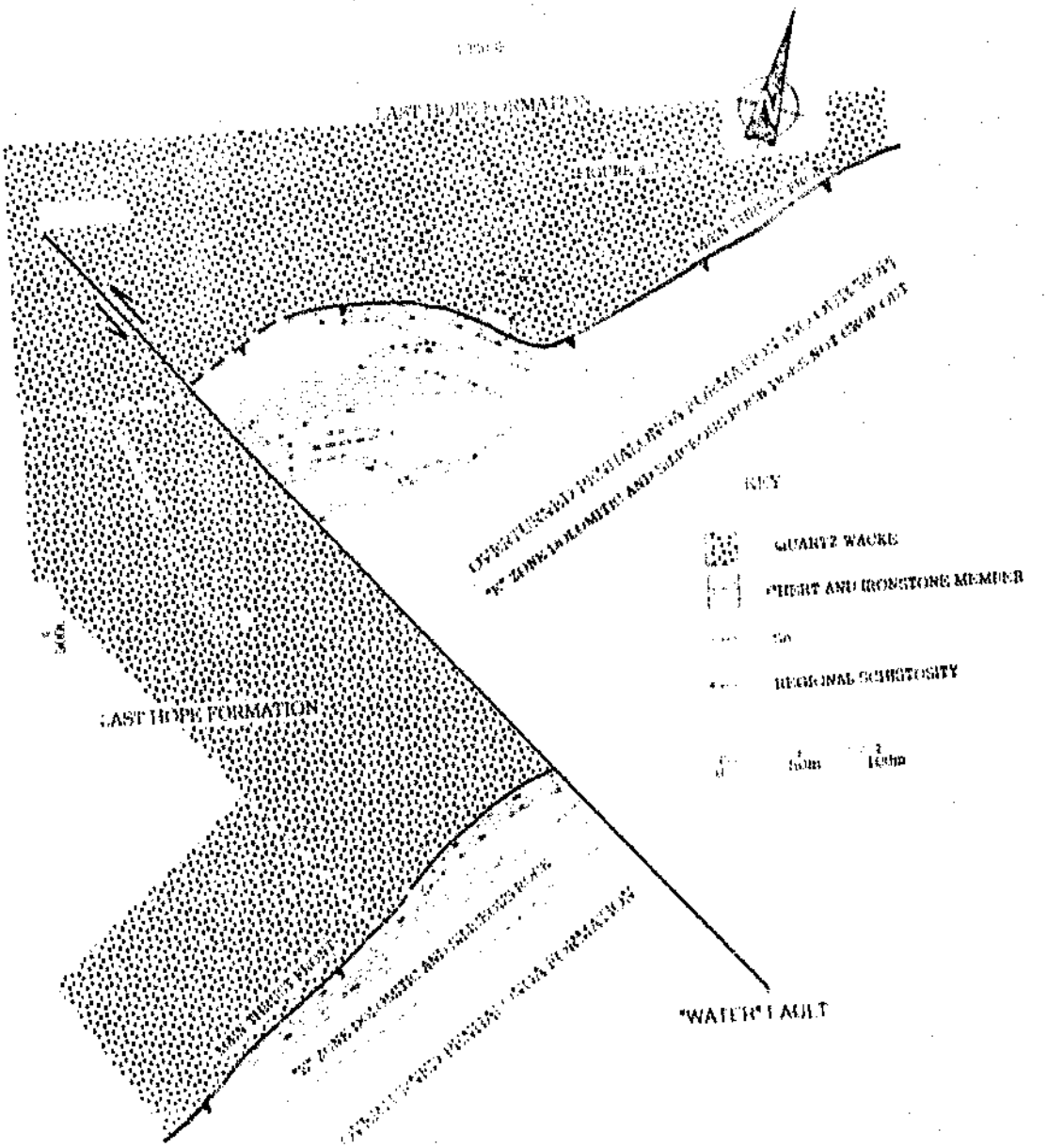


Figure 4.4: Chert and ironstone strata located southwest of the "WF" zone and stacked together to form foreland dipping duplex. The "Water" fault cross-cut and displaced the whole sequence.

below the Signal Hill ironstone.



Figure 4.3: Photo showing the contact between a chert stratum of the "B" Zone foreland dipping duplex structure and underlying quartz wackes. The contact dips at approximately 50° towards 190°.

It appears from the observations above that a major south dipping thrust fault brought the older overturned Penhalonga Formation to lie on the younger right way-up sequence of the upper Penhalonga and Last Hope Formations. The Main Thrust Front together with subsidiary thrust faults within the footwall, are responsible for the antiformal imbricate stack and foreland dipping duplex observed in chert and ironstone members of the right way-up upper Penhalonga Formation.

north of the contact between the overturned sequence and the right way-up succession.

B) chert and ironstone "blocks" of unit B show stacking of chert and ironstone strata in an antiformal imbricate stack (Fig. 4.1). The relative displacement of each individual stratum forming the imbricate stack, is about the same as the length of each individual chert and ironstone stratum.

C) southwest of the "B" Zone, several distinct chert and ironstone strata were stacked together to form a foreland dipping duplex (Fig. 4.4), the slip of individual stratum appears greater than the length of the strata. All of these strata dip moderately (30 to 50°) towards the south and southeast. The foreland dipping duplex sequence is cross-cut and displaced by the "Water" fault (Fig. 4.4). The northernmost members of the foreland dipping duplex, present unconformable contacts with underlying folded quartz wacke units (Fig. 4.3 and 4.4). Figure 4.3 present an almost perpendicular (90°) contact between the foreland dipping duplex (dipping at 50° towards 190°) and quartz wackes (dipping at 60° towards 270°). The contact is characterized by highly sheared and mylonitic material. The fault called Water Fault truncated and displaced the stack pile into its present position (Fig. 4.4). It is not clear whether these chert and ironstone strata were part of the Signal Hill ironstone or part of any other Penhalonga Formation's chert and ironstone formation located stratigraphically

4.3.2 Main thrust and associated "E" Zone

A structure, approximately 15 km long and forming a large-scale arc, separates the overturned Penhalonga sequence (South domain, Fig. 2.3) from both the right way-up members of the Penhalonga Formation (East domain, Fig. 2.3) and the Last Hope Formation (Figs. 1.2, 2.3 and Appendix VII). South of the "F" Zone, this structure separates the Penhalonga Formation overturned lithological units dipping at 30-45° towards 100-135°, from the upper Penhalonga Formation's right way-up chert, ironstone and volcanic units dipping at 50-60° towards 215° (Fig. 4.1). Further southwest along strike, this structure separates the overturned Penhalonga sequence from right way-up quartz wacke and diamictite facies of the Last Hope Formation, dipping 50-60° towards 140-160°. Although the contact between the overturned Penhalonga Formation and the right way-up formations crop out only in one location (Fig. 4.3), the structure is easily identified on aerial photographs and on the Landsat image. Figure 1.2 and Appendices VII to IX show the trace of this structure. Field evidence collected in the vicinity of the "F" Zone and the "E" Zone suggest that a major thrust, namely "Main Thrust Front", brought the older and overturned Penhalonga Formation over the younger right way-up sequence of upper Penhalonga and Last Hope Formations.

This field evidence is enumerated as follow:

A) as shown in Figure 4.1, the chert and ironstone "blocks" of unit A have been folded, faulted and abruptly terminate immediately

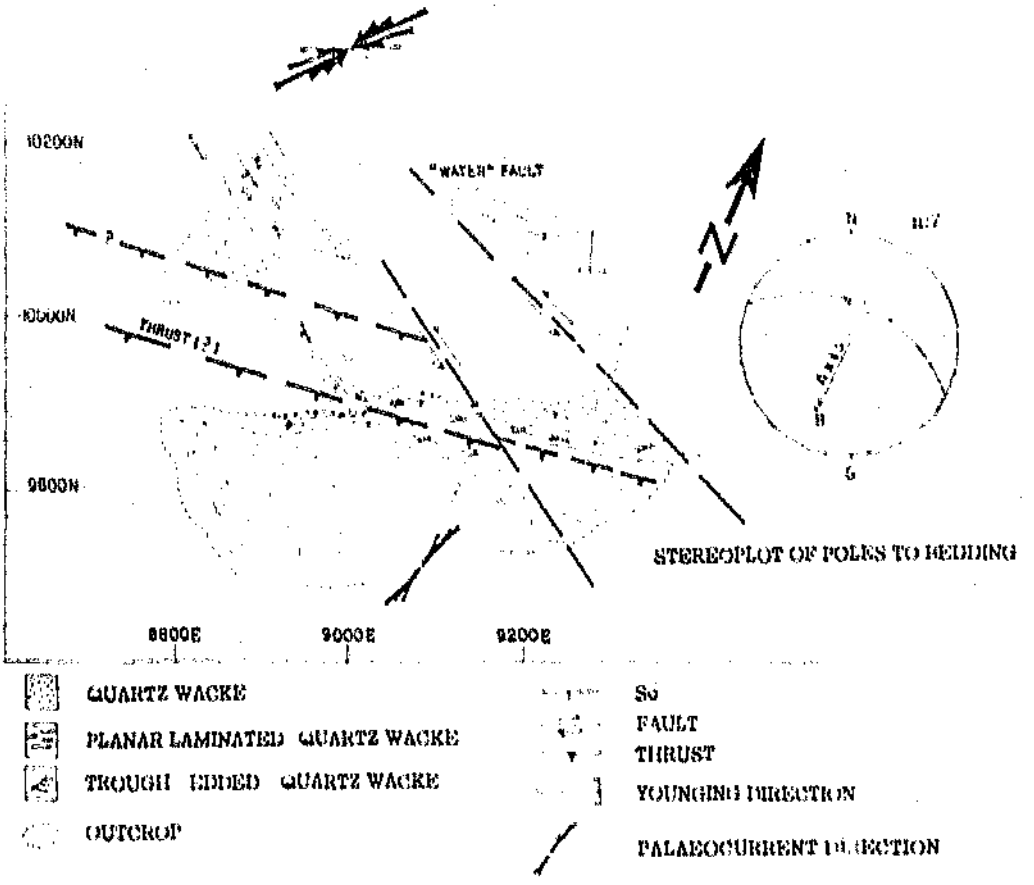


Figure 4.2: Detail of the antiform located approximately 1 Km west of the "A" Zone.

This antiform is interpreted to predate the regional schistosity (S2). This can be supported by the following: as indicated in section 4.4, the regional schistosity (S2) is generally a moderate to weak penetrative cleavage which developed mainly parallel to bedding. Over the "A" Zone the S2 is well developed and parallel to So, but over the antiform structure the S2 is absent. If the antiform structure post-date S2, a well developed S2 foliation folded together with the So should be seen.

the fold nose. Subsequently, the southern limb of the synform was faulted by F_5 and F_6 (Fig. 4.1). Thereafter, fault F_7 truncated the southern limb of the synform as well as faults F_5 and F_6. Figure 4.1, (detail 3) shows the faulted contact (F_7) between members A_1 and A_2. The presence of black gossan within members A_1 and A_2 indicates that A_2 is the extension of A_1 and therefore, implies a left lateral movement along fault F_7. The black gossan presents a short lateral extension, and is present in only three "blocks" of unit A chert and ironstone. The black gossan is therefore a useful marker to establish the sense of movement. Regardless of the S_0 orientation of units A and B chert and ironstone, the regional schistosity (S_2) is consistently dipping at 55-60° towards 290° and has not been affected by folding and faulting described above (Fig. 4.1, Appendix IX).

It is proposed that the chert and ironstone units in the vicinity of the "F" Zone were folded and subsequently faulted. These two deformation events predate the formation of the regional foliation (S_2).

An antiform has been outlined approximately 1 km west of the "A" Zone (Fig. 4.3). Only the southern limb of the antiform is out-cropping and has been affected by faults, as shown in Figure 4.2. The stereoplot of poles of lithological contacts between planar laminated quartz wackes and trough cross bedded quartz wackes (S_0) indicates a fold axis plunging at 35° towards 204° (Fig. 4.3). No fabric was generated by this early folding event.

was related to slumping of blocks of Penhalonga Formation in the Last Hope sediments at the edge of the basin. These apparent chaotic ironstone members belong to two distinct and laterally extensive chert and ironstone units, which form part of the Penhalonga Formation (Fig. 4.1, Appendix VIII). Geological mapping carried out northeast of the Signal Hill area shows two distinct, laterally extensive and sub-parallel chert and ironstone units within the Penhalonga Formation, namely Signal Hill chert and ironstone, and unit B chert and ironstone (Appendix VIII). Based on the interpretation of a Landsat image and aerial photographs, it is considered that the unit A "blocks" (Fig. 4.1) are an extension of the Signal Hill chert and ironstone formation, while unit B "blocks" (Fig. 4.1) are an extension of the unit B chert and ironstone formation (Appendix IX). However, as a result of approximately 400 meters of poorly outcropping area between the "F" Zone's chert and ironstone units (units A and B) and the two distinct chert and ironstone formations located north, no definite answer can be obtained regarding their relationship. The disposition of chert and ironstone "blocks" of units A and B in the vicinity of "F" Zone (Fig. 4.1), indicates that both units are folded, followed by faulting in unit A (F_1 to F_8 faults, Fig. 4.1) and imbrication in unit B (Fig. 4.1). The unit A fold is a close synform, the southern limb of the fold shows a right way-up sequence, with an inferred axial plane dipping approximately 50-60° towards 135°. This interpretation is based mainly on the overall disposition of these chert members. Collection of data suffered from lack of

4.3 Structure of the Signal Hill area

Interpretation of structural data collected from the Signal Hill area, and especially from the chert and ironstone units of the "F" Zone (Figs. 4.1, Appendix IX) outlined four distinct phases of deformation. The "F" Zone's chert and ironstone members, unit A, (Fig. 4.1) are extension of the Signal Hill's chert and ironstone members, which stratigraphically culminate the Penhalonga Formation and underlies the Last Hope Formation. Chert and ironstone members of unit B (Fig. 4 1) are located stratigraphically below the unit A. The unit B is the extension of the chert and ironstone unit located west of the Signal Hill's chert and ironstone (Appendix VIII). These members are useful stratigraphic markers which recorded deformation phases predating the development of the regional schistosity (Mason's S1, Table 4.1). Mapping in the vicinity of the "A" Zone, shows that the Au-As mineralization is located along faulted contacts between diamictite and quartz wacke facies, and has been deposited before the development of the regional schistosity.

4.3.1 D1 event

The apparent chaotic position of several chert and ironstone units in the vicinity of the "F" Zone (units A and B, Fig. 4.1), has not been satisfactorily interpreted by previous workers. Martin (1959), proposed that the chaotic position of these units

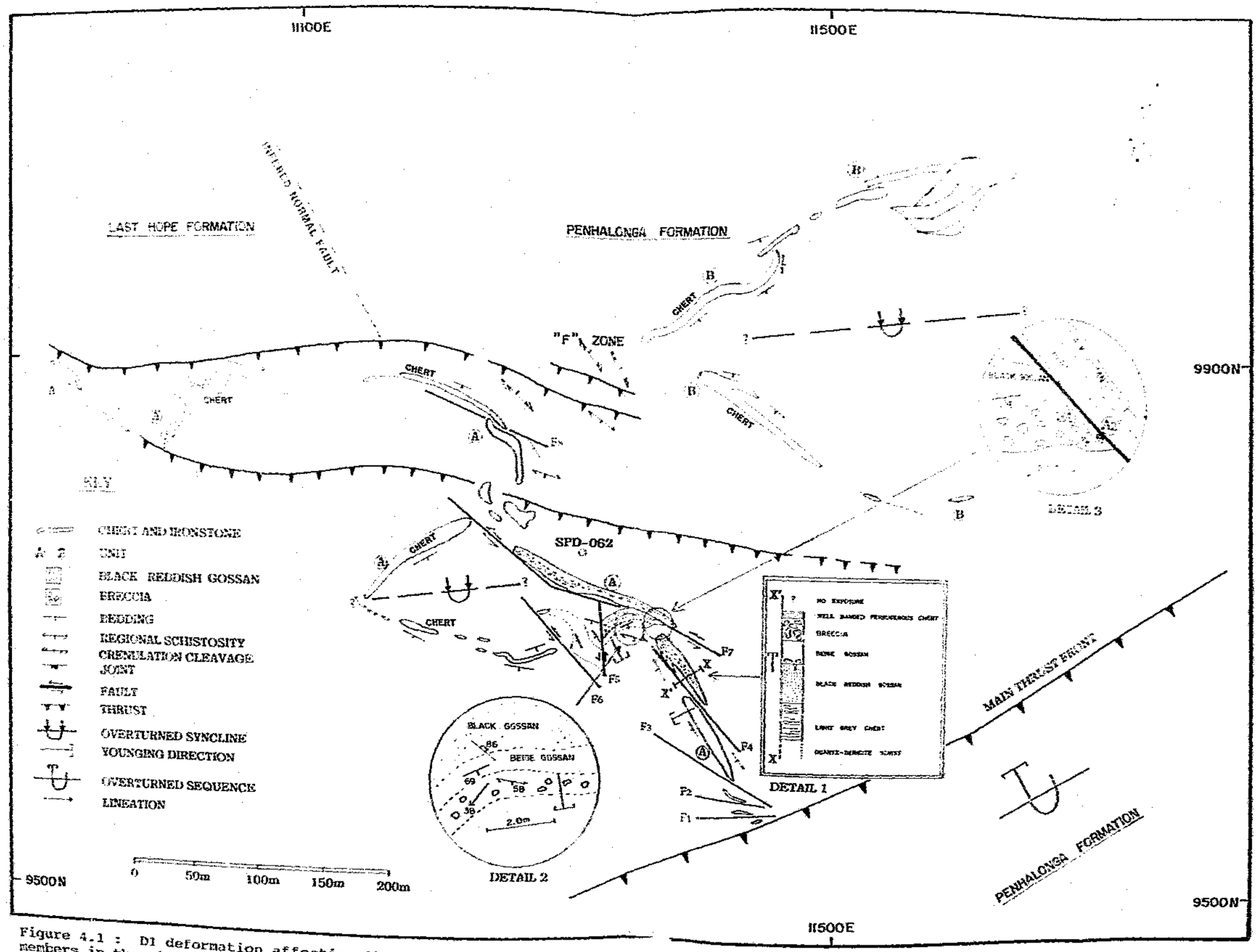


Figure 4.1 : D1 deformation affecting the chert and ironstone members in the vicinity of the "F" Zone mineralization.

localities. In most instances the schistosity (Mason's F1) has destroyed this cleavage. Both Mason's and Key's structural interpretations together with the present interpretation are summarized in Table 4.1.

Table 4.1: Tectonic events of the Tati schist belt after Mason (1970), Key (1976) and this study.

TECTONIC EVENTS AFFECTING THE TATI SCHIST BELT

MASON (1970)		KEY (1976)		THIS STUDY	
F5	SHEARING BROADLY PARALLEL TO S1 STRUCTURAL CONTROL FOR GOLD		OPEN WARPING AND SEVERAL AGES OF BRITTLE FRACTURING SET OF DEXTAL SHEARS WITH AURIFEROUS QUARTZ VEINS		
F4	CLEAVAGE DEFORMING F3			D3	CRENULATION CLEAVAGE
F3	REFOLDING F2 AND F1 WIDESPREAD CRENULATION CLEAVAGE	F4	LARGE MONOCLINES AND OPEN FOLDS CRENULATION CLEAVAGE		
F2	ISOCLINAL FOLDS NOT WIDELY OBSERVED	F3	ISOCLINAL FOLDS		CONJUGATED (?) FAULTS SYSTEM
F1	REGIONAL SCHISTOSITY FIRST RECOGNIZABLE PERIOD OF DEFORMATION	F2	REGIONAL SCHISTOSITY RARE MINOR FOLD	D2	REGIONAL SCHISTOSITY
				D1	THRUSTING AND MINOR FOLDS
					LARGE SCALE FOLDING
					DEPOSITION OF LAST BIFIF
		F1	SLATY CLEAVAGE NO F1 FOLD IDENTIFIED		EARLY DEFORMATION

north of the Tati schist belt (Tutume-Vukwe schist belts, Fig. 1.1) and were not seen in exposed outcrops within the Tati schist belt (Mason (1970), Litherland (1976) and Key (1976)). Neither Mason (1970), Litherland (1976) or Key (1976) described these folds in detail.

The third episode (F_3) is more widely developed. "It has refolded the earlier structures and is responsible for the widespread formation of one or more sets of crenulation cleavages. The crenulation cleavage, although locally intense, is essentially a non-penetrative structure dependent largely on the lithology of the host rock" (Mason 1970).

The fourth and fifth episodes recognized by Mason (1970) are of a more brittle type of deformation. The fourth episode involved the development of a later cleavage which locally deformed the crenulation cleavage (F_3). The final episode, believed to be closely associated with the fourth, includes faulting and shearing of both the schist belt rocks and the adjacent granitoids, with development of broad shearing parallel to schistosity, accompanied by quartz veins and mineralization. These structures trend between north and north-northeast. They are widespread throughout the schist belt and especially concentrated in the central-north sector and in the granodiorites to the north.

Key (1976) revised Mason's tectonic interpretation without introducing major changes to the sequence of events. He introduced an early phase of deformation, which predates Mason's F1. Key (1976) described it as a slaty cleavage observed in very few

4.2 Previous structural investigations

Mason (1970) recorded five deformational episodes in the Tati schist belt. The first episode (F1) involved the formation of the regional schistosity (Table 4.1). A mineral stretching lineation is frequently observed on schistosity surfaces. In the western sector of the schist belt, the lineation generally plunges towards the west-southwest, whereas further east it plunges to the south-west, south and southeast. Mason (1970) remarked, however, that the attitude of the lineation is usually constant in a given area. The schistosity and associated lineation are developed in all the formations of the schist belt. Mason (1970) considered that if the schistosity is regarded as an axial planar structure it must represent a period of folding earlier than any recognised folding in the schist belt. The apparent absence of early fold closures could be explained if the fold axes were more or less horizontal. Mason (1970), considered the regional schistosity to be a penetrative planar structure related to the first recognizable period of deformation. If the relationship of the stretch lineation, observed on the schistosity surfaces, with the lineations developed at the margins the granitoid plutons (New Zealand pluton, Fig. 2.7) is considered, the lineation probably represents a feature parallel to the direction of tectonic transport.

The second episode (F2) recognized by Mason (1970), involved the formation of isoclinal folds. These folds were identified

CHAPTER FIVE

MINERALIZATION

5.1 General Statement

This chapter discusses the nature and distribution of the Signal Hill mineralized zones, based on observations from surface mapping and from borehole core intersections.

These zones were briefly described by Von Spaeth (1970) and Molyneux (1971), and have been the subject of various internal reports from Seltrust Botswana and from Falconbridge (Byron (1983), Harwood (1986), Blaine (1986), Blaine et al (1990), Audet (1990)). Surface exposures of the known gold-arsenic-antimony mineralization are confined to four main zones, namely; "A" Zone, "B" Zone, "C" Zone and the "F" Zone. In addition a 1 km long arsenic-in-soil anomaly known as the "E" Zone has been identified. Only the "A", "B" and "F" Zones are considered to be potentially economically viable.

Extensive weathering has affected the country rock and oxidation of the mineralized zones occurs to 60 - 70 meters in depth.

The development of antithetic intrafolial shear and internal [illegible] in Unit and Ironstone members in vicinity of the "A" Zone, "B" Zone and "D" Zone, are synchronous to the thrusting event which brought the Superstition ophiolite sequence over both the right way up sequence of upper Intrusions and Lost Hope Formations. The Main Thrust Front and meridional thrust faults within the Lost Hope Formation were formed during this thrusting event. Intimately associated with the thrusting event was the injection of the "A" zone hydrothermal fluid into the hanging wall of the Main Thrust Front. Development of the regional schistosity [illegible] towards the end of the thrusting event.

Later tectonic events created normal and reverse fault systems, followed by the development of the crenulation cleavage.

Figure 4.14 summarizes these successive periods of deformation.

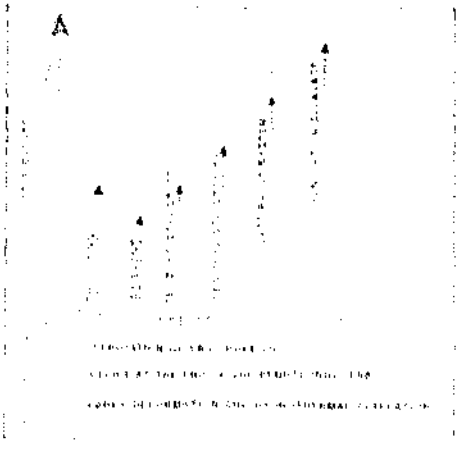


Figure 4.14: Summary of the deformation events in the Signal Hill area.

elements generated by such a conjugate system would be more or less parallel to the XoY plane of the strain ellipse. Figure 4.14 shows that XoY plane of the strain ellipse is parallel to the plane defined by σ1 and σ3, which corresponds to figure 4.11 should be a plane dipping at 30° towards 200°. No cleavage fabrics towards 200° has been observed within Grant Hill area.

The crenulation cleavage does not show any relation with the long axis of the strain ellipse and it is believed that the crenulation cleavage postdates the development of the late fault system.

It is interpreted that the development of the crenulation cleavage is related to a late tectonic event, which post-dated all earlier events, including the late fault event (F0B).

4.5 Discussion

The first stage of deformation is characterized by the development of folds and faults (D1 event), observed in the chert and limestone members which terminate the right way up Ordovician succession. These folds and faults produced no major movements to the development of the Main Thrust Front. According to Ramsay and Huber (1983), folds in the footwall of thrust faults can be developed by the formation of new thrust planes with ramp-flat geometry in the footwall, either by the forward propagation of the lower thrust plane at decollement layer, or by developing independent systems of thrust with ramp-flat geometry in strata beneath the thrust plane.

...deformation event that preceded the late ... event.

N



52° TOWARDS 045°

...e 4.12: Cyclowraphic trace shows the clockwise dipping at ... towards 045°.



Figure 4.13: Regional strain ellipse ... with a wrench/strike-slip fault system (Moxley ...).

If it is assumed that the normal fault and reverse fault systems are part of a conjugated system (section 4.4.1), then the

However, if these two fault systems are not part of a conjugate system, the reverse fault system represents a younger event than the normal fault system.

4.4.3 Crenulation cleavage

A non-penetrative crenulation cleavage, dipping at 30-40° to the northeast crenulates S0 and S1 and affects the entire Signal Hill sequence. This cleavage is particularly evident within the diamictite facies, where the crenulation cleavage is formed by the development of microfolds in the pre-existing schistosity (S2). Rock fragments of volcanic origin within diamictite facies, show strongly developed crenulation cleavage, while the surrounding matrix and limestone fragments show none or weakly developed crenulation cleavage. Quartz wacke facies show the development of the crenulation cleavage to varying degrees. The crenulation cleavage is fairly consistent throughout the Signal Hill area (Fig. 4.13). The stereoplot of poles to crenulation cleavage (Fig. 4.12) indicates an average dip of 52° towards 045°. Figure 4.8, shows that the crenulation cleavage post-dated the development of S0, the mineralization and the original schistosity. The crenulation cleavage was not affected by the drag fold created by the fault F098. Although the crenulation cleavage and the fault F098 have similar trends, the crenulation cleavage dips at shallower angles to the northeast than the normal faults.

Some could argue that the crenulation cleavage may be part of

dextral apparent sense of movement, varying from few centimeters to 2.5 kilometers. Neither quartz material or mylonitic material were observed within the fault's planes. It is difficult to establish, with the limited amount of data available, whether these reverse faults and normal faults, described above, are part of a conjugated fault system. If these two fault systems are part of a conjugated fault system, then the stereographic representation of these two fault systems, show that the axis of the maximum principal compressive stress (σ_1) plunges 20° towards 072°, the intermediate axis (σ_2) plunges 64° on 299° and the minimum principal compression stress (σ_3) plunges 20° towards 168° (Fig. 4.11).

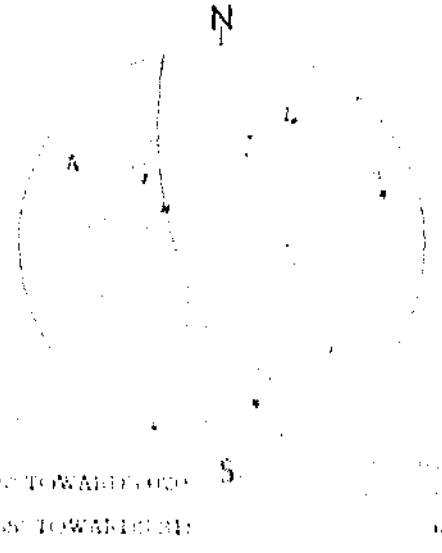


Figure 4.11: Stereoplot of the normal and reverse fault systems and the associated stress system. The axis of the maximum compressive stress (σ_1) plunges 20° towards 072°, the intermediate axis (σ_2) plunges 64° towards 299° and the minimum principal stress (σ_3) plunges 20° towards 168°

the movement along fault F098, affected S_0, the mineralization as well as the regional schistosity. Consequently this fault system is a younger event than the mineralization and the regional schistosity.



Figure 4.10: Exposure of the relationship between the reverse fault system and the normal fault system. The second system has been displaced by the reverse fault system, "A" Zone near 9900 E.

A series of reverse faults dipping 60° towards 305 to 315°, cross cuts the normal faults (Fig. 4.10). These faults show

frequently absent in any facies non oriented [illegible] to the schistosity. In the vicinity of the Signal Hill's "A" Zone, the schistosity dips at a shallower angle than the bedding (Fig. 4.8) and cross-cuts the folded and faulted chert and ironstone members south of the "F" Zone (D1 event, Fig. 4.1). In the "F" Zone area, the regional schistosity is well developed in felsic meta-tuff regardless their orientations (Figs. 2.6 and 4.1). There is a slight variation in the strike of the regional schistosity from the east ("F" Zone) to the west ("A" Zone), (Appendix IX).

4.4 Late structural events

4.4.1 Late faults

A series of normal faults dipping 85° towards 020° cuts the entire Signal Hill sequence (Figs. 3.11, 4.2, 4.7). These faults have a sinistral apparent lateral displacement ranging generally from 0.5 to 3 meters. However, several faults exhibit greater apparent displacements, up to 500 meters for the Water fault (Figs. 3.11 and 4.2), and approximately 35 meters for the fault F098 (Figs. 3.11 and 4.7).

Barren white quartz material is observed within several faults which crop out at the "A" Zone. When present the quartz vary from 1 mm to 2 cm in thickness, and is fairly consistent along the strike of the fault. Figure 4.7 shows that a drag fold due to

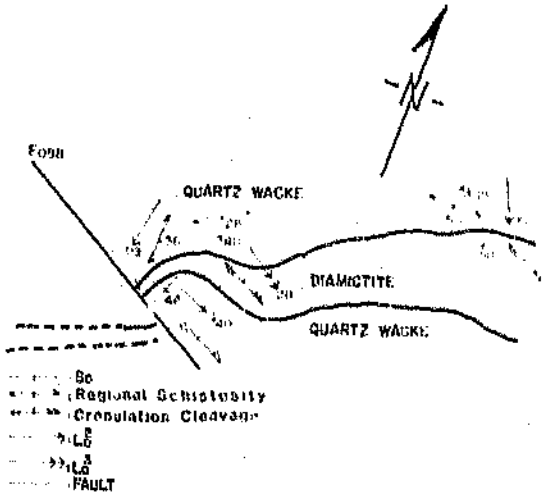


Figure 4.8: Figure showing structural relationship at the "A" Zone, between S0, S2, the normal fault F098 and the crenulation cleavage.

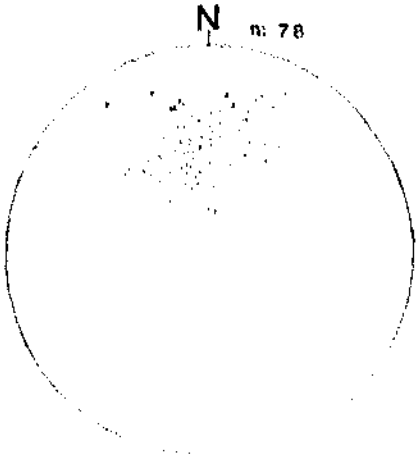


Figure 4.9: Stereoplot showing poles to S2 for "A" Zone and "F" Zone.



Figure 4.7: Fracture system filled with white quartz and affecting the whole "E" Zone host rock. These fractures dip at an average of 50° towards 015°.

4.3.3 D2 event

A generally moderate to poorly penetrative schistosity of regional extent, dips consistently at 30 to 40° to the south and affects the whole Signal Hill area. One of the characteristics of the regional schistosity, is that it is parallel to bedding planes and lithological boundaries (Mason, 1970). In the Signal Hill area, the regional schistosity is well developed within Last Hope's sedimentary rock which are subparallel to the schistosity. The regional schistosity is moderately to poorly developed or

The "E" Zone is located immediately south of the Main Thrust Front, and extends for several kilometers to the northeast and southwest of the Signal Hill block (Appendices VII and VIII). The "E" Zone is characterised by a highly dolomitic and siliceous rock. Erratically distributed within the "E" Zone dolomitic and siliceous rock, are several dragged and folded blocks of banded ironstone and what appear to be sheared felsic meta-volcanic "xenoliths". The surface area of these xenoliths varies from a few square meters to 400 square meters (Fig. 4.5).

A locally intense stockwork of kyanite, appears to have crystallized late within the dolomitic and siliceous host rock (Fig. 4.6). A series of late fractures, dipping at approximately 50° towards 015° can be locally observed cross-cutting the "E" Zone host rock (Fig. 4.7).

The "E" Zone pinches and swells along strike and can be locally absent, but it is invariably located south of the Main Thrust Front (Appendices VIII and IX). All folded and imbricated ironstone members described in section 4.2, are located either north or at the Main Thrust Front.

This implies that the "E" Zone structure could be intimately associated with the main thrusting event.

The xenoliths observed within the "E" Zone have been tectonically affected prior to their inclusion in the "E" Zone. Figure 4.5 indicates that these xenoliths have been dragged and folded by the "E" Zone structure, and thereafter affected by the development of the regional schistosity (S2) (see section 4.3.3).

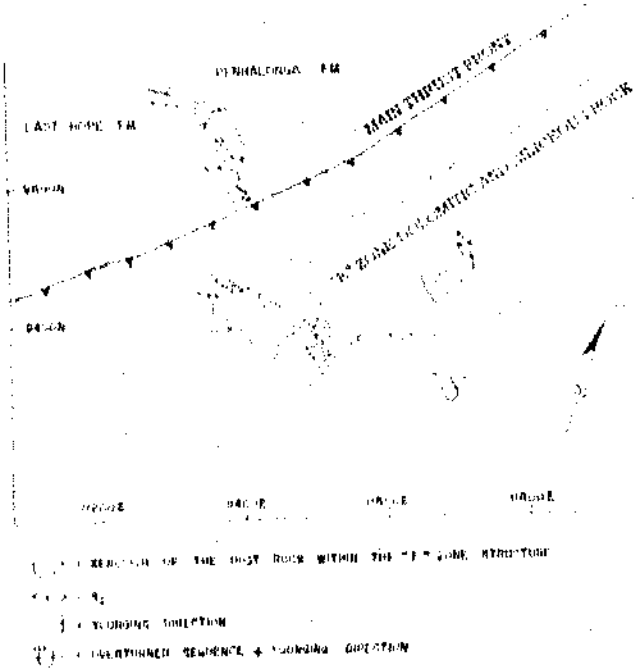


Figure 4.5 : Detail of the "E" Zone's geology, located south of the "F" Zone.



Figure 4.6: Breccia at Kyanite within the dolomitized and silicecous "E" Zone host rock.

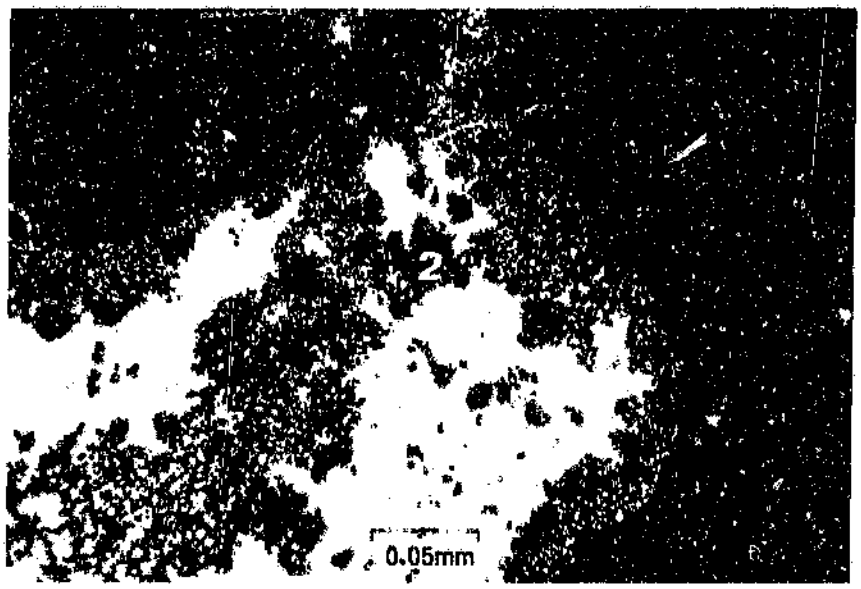


Figure 5.8: Stibnite (Sb) being replaced firstly by chalcostibite (1) and/or native antimony (1) and thereafter by metacinnabarite and/or tahlore (2), in a second generation gangue, SPD-083, 221m, (320 X, reflected light).

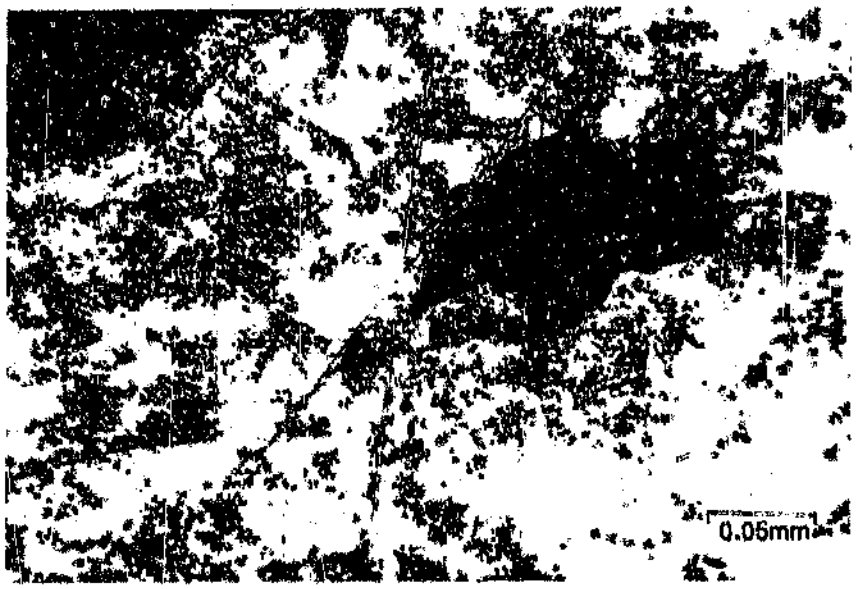


Figure 5.9: Stibnite (Sb) with inclusions of native antimony (1) and/or chalcostibnite (1) (high reflectance, white, top left) SPD-083, 220m, sample 10430 (320 X, reflected light).

Silver could perhaps be present as an alloy with the native gold and/or associated with the suspected tahlore phase.

5.3.1 Stibnite (Sb_2S_3)

The present study shows that the antimony mineralization occurs in two distinct phases:

A) an early phase, and
B) a remobilized phase

The early phase stibnite occurs as coarse, irregular shaped, hypidiomorphic granular aggregates. These are usually monomineralic but can have small inclusions of native antimony and/or chalcostibite. However, early stibnite is also observed in association with berthierite and sphalerite. It is not clear whether or not the monomineralic stibnite and the stibnite-berthierite-sphalerite association, represents two different phases. This early stibnite is replaced, firstly, by chalcostibite and/or native antimony and thereafter by a possible association of metacinnabarite and/or tahlore (see section 5.3.7) (Fig. 5.8). Figure 5.9, shows a concentration of mainly undeformed and unbrecciated stibnite with inclusions of native antimony and/or chalcostibite within a silicified and carbonated matrix (called the first gangue generation). This stibnite phase appears to have been well preserved within Footwall veins (Fig. 5.10). However, antimony mineralization observed in samples 1045 (Fig. 5.6), 1041 (Figs. 5.8, 5.11 and 5.12) and 1035 (Fig. 5.11) indicates intense

of approximately 150 meters. Unfortunately, no sulphide mineralization was intersected by drilling and, therefore, no fresh (unweathered) mineralized samples are available for this study.

Geological data collected from surface mapping, trenching and core boreholes, indicates that the gold mineralization seems to be shear-controlled, located within a sheared felsic lapilli meta-tuff unit as well as the underlying quartz-sericite schist unit (Fig. 5.7). These units are considered to be part of the upper Penhalonga Formation (Chapter 3). Gold mineralization is intimately associated with pervasive carbonatization and hematization and occasionally with ferruginous, antimony-bearing boudinaged veins. Although erratic high values of antimony, up to 2.0%, are associated with the ore zone, no visible antimony has been observed.

5.3 Mineralogy of the "A" Zone mineralization

A detailed study of the mineralogy has been carried out on over thirty polished sections (oxide and sulphide ore) from the "A" Zone. Identification of the ore minerals was carried out by means of reflected light microscopy. The principal ore minerals are: stibnite, berthierite, native antimony, chalcostibnite, chalcopyrite, sphalerite, pyrite, arsenopyrite and gold. The presence of metacinnabarite and/or tahlore (mercurian tetrahedrite) is suspected. Although low and erratic values of silver were detected in a few localities in the "A" Zone, no silver minerals were observed in this study.

Footwall veins).

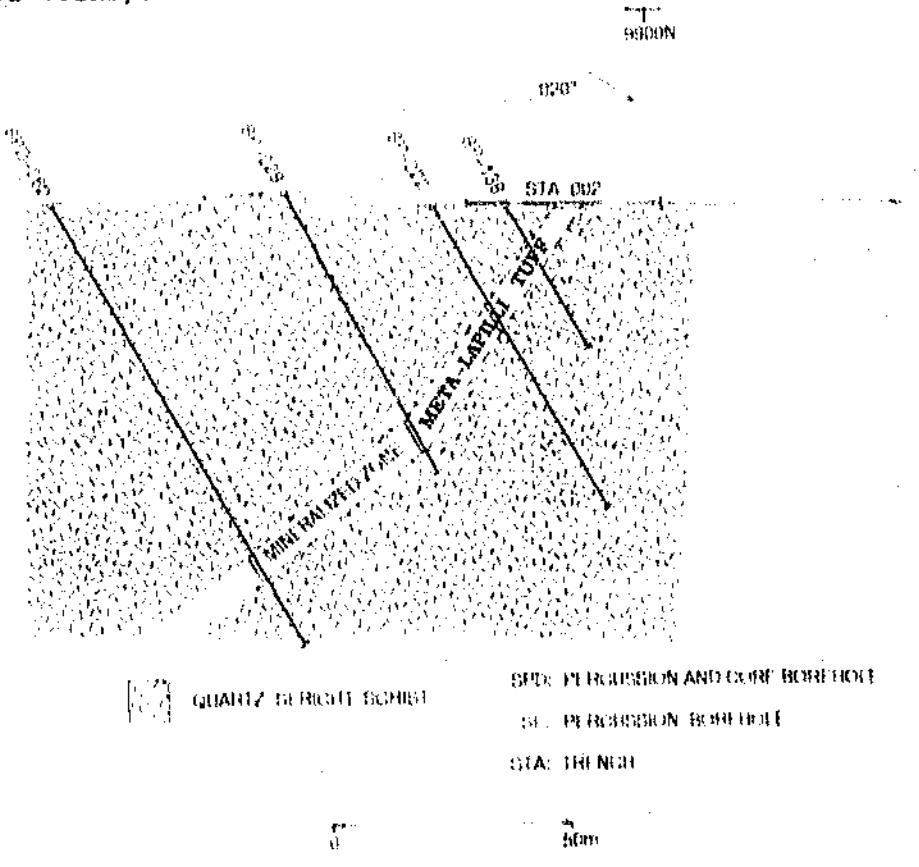


Figure 5.7: Cross section through the "F" Zone, the section is located along line 11285E (Appendix IX).

5.2.4 "F" Zone mineralization

The "F" Zone mineralization is located 400 meters east of the "A" Zone (Appendices VIII and IX). Numerous trenches, 45 percussion boreholes and 4 cored boreholes were drilled in the area and have indicated good potential for oxidized ore over a strike length

5.2.2 "B" Zone mineralization

The "B" zone mineralization is located approximately 500 meters south of the "A" Zone and has a 1.0 km strike length (Appendices VIII and IX). Along this strike, 40 trenches, 13 percussion boreholes and 2 cored boreholes have delineated a potentially economic ore body approximately 150 meters in strike length. It has some similar features to both the Footwall mineralization and the Contact mineralization of the "A" Zone. Once again, significant gold values on surface are associated with fine grained, white/yellow silicified and sericitic quartz wacke underlying a diamictite similar to that of the "A" Zone. Footwall veins contain massive stibnite in places.

5.2.3 "C" Zone mineralization

The "C" Zone mineralization is associated with deformed quartz veins within the highly sheared Northern diamictite package (Appendices VIII and IX). The surface strike extension is limited to less than 100 meters and only three shallow percussion boreholes were drilled into the zone. Therefore, no fresh (unweathered) mineralization has been studied and only little information about the mineralogy is presently available. Based on surface mapping, the gold mineralization is associated with a carbonated and slightly silicified host rock as well as deformed stibnite and stibiconite-bearing quartz veins (similar to the "A" Zone's



Figure 5.5: Detail of the contact between a Footwall vein and the sheared, silicified and mineralized quartz wacke host.

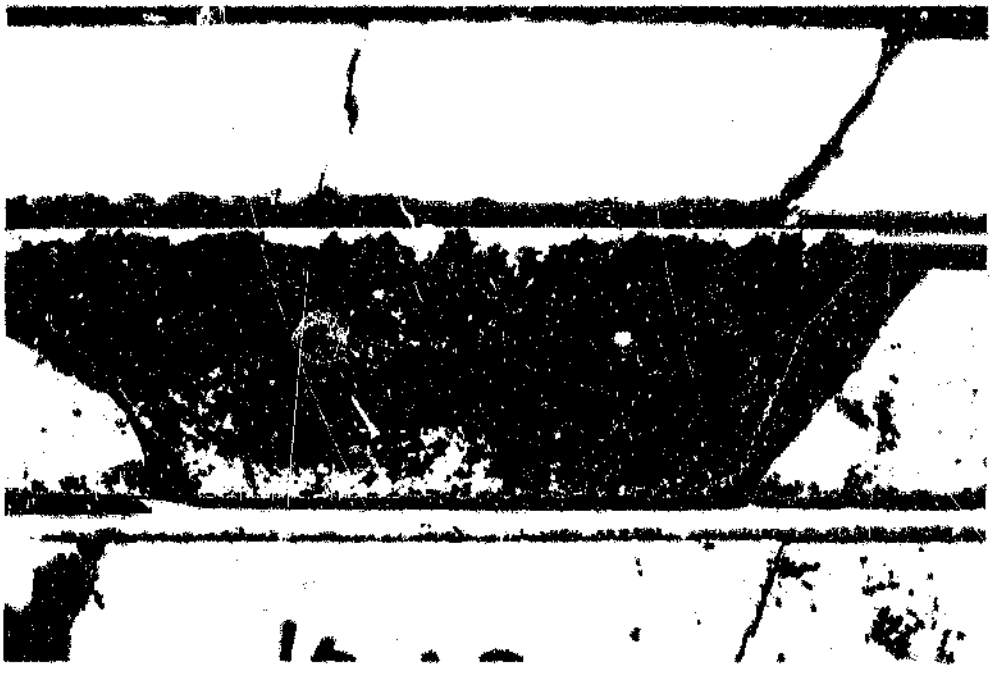


Figure 5.6: Silicified quartz wacke, tectonically brecciated and thereafter altered by the precipitation of pyrite and arsenopyrite by mineralizing fluids, Alberose, sample 10426.

while the core of the Footwall veins remain unaffected. This suggests that the Footwall veins predate the formation of the S_2 schistosity. Figure 5.5, shows a Footwall vein with massive and finely disseminated stibnite in sharp contact with the surrounding sheared, silicified and mineralized quartz wacke. Several fine fractures, mainly near the contact, but also throughout the Footwall vein, have been filled by pyrite and arsenopyrite which suggests two possible scenarios. Firstly, the Footwall vein preduces the pyrite and arsenopyrite mineralization, or the pyrite and arsenopyrite-rich mineralization predates the Footwall vein and has been remobilized and filled fractures and cleavages created during the development of the regional schistosity. However, Figure 5.6 shows that the silicified and slightly mineralized (stibiconite ($Sb_3O_6(OH)$) staining) quartz wacke was tectonically brecciated and thereafter replaced by pyrite and arsenopyrite-rich fluids. This observation indicates that the silicification and the antimony enrichment of the quartz wacke facies appeared earlier than the pyrite and arsenopyrite mineralization.

While there are some impressive gold values in lenses of Footwall mineralization, the distribution of gold is of an erratic nature. Surface mapping and drilling indicates that both zones of Footwall and Contact mineralization diverge westward and upward (Fig. 4.1). No trace of the Footwall mineralization has been found in the eastern portion of the "A" Zone.

typical quartz vein material, sometimes present, could have resulted from metamorphism and/or later quartz vein formation. These chert boudins and/or quartz veins called thereafter Footwall veins occur exclusively within the footwall quartz wacke assemblage. None of these Footwall veins have been observed within the Fat Boy package.

Footwall veins together with the quartz wacke assemblage dip towards the south at shallower angles than the contact between the Fat Boy package and the quartz wacke assemblage (Figs. 5.1 and 5.4)



Figure 5.4: Footwall vein plunging 15° towards the southeast, located near Ingolf and 3 Mile.

At surface, the contact between these Footwall veins and the quartz wacke host rock show that the quartz wacke as well as the margins of the Footwall veins are affected by the S2 schistosity,

"A" Zone, at its western extremity (Fig. 5.3). The mineralization is hosted within lenses of sheared, silicified and sericitized rocks, associated with boudinaged "chert" and/or quartz veins within the silicified footwall assemblage of the quartz wacke (Fig. 5.1). These chert boudins and/or quartz veins are the main host to the antimony mineralization and were exploited at surface by previous prospectors. Individual lenses of Footwall ore were mined for antimony in the late 1940's (the deposit was known as the "Last Hope" antimony deposit)

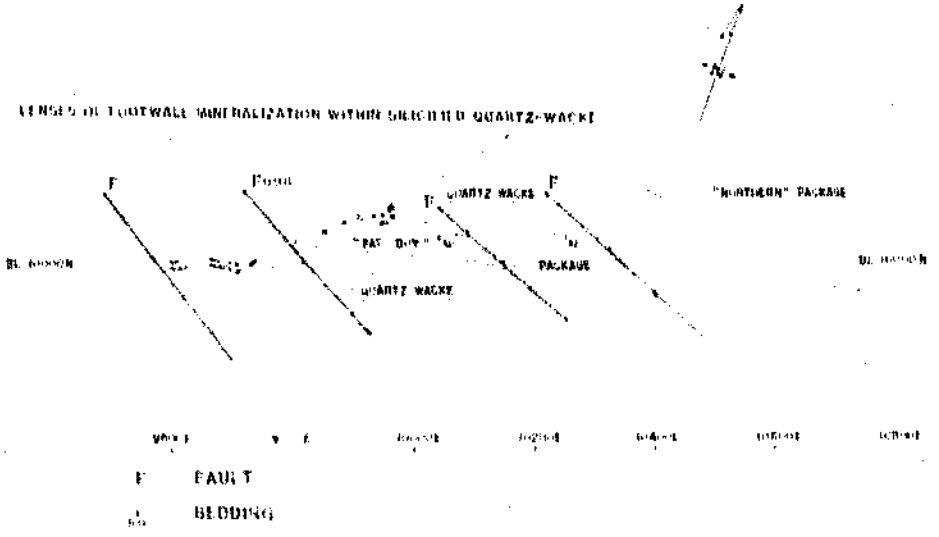


Figure 5.1 : Lenses of Footwall mineralization within the silicified quartz wacke facies, located in the western end of the "A" Zone.

Byron (1983) described this material as "chert" as it has a fine-grained, slightly sugary texture and it was felt that the more

strike and down dip, gold is not distributed uniformly within the ore body.

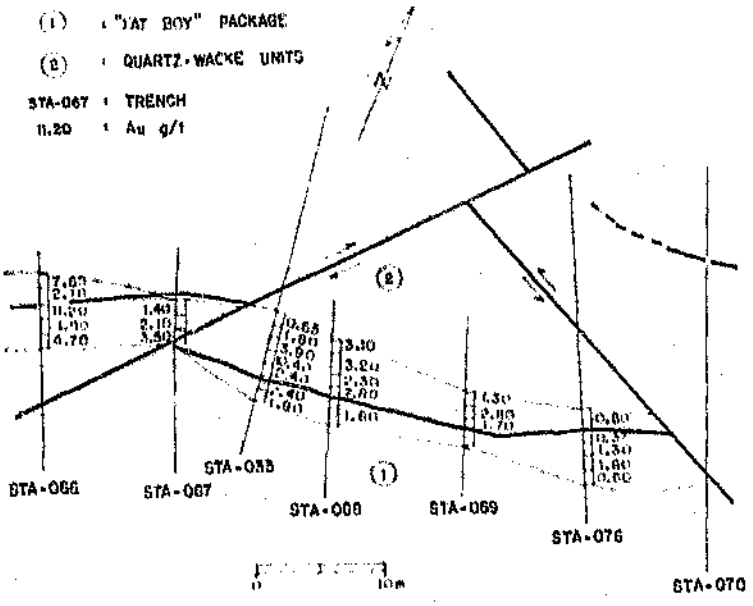


Figure 5.2: Distribution of gold within the "A" Zone ore body. The ore body is defined by a cut-off grade of 0.5 Au g/t.

From one trench to the other (10 meters apart) gold is located within the diamictite layers and/or within the silicified quartz wackes. Figure 5.2, shows that in trench STA-076, the ore is located mainly within the bottom member of the Fat Boy package, while in trench STA-069, most of the ore is located within the quartz wacke. In trench STA-067, the ore is exclusively within the Fat Boy package, while in trench STA-066 gold is evenly distributed between both units.

Footwall Mineralization

The Footwall mineralisation is present in the footwall of the

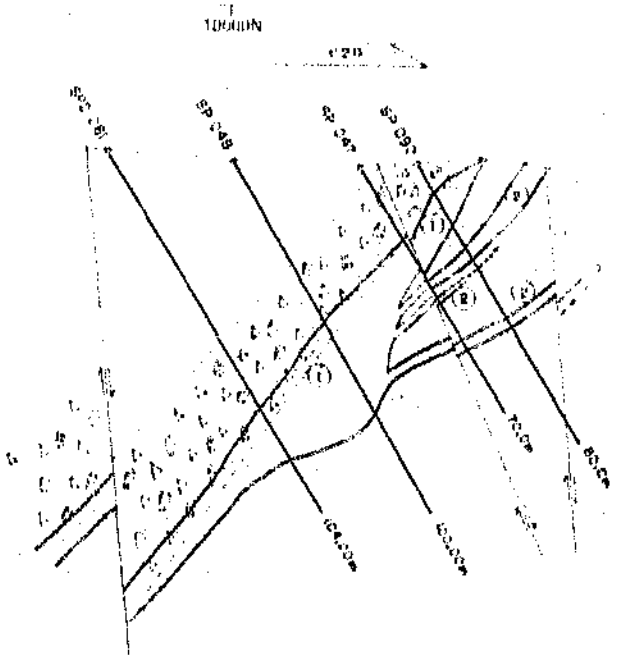


Figure 5.1 : Cross-section showing both the Contact mineralization and the Footwall mineralization, along the line 9875 E ("A" Zone grid).

The bottom portion of the Fat Boy package (Fig. 5.1) shows diamictite layers which are sheared, weakly silicified and show a weak limonite staining. Westward and along the "A" Zone strike, underlying quartz wackes show increases in silicification. While in the eastern part of the "A" Zone, the carbonatization is very intense in both hosts and decreases slightly towards the west.

The economic ore body of the "A" Zone mineralization is defined by a series of intersections, from boreholes and trenches, of a minimum width of 1 meter grading 0.5 g/t Au and above. Along

5.2 Mineralization types and distribution

5.2.1 "A" Zone mineralization

The surface mineralization of the "A" Zone has a strike length of more than 1.5 km. One hundred and fifty trenches, 88 percussion boreholes and 29 cored boreholes have delineated potentially economic ore over 1.1 km. The termination at depth of the sulphide phase of the "A" Zone mineralization is not known with the deepest drill intersection at 250m vertical depth. Two zones of Au-Ag-Sb mineralization have been identified, namely

A)- Contact mineralization, and
B)- Footwall mineralization

The cross-section presented in Figure 5.1, shows the occurrence of both zones of Au-Ag-Sb mineralization and their relationship to one another.

Contact mineralization

The zone of contact mineralization dips at 45-50° towards the south and occurs both in the basal portion of the Fat Boy package and in the upper portion of the underlying quartz wacke facies (Fig. 5.1). The zone of mineralization is usually three to four meters thick, but may range from less than one meter up to about fourteen meters. The mineralized zone shows varying degrees of hydrothermal alteration, mainly silicification and carbonatization.

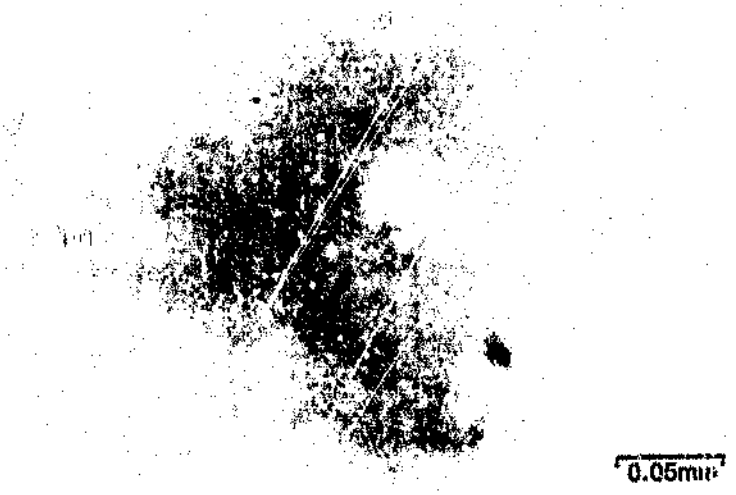


Figure 5.21: Native gold occurring with the second quartz generation, sphalerite, galena, 1200 X, reflective light).



Figure 5.22: Native gold occurring with the second quartz generation, high reflectivity, top left, chromite, 1200 X, reflective light).

5.3.9 Pyrrhotite ($Fe_{1-x}S$)

Pyrrhotite was observed in only one sample, where it occurs as an anhedral phase in close relationship with arsenopyrite.

5.3.10 Pyrite (FeS_2)

Minor xenomorphic to hypidiomorphic pyrite with multiple inclusions of gangue material is found in close association with the arsenopyrite (Figs. 5.16 and 5.20). Late pyrite also fills open fractures and cleavage planes related to late deformation of the country rock and the ore zone.

5.3.11 Gold (Au)

Native gold was found exclusively as very fine, free grains within the second gangue generation (Figs. 5.21 and 5.22). The gold mineralization is associated with the second pulse of hydrothermal fluids which also resulted in the precipitation of the arsenopyrite and pyrite (see section 5.3.12).

5.3.12 Gangue minerals

Gangue minerals are predominantly quartz, carbonate and to a lesser amount sericite and chlorite. Quartz is by far the most common constituent, whereas the carbonate content can be highly

this alteration phase represent meteriumbarite or Fahlore.

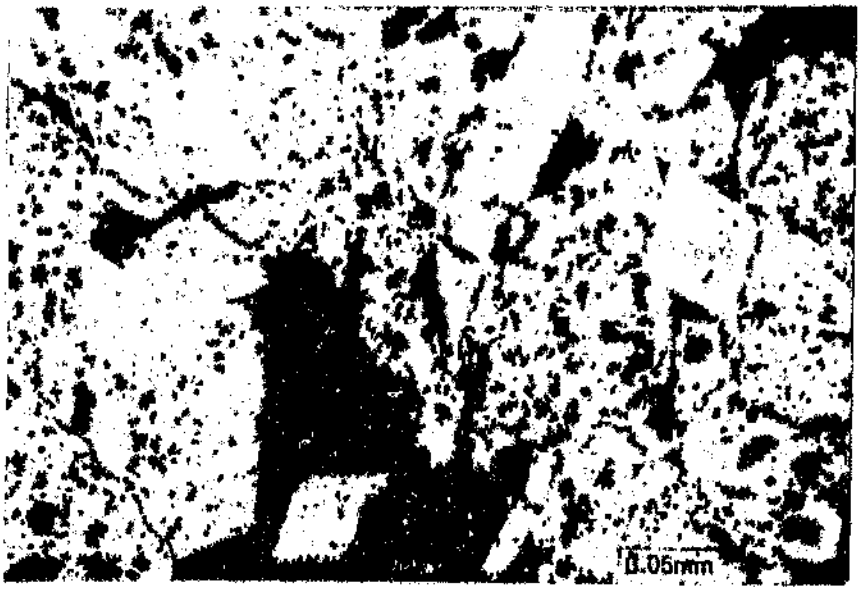


Figure 5.20: Assemblage of euhedral arsenopyrite (Apy) and porous xenomorphic pyrite (Py). Both phases are related to the second hydrothermal event, SD-003, 55m, (330 X, reflected light).

5.3.8 Arsenopyrite (FeAsS)

Arsenopyrite is by far the most abundant sulphide mineral observed. It is present as fine to coarse idiomorphic to hypidiomorphic crystals with inclusions of gangue minerals. Arsenopyrite is frequently associated with pyrite. Arsenopyrite is exclusively associated with the second generation of gangue (see section 5.3.1?) (Plate 5.11, 5.16 and 5.20).

stibnite and berthierite, have been replaced first by chalcostibite and/or native antimony and chalcopyrite. A dark greyish mineral phase, which is weakly anisotropic, replaces the early antimony ore as well as the chalcostibite and native antimony. It is suspected that metacinnabarite and/or [illegible] (Fig. 5.8) could represent this mineral phase. Unfortunately, microscopic identification of these phases remains uncertain. A Cambridge microscan 5 (1972) electron microprobe (detection limit of 0.05 wt % Hg) was used in order to detect any Hg content within this alteration phase. Twelve points were analyzed within the unaltered stibnite core, the stibnite rim close to the alteration phase and within the alteration phase.

Table 5.1: Mercury (Hg) content in stibnite core, stibnite rim and within the alteration phase.

Point	Wt. % Hg	Description
1	0.11	Alteration phase
2	0.10	Alteration phase
3	0.15	Alteration phase
4	0.11	Alteration phase
5	0.08	Alteration phase
6	<0.04	Stibnite rim
7	<0.03	Stibnite rim
8	<0.03	Stibnite rim
9	0.04	Stibnite rim
10	<0.03	Stibnite core
11	<0.03	Stibnite core
12	0.03	Stibnite core

The results presented in Table 5.1, indicate that the alteration phase is enriched in Hg (0.08 - 0.15 wt %, avg. 0.11 wt %) while within the stibnite core and rim the Hg content is below the limit detection. Unfortunately no final conclusion can be drawn whether

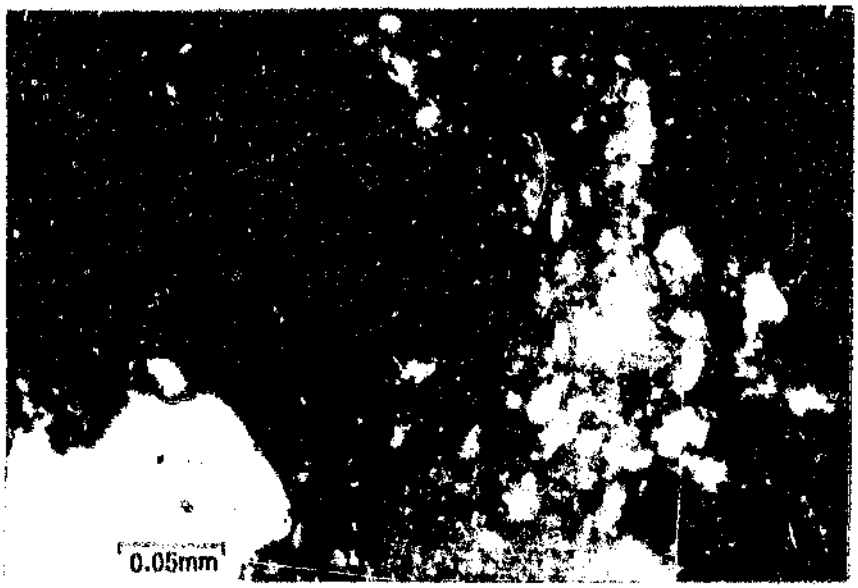


Figure 5.19: Brecciated early sphalerite in a quartz-carbonate, first generation gangue material, thereafter affected by a later tectonic event and the associated second gangue generation and the growth of arsenopyrite, 30-003, 56m (320 X, reflected light)

5.3.6 Sphalerite (ZnS)

Sphalerite is found in close association with stibnite, berthierite and chalcopyrite but can also occur independently within the first gangue generation. Sphalerite is usually irregularly shaped and is commonly intensely brecciated by a later tectonic event and the associated second pulse of gangue material (Figs. 5.11, 5.12, 5.17, 5.18 and 5.19).

5.3.7 Meteorimaboarite (HgS) and/or Famlorce (Cu$_2$ (As,Sb,Hg) S$_3$)

The mineralogical study does that the antimony minerals,

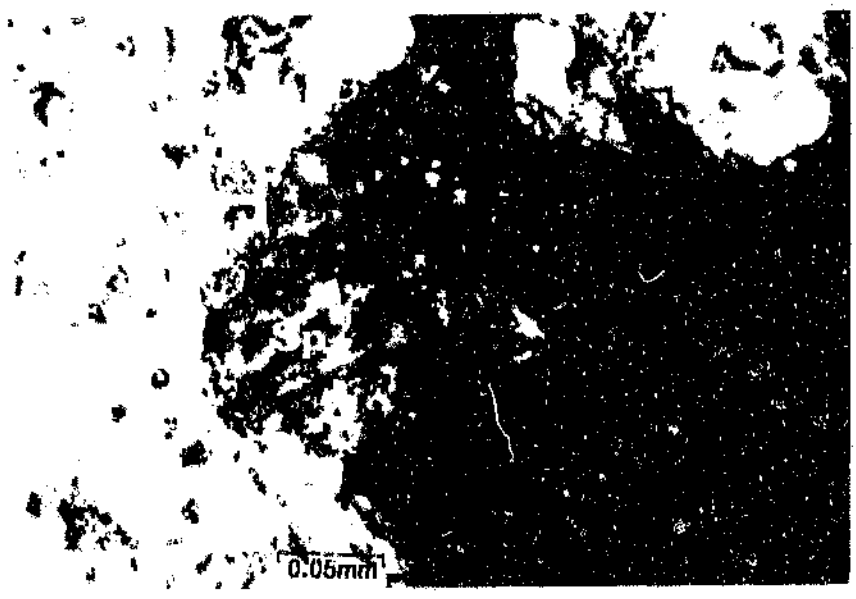


Figure 5.17: Brecciated early sphalerite (Sp) cut off by a late pyrite crystal (Py). Assemblage occurs within the second gangue generation, SD-107, 126m, (330 X, reflected light).



Figure 5.18: Early sphalerite (Sp) brecciated by a later tectonic event and associated second gangue generation, within gangue associated to the third hydrothermal event, SPD-067, 85m, (330 X, reflected light).

5.3.3 Berthierite ($FeSb_2S_4$)

Berthierite is present as anhedral crystals in close association with stibnite (Figs. 5.12 and 5.16). It is not clear if the relationship is one of a replacement or of a mutual intergrowth. However, replacement to varying degrees of berthierite by chalcostibite and/or native antimony is common.

5.3.4 Chalcostibite ($CuSbS_2$)

Chalcostibite is found as the first phase of replacement of stibnite and berthierite. It is exclusively anhedral, and generally does not exceed 3 μ in diameter. Due to the close optical characteristics of the chalcostibnite with native antimony, these two phases can easily be confused (Figs. 5.8, 5.9 and 5.12).

5.3.5 Chalcopyrite ($CuFeS_2$)

Chalcopyrite has been found in trace amounts, in association with stibnite and occasionally with sphalerite. It is present as very fine, irregular shaped crystals in, and adjacent to, stibnite and sphalerite (Fig 5.12).

event (Figs. 5.11, 5.14, 5.15).

5.3.2 Native Antimony (Sb)

Minute flakes of native antimony are associated with the monomineralic stibnite and the stibnite-berthierite intergrowths. They are present as anhedral inclusions more often within stibnite than within berthierite. However, due to the small size of these inclusions (3 to 5 μ) and the similarities in optical characteristics to chalcostibite, these two phases can be easily confused (Figs. 5.8, 5.9 and 5.12).



Figure 5.16: Early stibnite (Sb) and berthierite (Be) partially replaced by chalcostibnite and/or native antimony and the growth of late pyrite (Py) and arsenopyrite (Apy), SD-003, 55m, (320 X, reflected light).

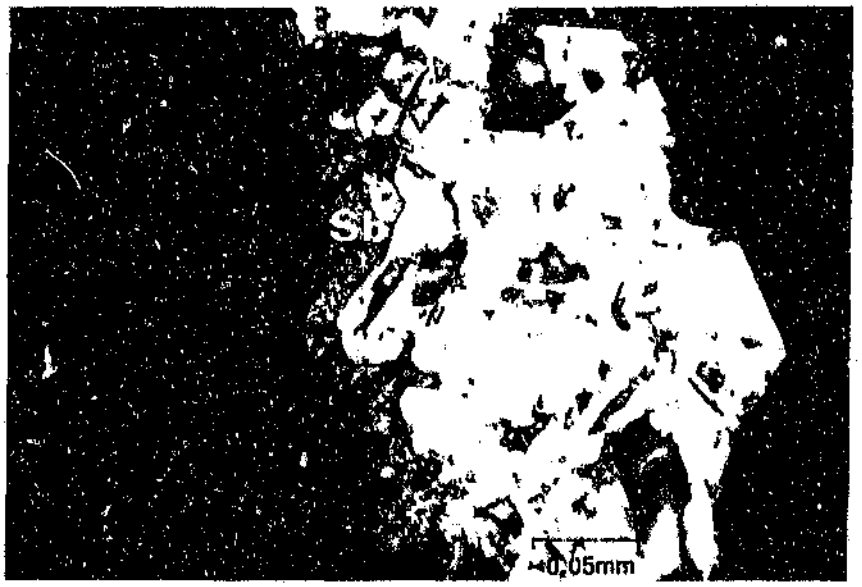


Figure 5.15: Stringer of remobilized stibnite located adjacent to a pyrite crystal, SPD-083, 221m, (320X, reflected light).

brecciation and remobilisation by a later tectonic event. The pyrite and arsenopyrite crystals appear to be precipitated from a hydrothermal fluid related to this later tectonic event. Figure 5.6 suggests that the antimony mineralization is related to the early pervasive silicification and carbonatization of the quartz wacke host rock, rather than to the late pyrite and arsenopyrite bearing hydrothermal event.

The early stibnite has been reconstituted due to increases in pressure and temperature conditions generated by a later tectonic event, and has filled fine fractures within the gangue material. These fractures were probably generated during this later tectonic

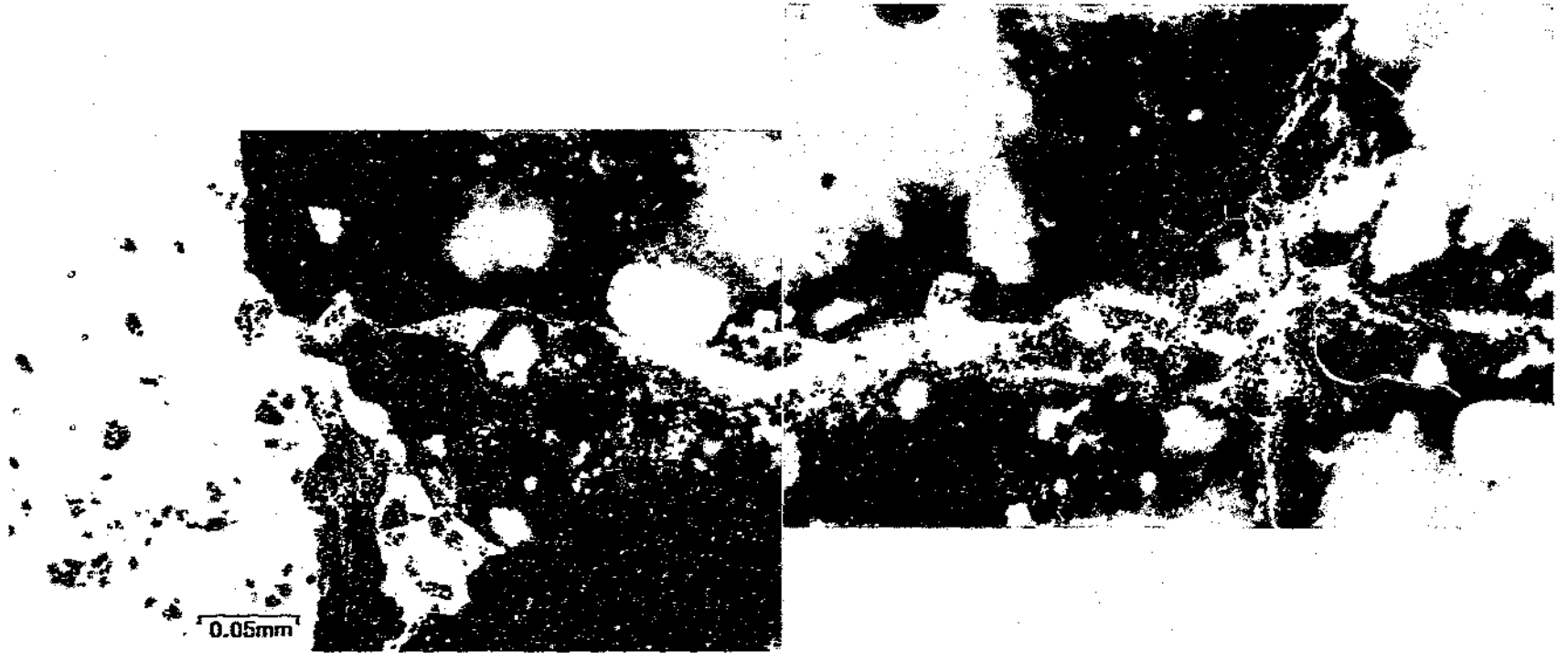


Figure 5.14: Pemchillination of early stibnite (Sb) into stibnite veinlets, SD-100, 221m, (320 X, reflected light).



Figure 5.12: Stibnite (Sb) and berthierite (Be) (replaced by chalcostibite and/or native antimony) in close relationship with sphalerite (Sp) and chalcopyrite (Cc), SPD-083, 255m, (320 X, reflected light).

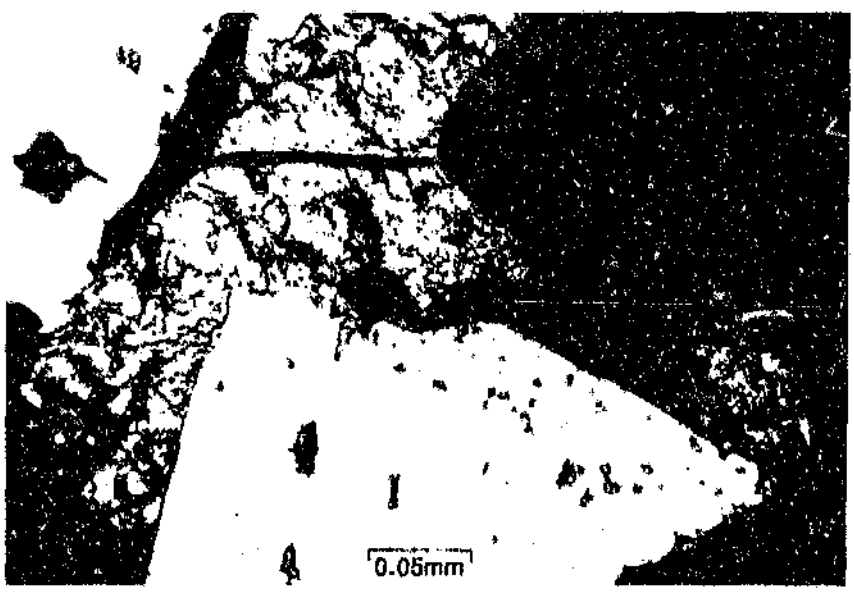


Figure 5.13: Stibnite (Sb) affected by a later tectonic event (fractures infill by the second generation of gangue material) and the growth of late euhedral arsenopyrite (Apy), SD-003, 221m, (320 X, reflected light).

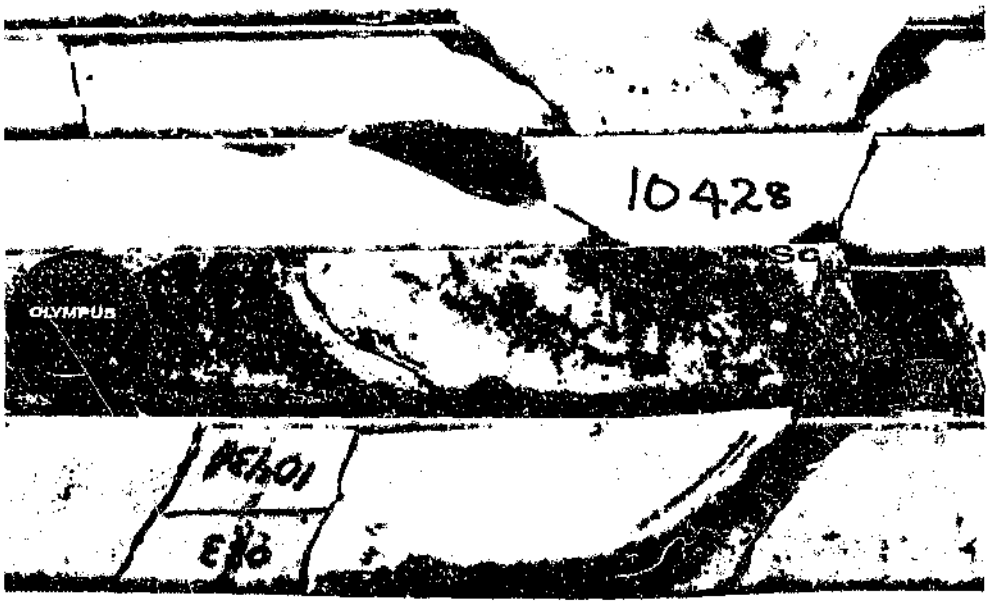


Figure 5.10: Footwall vein with massive and disseminated stibnite partially replaced by stibiconite (Sc). The photo shows a sharp contact between this footwall vein and the surrounding pyrite and the arsenopyrite mineralized zone. Several fine fractures through the footwall vein has been filled by pyrite and arsenopyrite, SPD-083, sample 10428.

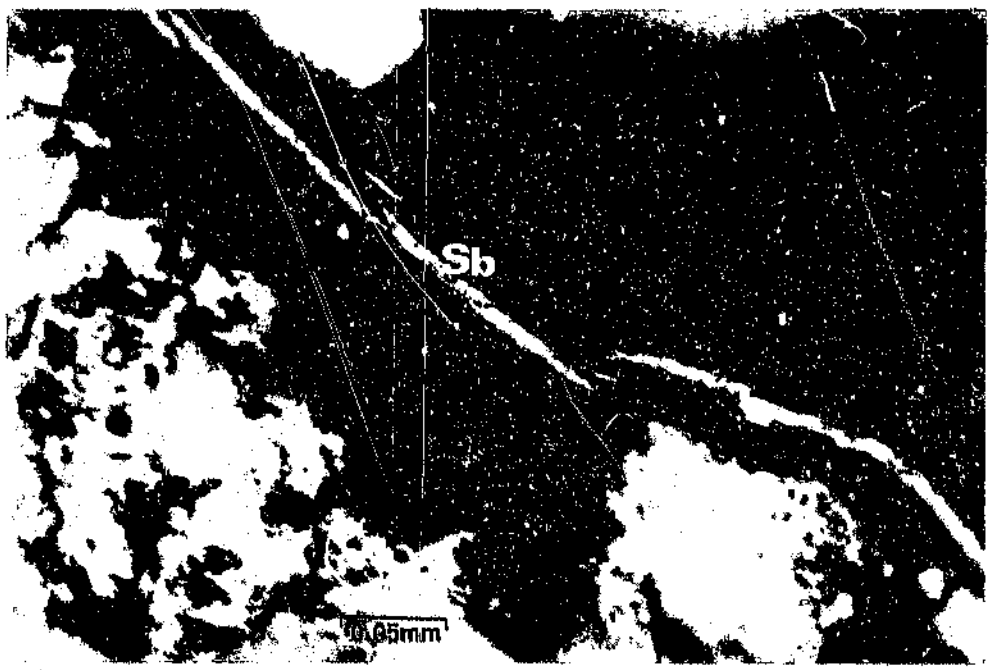


Figure 5.11: Remobilized stibnite as fine stringers in fractures created by a later tectonic event. Sphalerite (Sp) occurs at the bottom left. SPD-083, 221m, (430 X, reflected light).

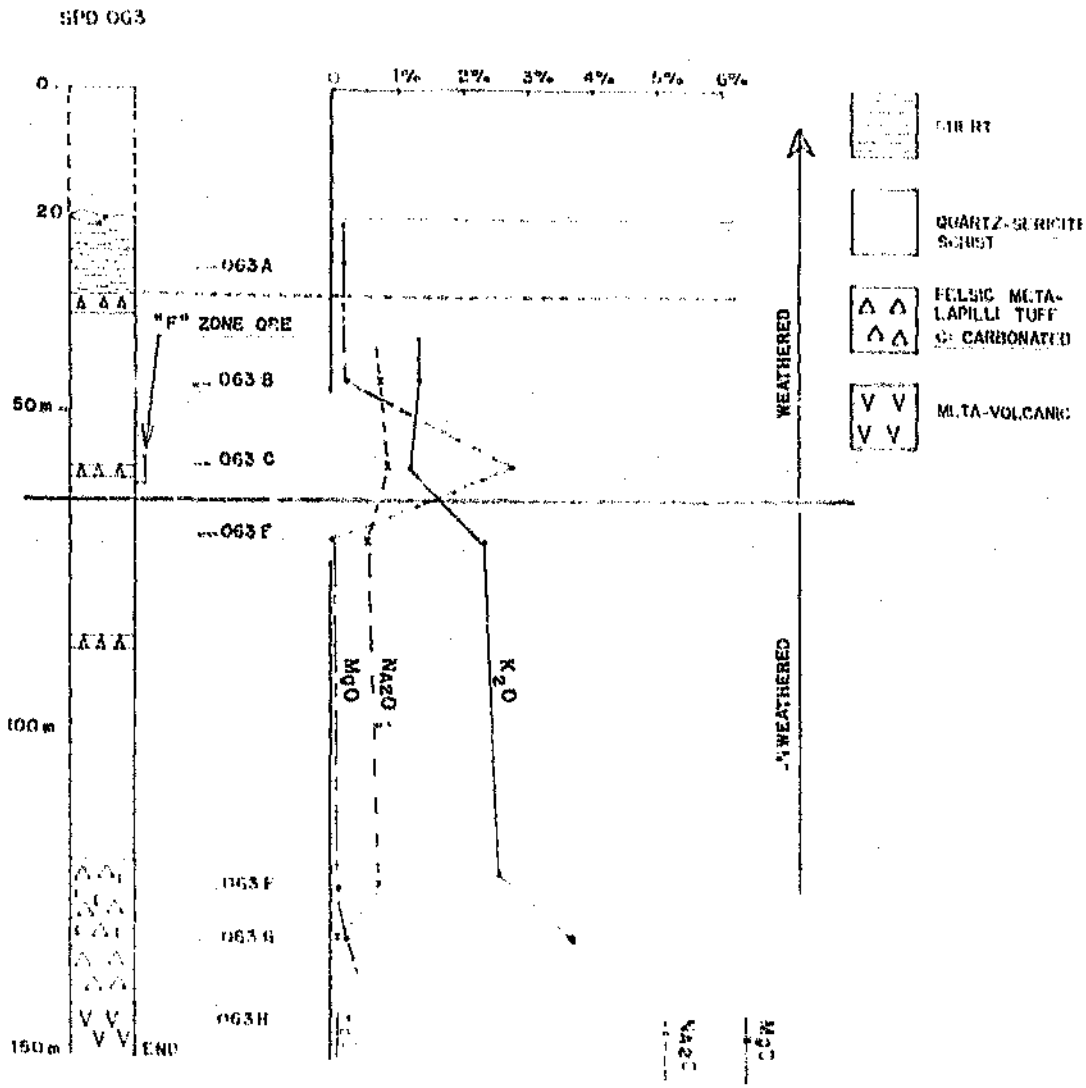


Figure 6.1: Schematic stratigraphic profile showing the variation of Na_2O, K_2O and MgO for rocks of the upper Penhalonga Formation. (Borehole SPD-063)

sediments. The reliability of the Zr/TiO2 versus Nb/Y plot is based on the apparent immobility of these elements during hydrothermal alteration (Cann, 1970; Pearce and Cann, 1973; Floyd and Winchester, 1978). Foster et al (1986b) used this plot to classify the volcanic and volcaniclastic sediments at Shamva Gold mine, Zimbabwe.

[illegible] the [illegible] of the upper Penhalonga Formation [illegible] may have resulted during the successive periods of deformation and alteration than the Last Hope Formation sedimentary rocks. [illegible] of the upper Penhalonga Formation, that is, [illegible] to be the least altered and [illegible]. However, [illegible] it is unlikely that the [illegible] altered.

6.2 Upper Penhalonga Formation.

It has been indicated previously (chapters 3 and 4) that the lithologies of the upper Penhalonga Formation volcanic sequence in the vicinity of the "J" Zone have undergone several periods of

product. This is especially crucial when attempting to establish the protolith of an altered and/or weathered rock or the alteration process that the rock has undergone. If certain elements are mobile during alteration any classification based on these elements is suspect. Over the years numerous papers have addressed some facets of element mobility (Smith (1968), Cann (1970), Floyd and Winchester (1978), [illegible] et al (1979), Kranidiotis and MacLean (1987)). An overview of the literature indicates that the following elements are considered relatively immobile: Ti, Al, Zr, Y, Nb, Ni Co, Cr as well as rare earth elements. Those considered to be mobile include Na, Ca, K, Sr, Rb, Mn and Ba, and those which behave in an unpredictable manner include Si, Mg and Fe. However, at present there still exists considerable debate as to whether Al is an immobile element or in contrast, is one of the most mobile elements. Kerrick (1990) concluded from his study of aluminum silicates in the aureoles of the Donegal Granites (Ireland) that late-stage metamorphic fibrolite (Quartz-K feldspar segregation) formed from the influx of acidic, magmatic fluids containing aluminum, boron and alkalies. Accordingly, Kerrick (1990) suggested considerable caution when utilizing a constant Al reference frame to model metamorphic processes during metamorphism of pelites and quartzo-feldspathic lithologies.

The use of Ti/Zr versus Nb/Y ratios for apparent petrographic identification of volcanic rocks and their derivatives is of great help in establishing the protolith of the Pembroke Formation and the exact nature of the [illegible] formation

CHAPTER SIX

LITHOGEOCHEMISTRY

6.1 General statement

The purpose of this chapter is to supplement the petrographic identification of volcanic rocks and their derivatives, to establish geochemical correlations between Au, As, Sb and other associate minerals, and to tentatively establish a correlation pattern between hydrothermal alteration indicators and the Au, As and Sb mineralization.

Geochemical analysis were carried out on 63 borehole core samples from the Signal Hill area. Fifty-five samples were collected from borehole intersections of the "A" Zone, and 8 samples were collected from the "F" Zone. The locations of these drill holes are given in Appendix IX.

Of the 55 samples from the "A" Zone, 13 are unweathered ore samples, the remaining samples were collected from footwall and hanging wall lithologies.

All samples were analyzed by XRF for major elements and for 15 trace elements at the Department of Geology, University of the Witwatersrand. Gold (standard fire assay), as well as arsenic and antimony (XRF) for the 13 "A" Zone ore samples were analyzed by Bergstrom And Bakker laboratories in Johannesburg, R.S.A.

In dealing with altered lithologies it is necessary to establish a link between the parent rock and its alteration

CHAPTER SIX

LITHOGEOCHEMISTRY

6.1 General statement

The purpose of this chapter is to supplement the petrographic identification of volcanic rocks and their derivatives, to establish geochemical correlations between Au, As, Sb and other associate minerals, and to tentatively establish a correlation pattern between hydrothermal alteration indicators and the Au, As and Sb mineralization.

Geochemical analysis were carried out on 63 borehole core samples from the Signal Hill area. Fifty-five samples were collected from borehole intersections of the "A" Zone, and 8 samples were collected from the "F" Zone. The locations of these drill holes are given in Appendix IX.

Of the 55 samples from the "A" Zone, 13 are unweathered ore samples, the remaining samples were collected from footwall and hanging wall lithologies.

All samples were analyzed by XRF for major elements and for 15 trace elements at the Department of Geology, University of the Witwatersrand. Gold (standard fire assay), as well as arsenic and antimony (XRF) for the 13 "A" Zone ore samples were analyzed by Bergstrom And Bakker Laboratories in Johannesburg, R.S.A.

In dealing with altered lithologies it is necessary to establish a link between the parent rock and its alteration

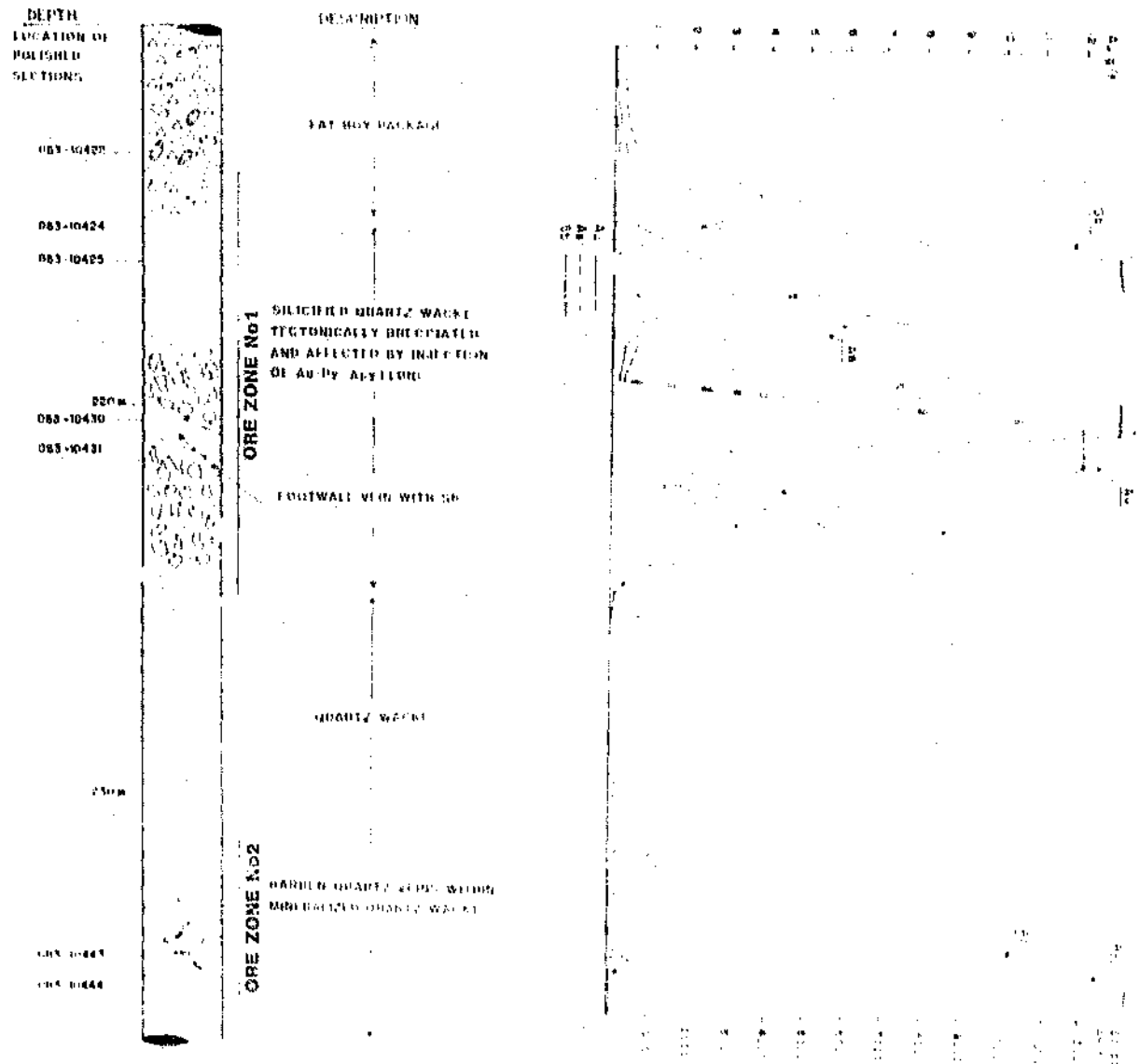


Figure 5.38: Intersection of "A" Zone mineralization in borehole SPD-083 showing two distinct ore zones. The Au, As and Sb distribution is also shown.

ore combined with a Footwall vein in silicified quartz wackes. This Ore Zone 1, shows a close relationship between Au and As, and a more erratic association with Sb. The Ore Zone 2 is located approximately 10 meters further in the footwall, and is characterised by brecciated Au-Py-Apy mineralized quartz wacke facies and injected by barren quartz veins. In Ore Zone 2, the same close relationship between Au and As exists, but Sb is practically absent. Assuming that the Au-As mineralization of Ore Zone 1 and Zone 2 are of the same origin, and if the antimony mineralization was the latest phase associated with gold to precipitate, as proposed by Harwood (1986), then it could be anticipated that the Au-Sb relationship in Ore Zone 1 and in Ore Zone 2 would be the same. Figure 5.28 shows that the Au-Sb relationship in Ore Zone 1 and in Ore Zone 2, is not the same, which suggests that the Au-As association has no relationship with the antimony mineralization.

Furthermore, evidence of brittle deformation of the early antimony mineralization by a later tectonic event with associated gold-bearing hydrothermal fluids has been described and observed megascopically and microscopically. These observations indicate that early antimony mineralization took place before the Au-Py-Apy mineralization.

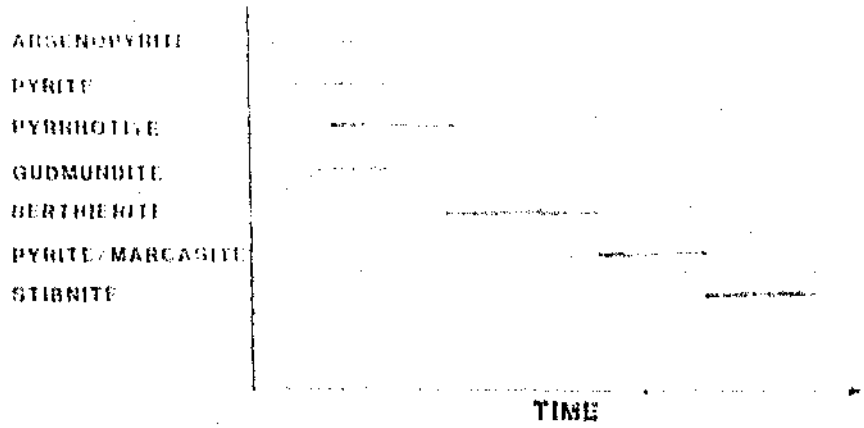


Figure 5.27: Paragenetic sequence of mineralization after Harwood (1986). Although gold has been observed and described by Harwood, he did not included gold in the paragenetic sequence.

is the timing of the antimony ore emplacement. Harwood (1986), considered the stibnite to be introduced as a late sulphide phase, while the writer argues that the antimony mineralisation predates the main gold mineralization. According to Boyle (1979), stibnite is invariably a late mineral in gold deposits. Most antimony minerals form at very low temperatures that even in the case of a solution from volcanic rocks, the water might be below its condensation point (Saunders, 1990). Considering these statements, Harwood's paragenesis appears quite acceptable.

However, Figure 5.27, presents mineralized intersections of borehole [illegible]. Using [illegible] results, these intersections can be subdivided into two distinct paragenetic ore associations; namely ore Zone I and ore Zone II. Ore Zone I is characterized by contact

the "A" Zone Au-As-Sb deposit is presented in Figure 5.26.

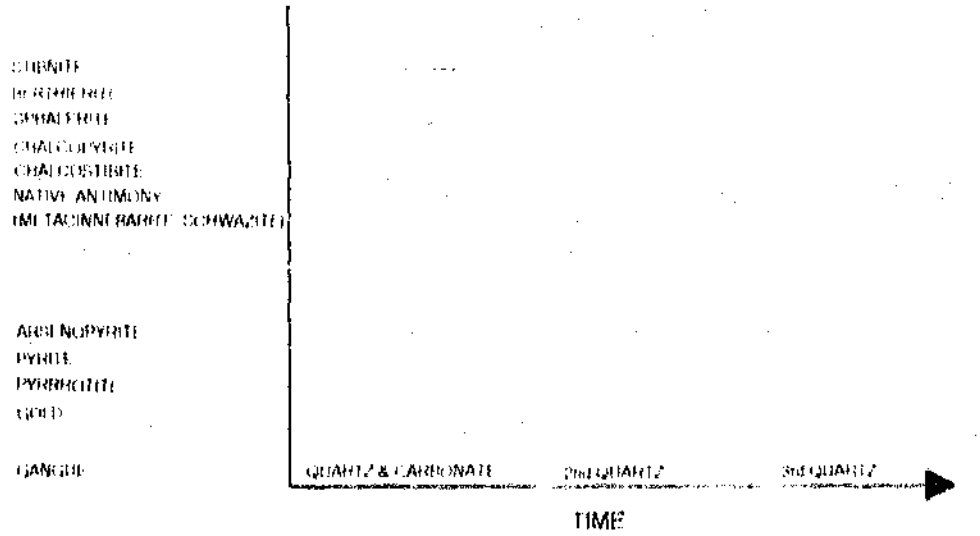


Figure 5.26: Ore paragenesis of the "A" Zone mineralization, Signal Hill area.

Harwood (1986), reported gudmundite (FeSbS) "in close intergrowth with stibnite which it appears to be replacing with a cavcous texture". He also reported a gudmundite-arsenopyrite paragenesis. However, in this study gudmundite was not observed.

5.4 Discussion

Harwood (1986), in his study of sulphide ore from the "A" Zone proposed the paragenesis presented in Figure 5.27, for the Au-Sb-As mineralization.

However, the paragenetic sequence described in section 5.3.13 is different from Harwood's (1986) interpretation. The main point

B) A subsequent introduction of siliceous material is associated with a tectonic event which brecciated phase "a", and created coarser grained dark grey idiomorphic quartz crystals. These quartz crystals are associated with arsenopyrite-pyrite mineralization. Gold is found interstitially or fills in microfractures. Figure 5.24 shows brecciated first gangue replaced by quartz-carbonate-sericite with associated pyrite and arsenopyrite.

C) A milky white barren quartz vein cross-cuts the two earlier phases. The quartz crystals within this quartz vein are very coarse grained and do not host any mineralization (Fig. 5.25).

5.3.13 Ore paragenesis

It appears that several phases of hydrothermal alteration and mineralization took place within the sedimentary assemblage of the "A" Zone. It is proposed that the stibnite, berthierite, sphalerite, as well as chalcopyrite, chalcostibite, native antimony and possible metacinnabarite and/or schwazite were related to an early phase of mineralization. It is not clear whether or not a certain amount of gold was associated with this early phase. A second influx of hydrothermal fluids was introduced, which resulted in the arsenopyrite + pyrite + gold mineralization. A third barren hydrothermal event is related to later brecciation of the two earlier phases. In addition, the early antimony mineralization has undergone later local remobilization. The paragenetic sequence of



Figure 5.25: Brecciation due to brittle deformation of the gold bearing second gangue generation (dark colour) and injection of white barren quartz material, SPD-083, sample 10444.

variable. Three periods of hydrothermal alteration have been identified.

A) The first is an early fine grained grey to brownish quartz-carbonate gangue related to an intense and pervasive alteration of quartz wacke. This pervasive intense silicification and to a lesser extent carbonatization took place in the western portion of the "A" Zone (Fig. 5.3). Stibnite-rich Footwall veins are located within these altered quartz wackes. Figure 5.25, shows a Footwall vein with stibnite-berthierite-sphalerite mineralization. The gangue is composed almost exclusively of fine grained quartz.

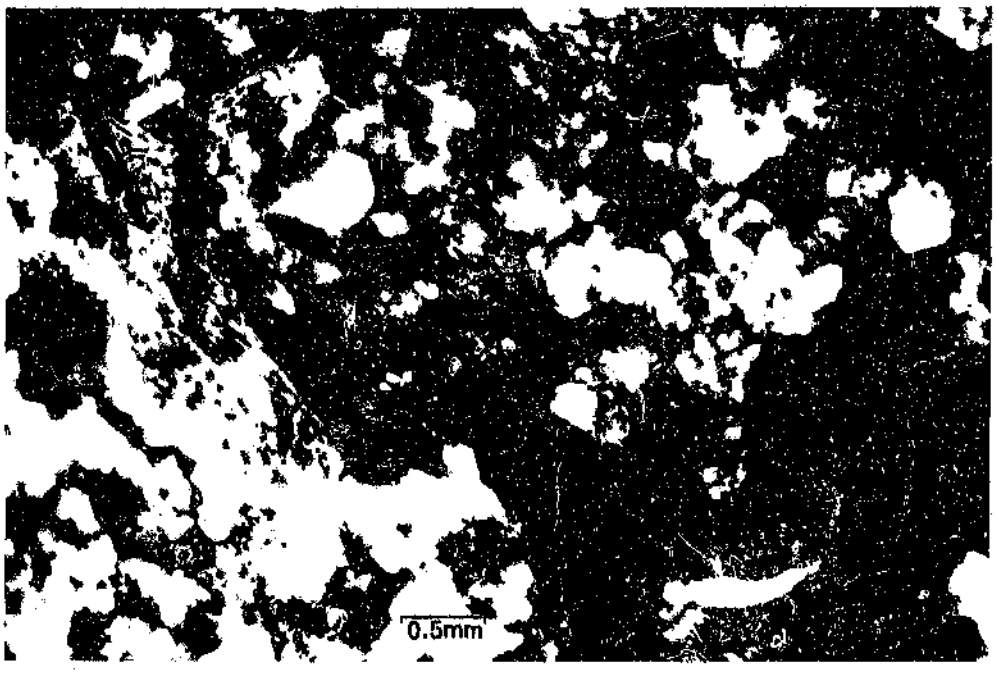


Figure 5.23: Footwall vein with stibnite-berthierite-sphalerite mineralization. The gangue is composed almost exclusively of quartz, SPD-083, 220m, (25 X, + Nic).

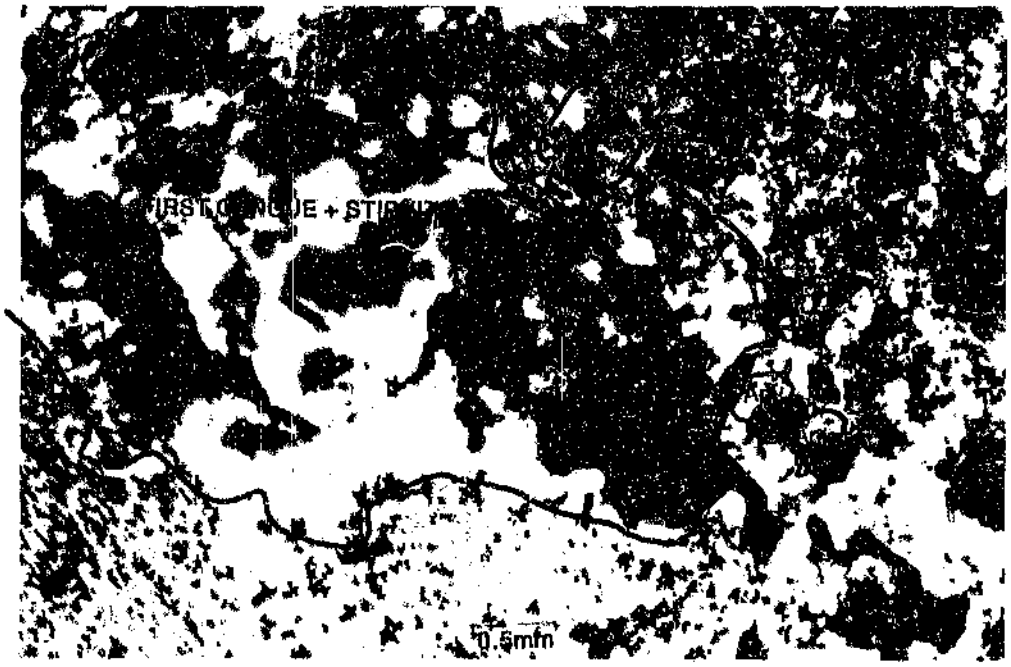


Figure 5.24: First fine-grained, grey quartz gangue tectonically affected by an later event with subsequent replacement by carbonatization and sericitisation, SPD-083, 215m, (25 X + Nic).

contents of the whole rock (Foscar et al (1986b)). According to Boyle (1979), for most of the gold deposits associated with gold-quartz veins and/or shear zones, Rb shows an increase as gold zones are approached while Sr decreases.

Figure 6.8 shows that Sr and Rb [illegible] the distribution pattern [illegible] Zone mineralization. Both decrease slightly towards the ore zone (hanging wall), drop at the ore zone and rise in the footwall away from the ore zone. None of the other "ore" elements (As, Sb, Zn, Ni and Cu) show any correlation with Sr (Fig. 6.10) and Rb (Fig. 6.11) in the host rock. Figure 6.9 indicates that for all mineralized [illegible] as listed in Appendix IV, a broad correlation exists between the decrease of Sr and Rb and the increase in gold. This pattern does not correlate well with a typical gold-quartz vein in a shear zone system (Boyle, 1979).

[illegible]

6.5), while no statistical significant correlation exists between Au and Sb (r= 0.32). Figure 6.6 indicates that no direct correlation can be drawn between high gold values and Zn, Ni and Cu contents. Also, no correlation exists between Zn, Ni, Cu and Sb (Fig. 6.7).

Although mercury (Hg) has been reported to be associated with diverse mineralized zones ("A" and "C" Zones, Appendix V), no direct correlation between Hg and Au, As and Sb can be obtained from this data (Fig. 6.8). However, results from two samples of undeformed massive antimony ore (Table 6.1) show that high mercury content (629 ppb, 4120 ppb) is associated with the antimony ore. The presence of schwazite (fahlore group mineral, $Cu_{12}(As,Sb,Hg)S_{13}$) as suggested in section 5.3.7, could explain these mercury values as well as the high As contents (408 ppm, 624 ppm). No gold has been detected in these samples.

Table 6.1: As, Sb, Hg and Au contents of two samples of massive antimony ore from "A" Zone mineralization.

Sample	As (ppm)	Sb (ppm)	Hg (ppm)	Au (ppm)
HG-1	408	140000	629	nd
HG-2	624	120000	4190	nd

6.5 Hydrothermal alteration

The role of the various tectonic and hydrothermal events, (Chapters 3 and 5) can be investigated further by using Rb and Sr

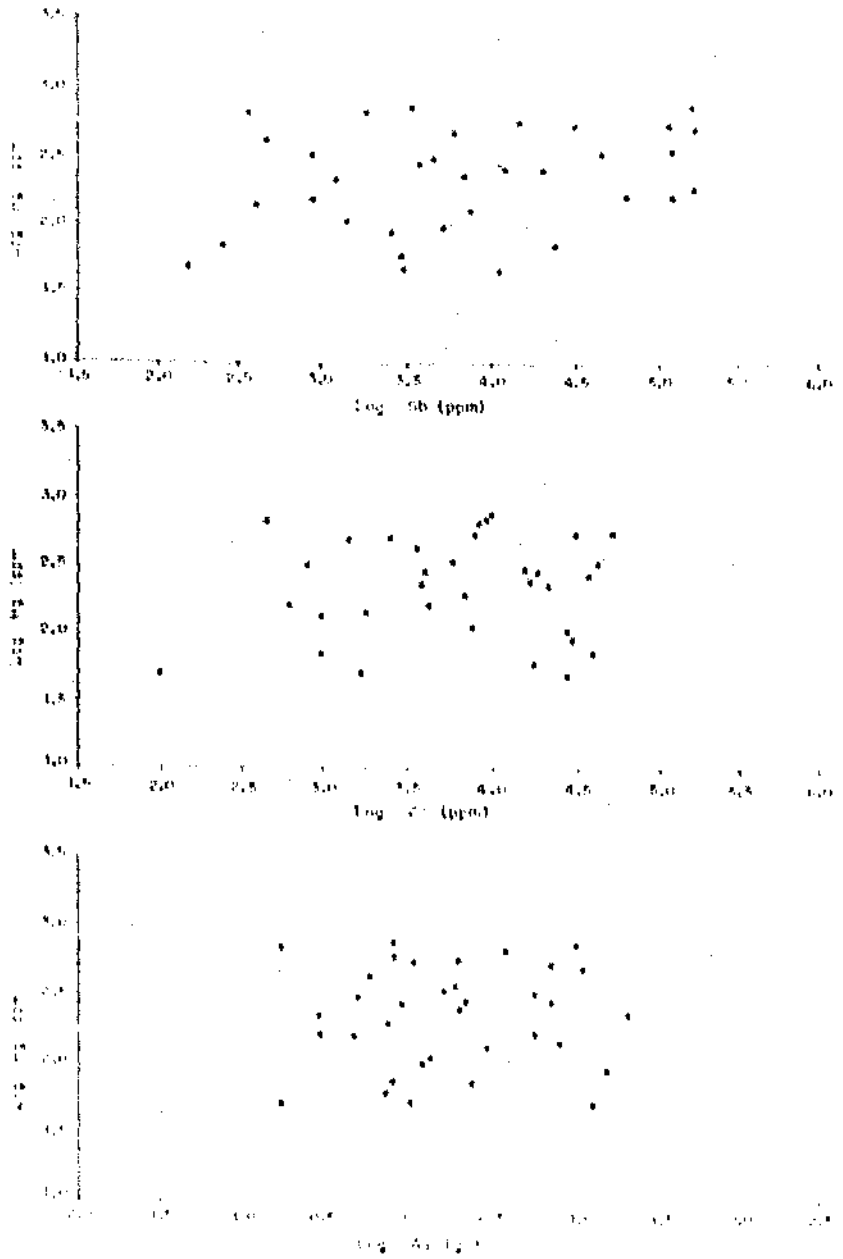


Figure 6.8: Variation diagrams for Hg vs Au, Hg vs As and Hg vs Sb, samples are listed in Appendix V.

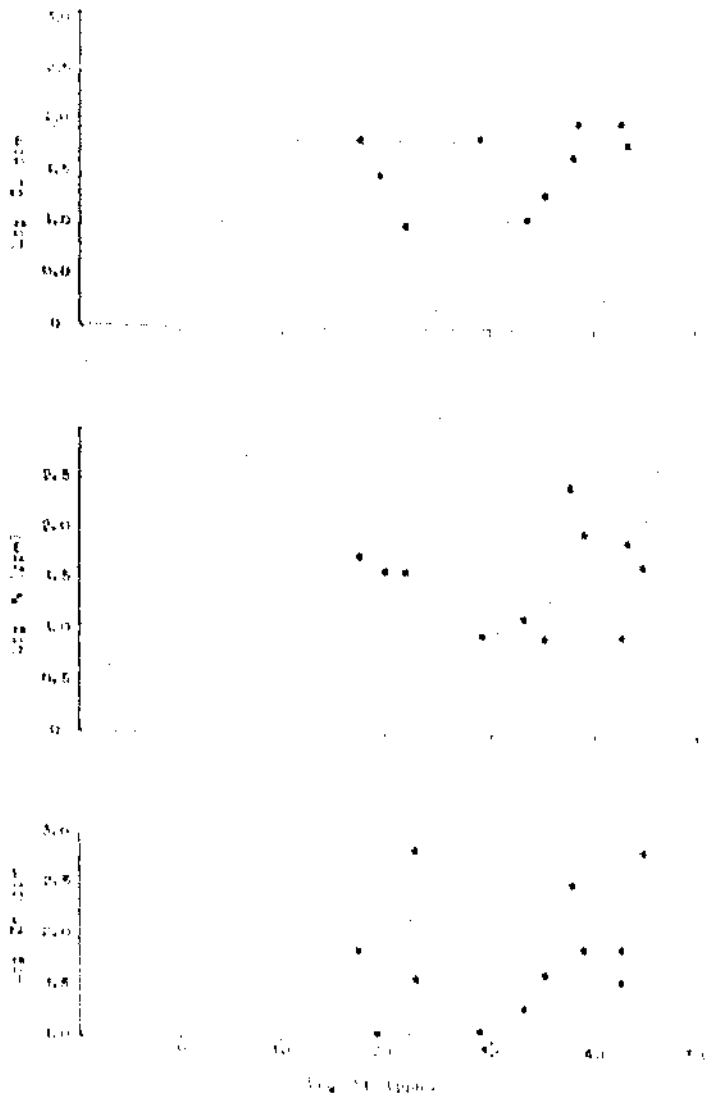


Figure 6.7: Variation diagrams for Zn, Ni and Cu vs Sb, samples are listed in Appendix IV.

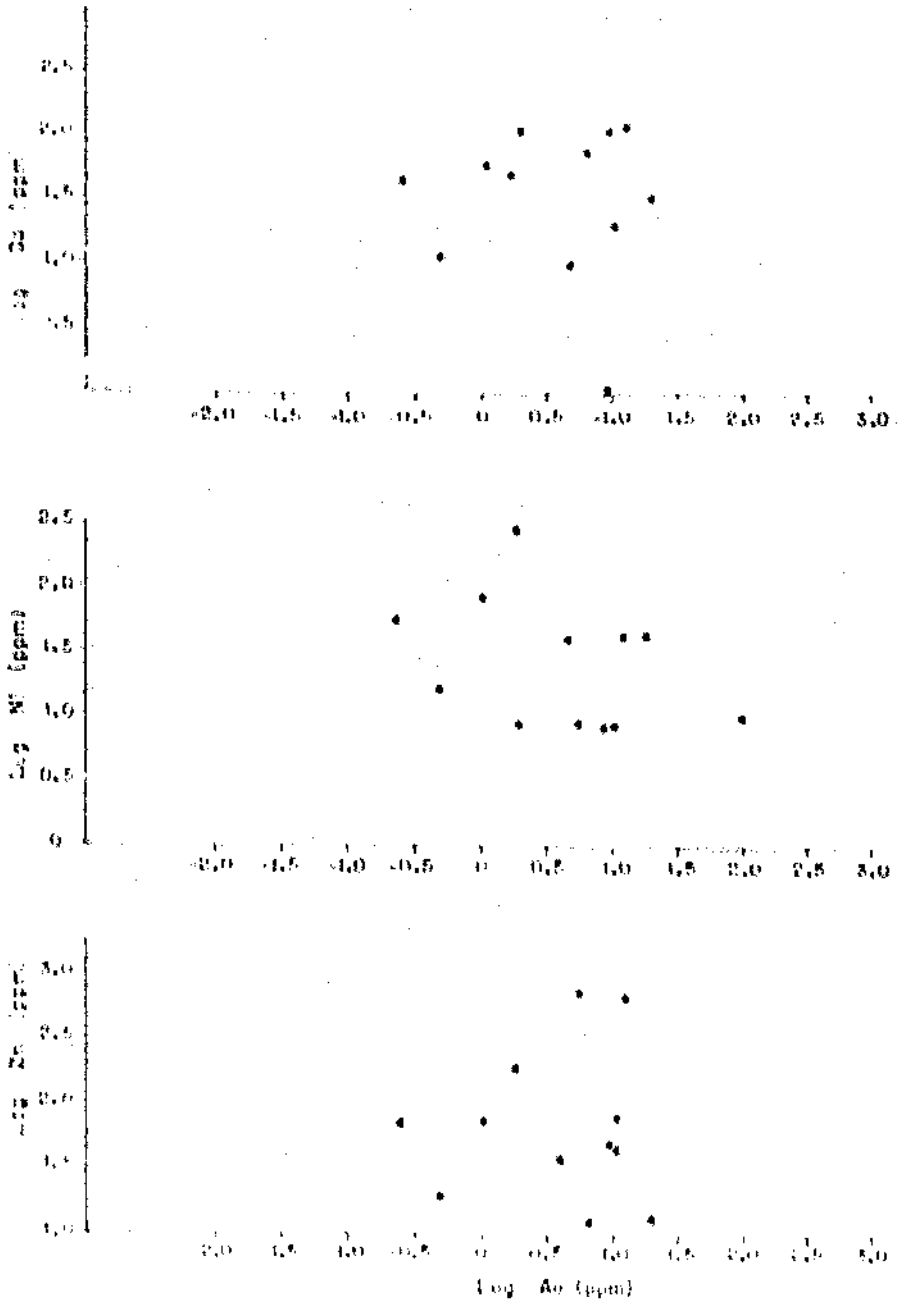


Figure 6.61 Variation diagrams for Pb, Ni and Cu vs Au, samples are listed in Appendix IV.

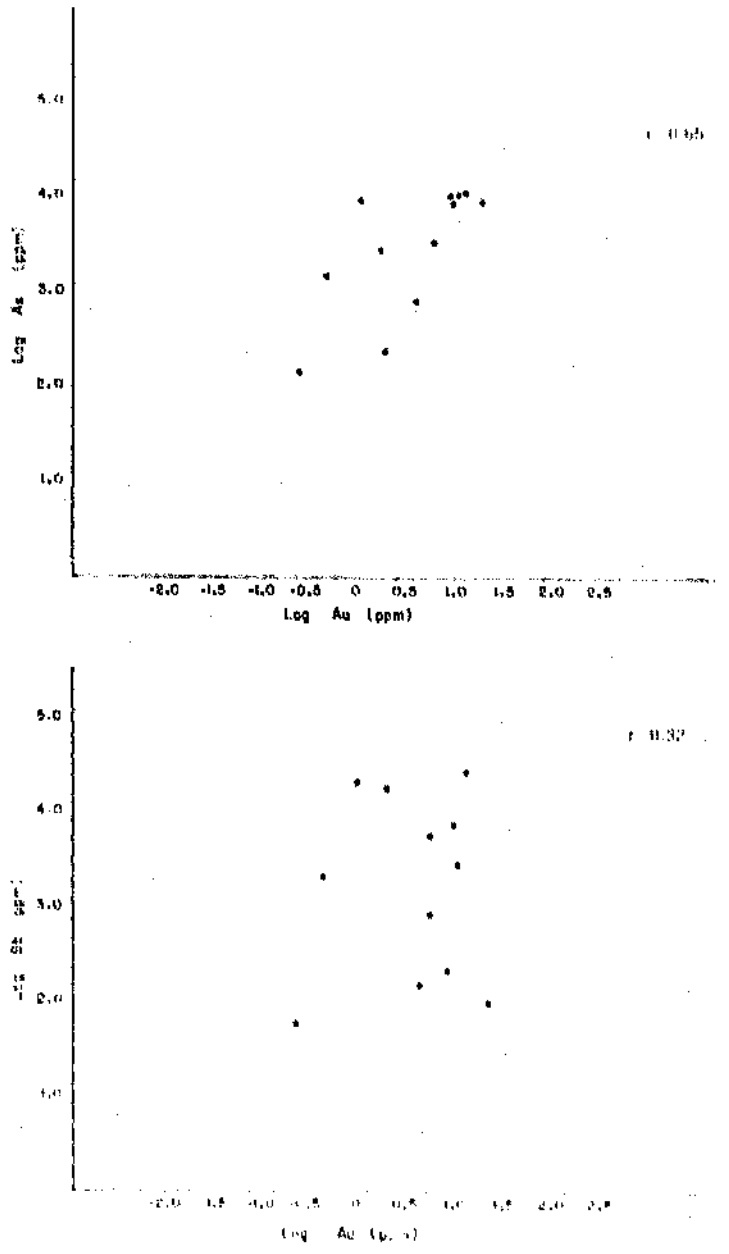


Figure 6.5: Variation diagrams of Sb and As vs Au, samples are listed in Appendix IV.

where a slight build-up of these elements is observed. According to Figure 6.3, a chaotic pattern for both K_2O and Na_2O can be observed throughout the ore zone.

The chemistry of the clastic components indicates derivation of the material from a relatively Ti-enriched and Zr-depleted source (Fig. 6.4). The chemistry of unaltered volcanic fragments collected from diamictite facies (Appendix III), indicates a variety of origins, from sub-alkaline basalt to andesite (Fig. 6.4).

6.4 "A" Zone mineralization

The gold rich samples (≥ 0.50 g/t) are characterized by As contents varying from 0.024% to 5.13% (avg. 0.72%) and Sb varying from 0.010% to 2.74% (avg. 0.81%), (Appendix IV). Gold mineralization is also associated with Zn (13.1 to 744 ppm, avg. 206 ppm), Ni (0.05 to 295 ppm, avg. 63 ppm) and Cu (nd to 138 ppm, avg. 59 ppm) (Appendix IV). Mercury (Hg) has been detected in gold-rich samples collected at surface along the "A" Zone with values ranging from 22 ppm to 740 ppm (avg. 265 ppm) (Appendix V). All these elements are enriched within the ore zone, compared to the unaltered quartz wacke facies away from the ore zone (Fig. 6.3). The Co, Cr and Ba contents do not show any significant increase or decrease between the ore zone and the unaltered host rock (Fig. 6.3).

A correlation between Au and As is evident (r= 0.65, Fig.

at 1.9% (Appendix III). Consequently, direct comparison of element contents in unaltered and altered rocks without any mass and volume adjustment was deemed acceptable.

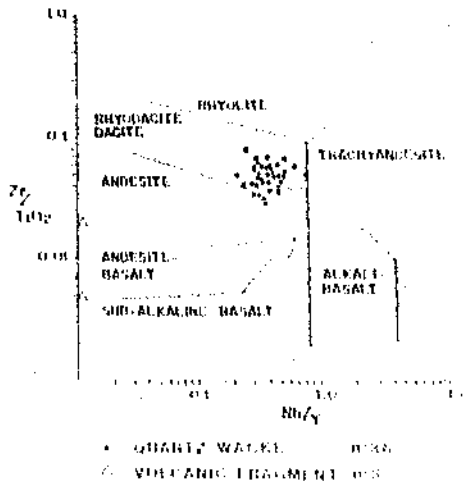


Figure 6.4: Zr/TiO2 - Nb/Y plot showing the classification of the quartz wacke facies of the Last Hope Formation and volcanic fragments of diamictite facies (after Floyd and Winchester, 1978).

6.3.1 Major and trace element behaviour.

The K2O content of the Last Hope Formation ranging from 0.87 to 2.43 wt %, (avg. 1.09 wt %) correlates well with the minor quantity of sericite observed within the matrix of these sediments (Appendix III). These rocks appear to be almost free of Na2O and MgO, with the exception of the "A" Zone mineralization (Fig. 6.3),

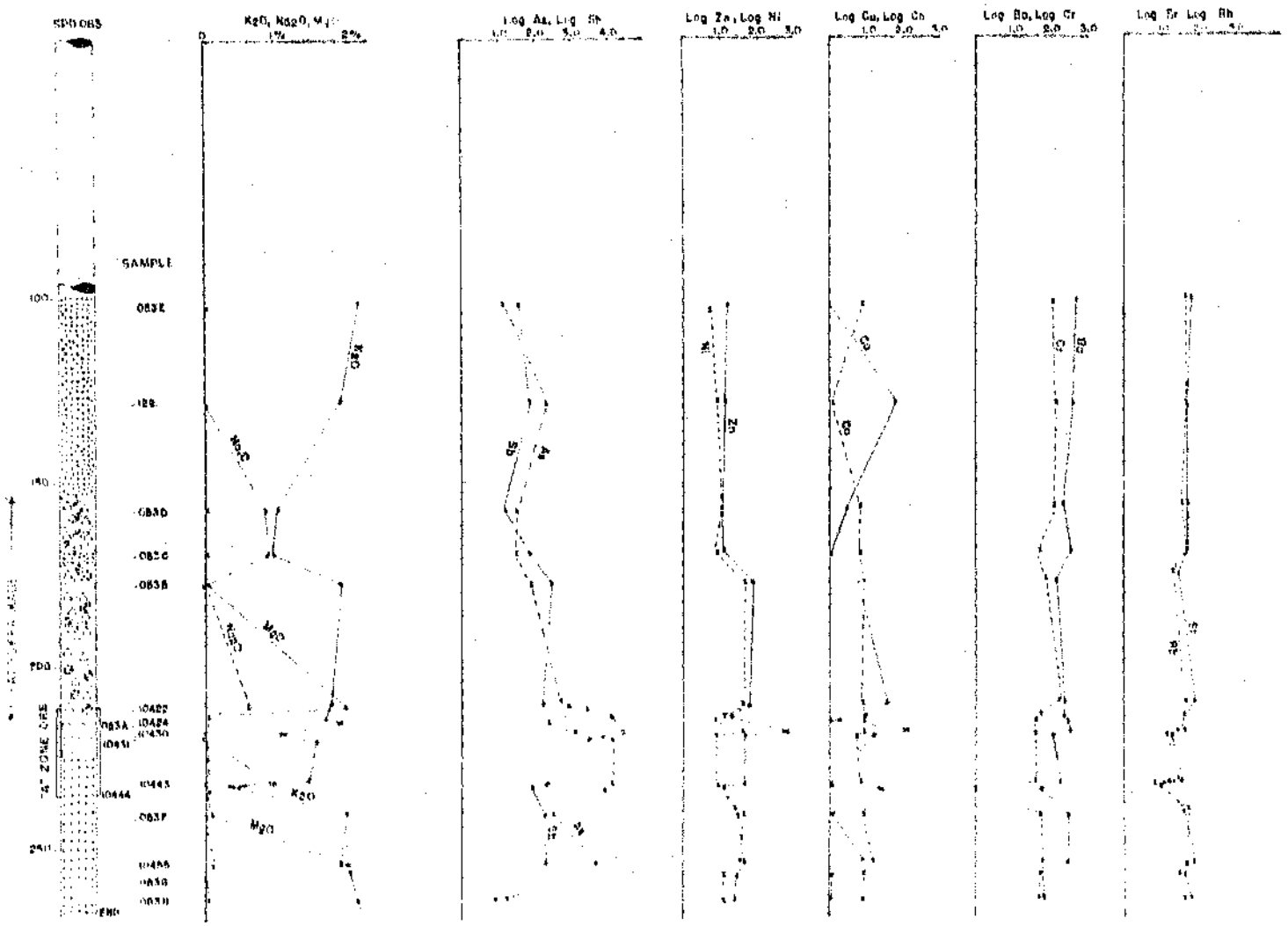


Figure 5.3: Variation of major and trace elements in the Last Hope Formation rocks. (borehole SPD-083)

remains generally very low throughout the whole succession with one exception near the "F" Zone mineralization, where the values increase dramatically by approximately 28 times the background (Fig. 6.1). The Zr/TiO2 versus Nb/Y plot indicates an acid volcanic protolith (andesite to dacite)(Fig. 6.2).

6.2.3 Chert unit

The third assemblage is characterized by 94.00 wt % SiO2, 0.85 wt % Fe2O3 and 2.99 wt % Al2O3. Petrographic observations (Chapter 3) and chemical results, (less than 1% loss on ignition and very low CaO and Fe2O3) indicate that this unit is unaltered. This unit belongs to the unit A chert and ironstones (Chapter 4, Fig. 4.1)

6.3 Last Hope Formation

[illegible] all the [illegible] of this Formation, [illegible] [illegible] relatively low degree [illegible] deformation. [illegible] [illegible] and the development of [illegible] [illegible] the [illegible], the [illegible] [illegible] [illegible].

The maximum dilution due to possible hydration and carbonatization, as detected by loss on ignition, was [illegible] with the average

1). Although this unit is heavily chloritized and carbonated (mainly calcite), the chemical composition outlined by K_2O, Na_2O and MgO undoubtedly differs from the quartz-sericite schist assemblage (Fig. 6.1). The chemical composition, as well as the Zr/TiO$_2$ - Nb/Y plot (Fig. 6.2), suggests, although not conclusively (only one sample), a sub-alkaline basalt protolith.

6.2.2 Quartz-sericite schist units

The quartz-sericite schist units were heavily affected by the successive tectonic events and accompanying alteration processes. Therefore, the interpretation using the major elements of these rocks will be limited to the identification of general trends in the alteration process. The interpretation is also complicated by the fact that intense weathering has affected these rocks at a depth down to 65 meters.

Chemically, the whole assemblage is characterized by highly variable amounts of SiO_2, varying from 48.90-77.00 wt % (avg. 62.5 wt %), 2.76-0.00 wt % (avg. 0.68 wt %) of MgO and [illegible]-0.86 wt % (avg. 0.38 wt %) of TiO_2. Ba ranges from 164 ppm to [illegible] ppm (avg. 344 ppm), and Nb from 4.47 ppm to 10.6 ppm (avg. 8.0 ppm) (Appendix I). From bottom to top, this rock succession shows a broad decrease in K_2O accompanied by a slight increase in Na_2O (Fig. 6.1).

A drop of 1.0% in FeO and an increase of 0.4% in Na_2O are associated with the "I" zone mineralization. The MgO content

deformation and alteration. In addition, dilution due to possible hydration and carbonatization, as defined by loss on ignition, is highly variable but remains on average very high (Appendix I). Consequently, the interpretation of the chemistry of the members of the upper Penhalonga Formation, without mass and volume adjustment, will remain speculative.

Figure 6.1, shows that three distinct units can be outlined by the general trend of K_2O, Na_2O and MgO.

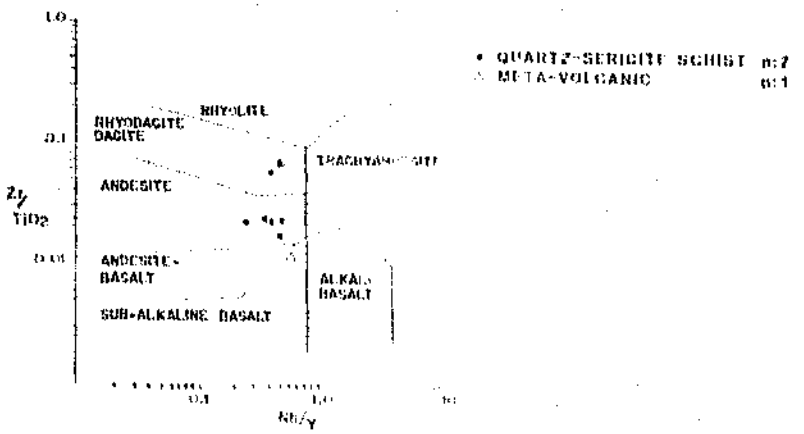
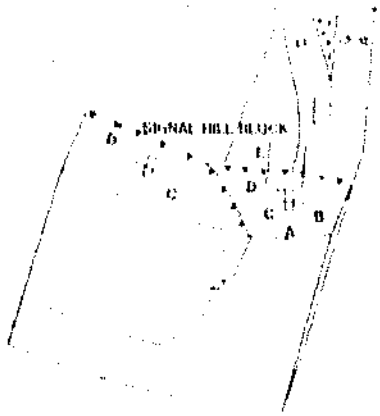


Figure 6.2: Zr/TiO_2 - Nb/Y plot showing the classification of the volcanic rocks of the upper Penhalonga Formation (after Floyd and Winchester, 1978).

6.2.1 Meta-volcanic unit

Chemically, this unit is composed of 51.45 wt % SiO_2, 14.68 wt % Al_2O_3, 6.45 wt % MgO, 365 ppm of Cr and 104 ppm of Ni (Appendix

1



A MAYBLOOM
B OLD TATE
C LADY MARY
D PENHALONGA
E LAST HOPE

2



3

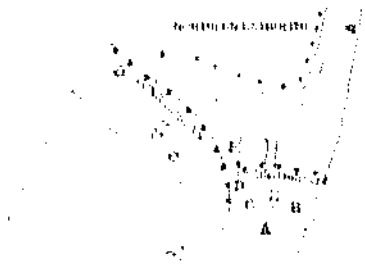
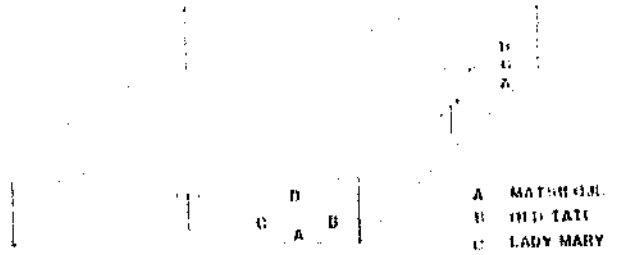
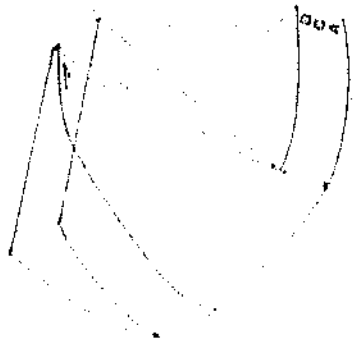


Figure 2.23: Block diagrams showing the "splits" of the right way-up northern limb by the intrusion of the Northern Batholith, together with the thinning (shown by the dotted line) of a portion of the overturned southern limb.

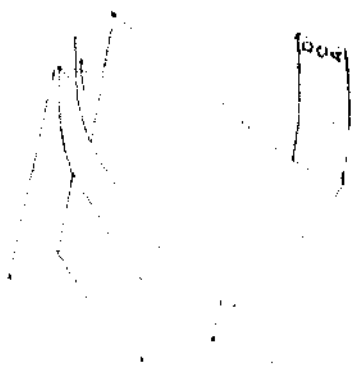
1



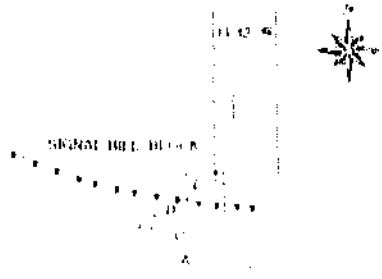
2



3



PLAN VIEW



the schist belt on markedly different bearings. The regional dip throughout most of the schist belt is to the south or southwest, but westerly dips are recorded in the extreme east. The subdivision of the Penhalonga Formation into distinct structural domains can also apply to the whole schist belt. In the south and southwest domains the stratigraphic succession is inverted, with the ultramafic/mafic phases occurring at the top of the structural succession. The north and east domains show right way-up rock successions. Except for the broad arcuation of the schist belt, major fold structures are not prominent.

Positions of tonalitic batholiths and their marked effect on the schist-batholiths contacts, suggests that the schist belt collapsed between them as they moved upwards into their present positions (Mason 1970). Based on Mason's statement and in light of field observations and a detailed examination of the Landsat image of the Tati schist belt, an interpretation of the structural history of the Tati schist belt is presented.

At an early stage in the development of the Tati schist belt, the stratigraphic succession was initially subjected to large scale folding caused by a combination of the sinking of the volcanic pile and the diapirically rising granitoid complexes, and possibly by other tectonic mechanisms (nappe like structures ?, Litherland (1976)) (Fig. 7.1). This early deformation produced a large-scale synform with an overturned southern limb and a right way-up northern limb. The continuous rising of batholiths and/or other tectonic forces, caused the amount of folding to increase and the

CHAPTER SEVEN

DISCUSSION

7.1 General Statement

The sedimentological, structural, mineralogical and geochemical data presented in earlier chapters of this dissertation, provide the framework for establishing a model of the genesis of the Signal Hill Au-As-Sb deposits. These complex deposits formed as a response to inter-related geological processes. These include early phases of tectonic activities responsible for the deposition of the Last Hope sediments, early formation of the antimony mineralization, later thrusting and folding events which control the gold and arsenic mineralization and finally post-mineralization tectonic activities.

7.2 Structural deformation affecting the Tati schist belt

Before one can understand the structural deformation which affected the Signal Hill area and its control on the location of Au-As-Sb deposits, an understanding of the regional structure affecting the whole Tati schist belt is necessary.

The whole succession is weakly metamorphosed under greenschist facies conditions and is intruded between a series of tonalitic batholiths. The Tati schist belt possesses an overall south-easterly trend, although appendages lead off from the main body of

less than 1 ppm. However, a few exceptions to this rule exist, in the Puhipuhi gold deposit in New Zealand (hot springs), the range is 360-760 ppm Hg. Boyle (1979), described favourable conditions for mercury enrichment in gold deposits as the following:

1) [illegible]

2) the presence of sphalerite and/or sulphosalts and cinnabar are the controlling factors for enrichments.

3) under most conditions mercury is lost from the oxidized zones of gold deposits especially where the oxidation has been intense and prolonged. Where the oxidation is less severe mercury may exhibit an enrichment.

In section 5.3.7, it has been proposed that for the "A" Zone mineralization the mercury could have been intimately associated with the early phase of stibnite mineralization, rather than being associated with the later gold mineralization.

This relationship between Hg and the antimony mineralization is also supported by chemical evidence. Results from undeformed, unweathered massive antimony ore have proved that antimony and Hg mineralization are related.

[illegible]

mass and/or volume changes, the rock assemblages were defined using general trends of K_2O, Na_2O and MgO as well as Zr/TiO_2 versus Nb/Y plots. According to the chemical classification the rock succession can be defined as follows: a meta-volcanic unit of sub-alkaline basaltic origin occurs at the base, followed by a sequence of quartz-sericite schists of acid volcanic affinity (andesitic to dacitic), which in turn is overlain by cherty units.

The chemistry of the quartz wacke facies of the Last Hope Formation indicates derivation from a relatively Ti-enriched and Zr-depleted source. Furthermore, volcanic fragments from the diamictite units indicate a sub-alkaline basaltic to andesitic origin.

The "A" Zone gold mineralization is characterized by a high concentration of As, Sb and Hg. Gold-rich samples show a direct relationship with As, but there is no correlation with Sb and Hg. Although the "A" Zone ore shows a slight enrichment in Zn, Ni and Cu, gold does not show any correlation with these elements.

Interpretation of mercury within the "A" Zone ore is complicated by the fact that mercury is a mobile element which could have been affected by successive hydrothermal activities and by several deformational events. Weathering could also have caused either enrichment or depletion of the mercury content (Boyle 1979).

According to Boyle (1979), mercury is a common associate of gold in practically all types of hypogene gold deposits, but the element is invariably present only in small amounts, often much

6.6 "E" Zone Structure

This zone is characterised by a strong 1 km long arsenic anomaly in soil samples.

The results listed in Appendix VI indicate that the rock is composed of 5.79 to 6.34% Fe_2O_3, 7.10 to 14.40% CaO, 21.00 to 24.30% MgO, 13.70 to 33.80% SiO_2 and high L.O.I (30.0 to 39.7%). The Fe_2O_3, CaO, MgO and the L.O.I (mainly due to CO_2) are related to the intense dolomitization (ankerite) observed in the "E" Zone rocks. Two rock samples collected from the "E" zone, show As values ranging from 133 to 1263 ppm, Sb values from 109 to 410 ppm and one sample returned an anomalous gold value of 0.6 ppm (Appendix VI).

[illegible] described above indicate that the "E" Zone is related to an alteration system [illegible] the [illegible] contact zone. The "E" Zone structure could have acted as the conduit for the migration of hydrothermal fluids. [illegible] and be related to the [illegible], a major " " [illegible] structure, of early [illegible] the [illegible].

6.7 Discussion

Three distinct assemblages can be outlined using major and trace elements distribution from the lithological units of the upper Penhalonga formation. Due to the intense deformation and alteration of these units, and the impossibility of establishing

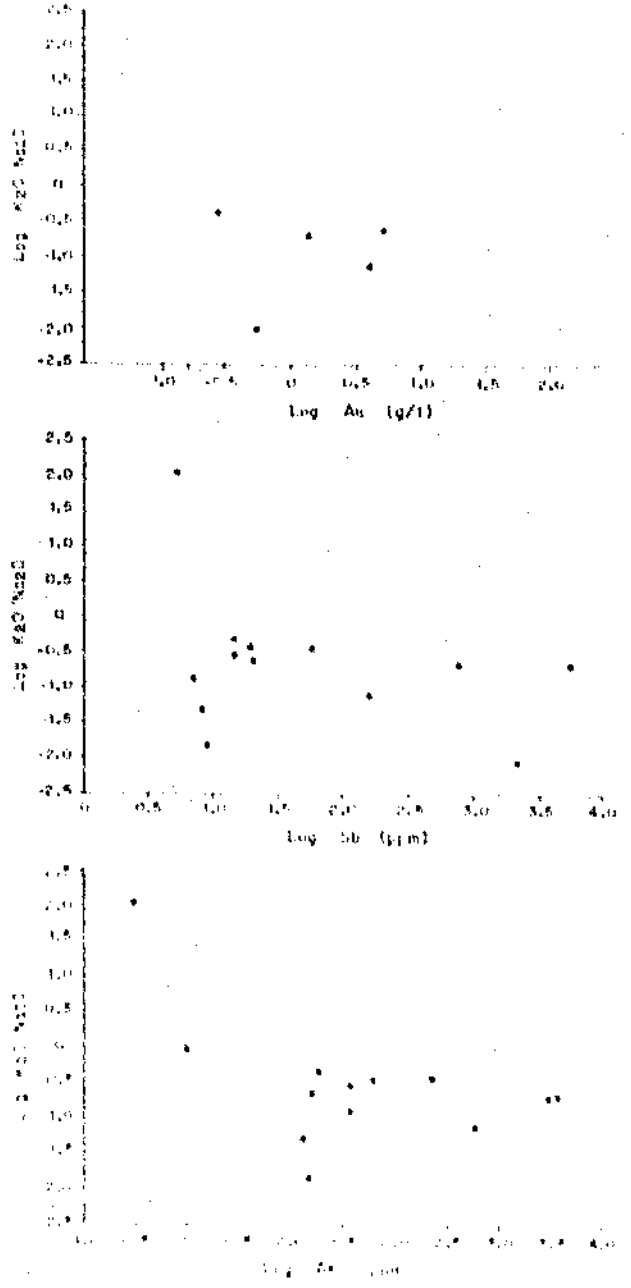


Figure 6.12: Variation diagrams for As, Sb and Au versus the K2O/Na2O ratio, samples are listed in Appendix IV.

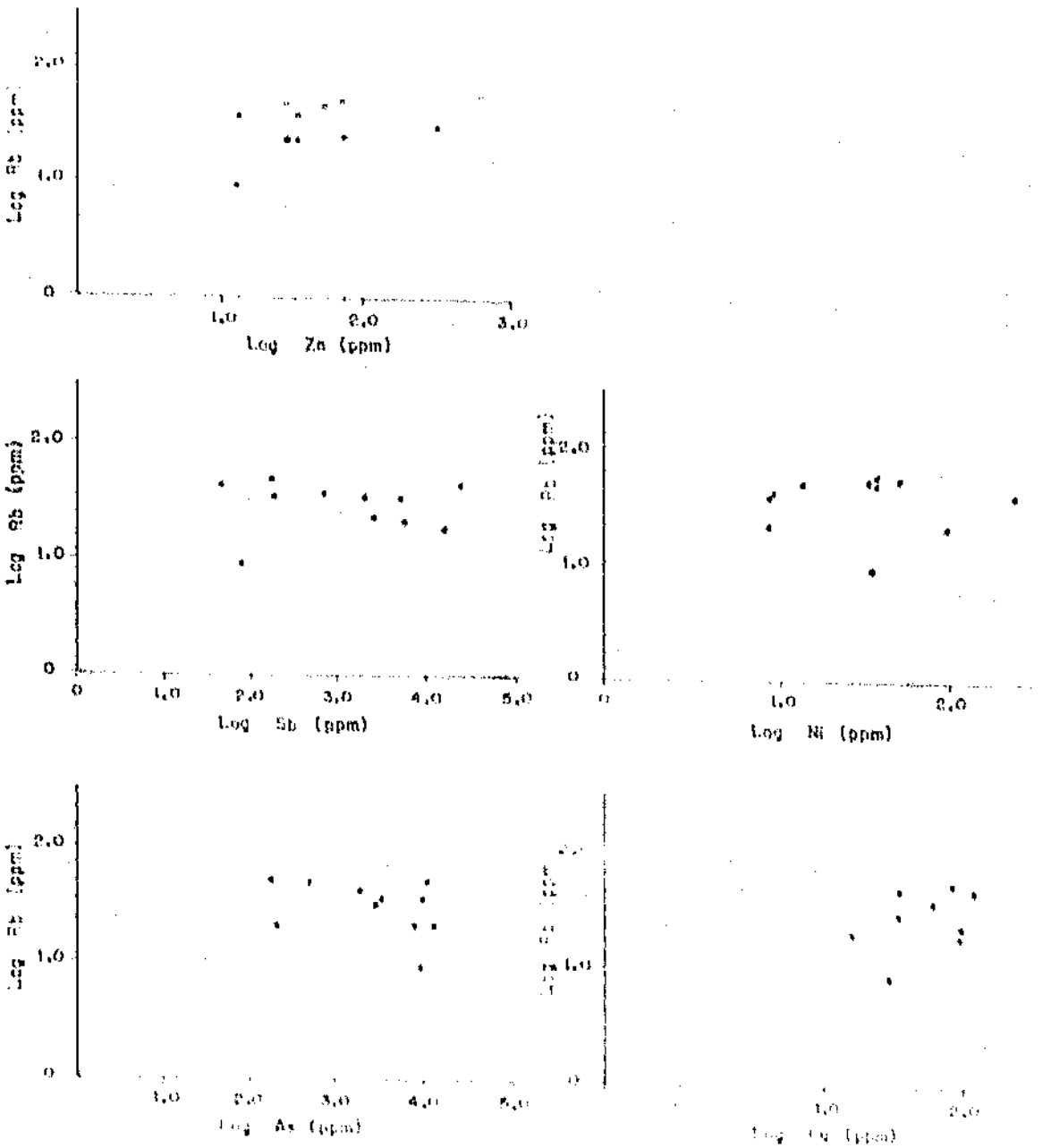


Figure 6.11: Variation diagrams for As, Sb, Zn, Ni and Cu with Rb, Samples are listed in Appendix IV.

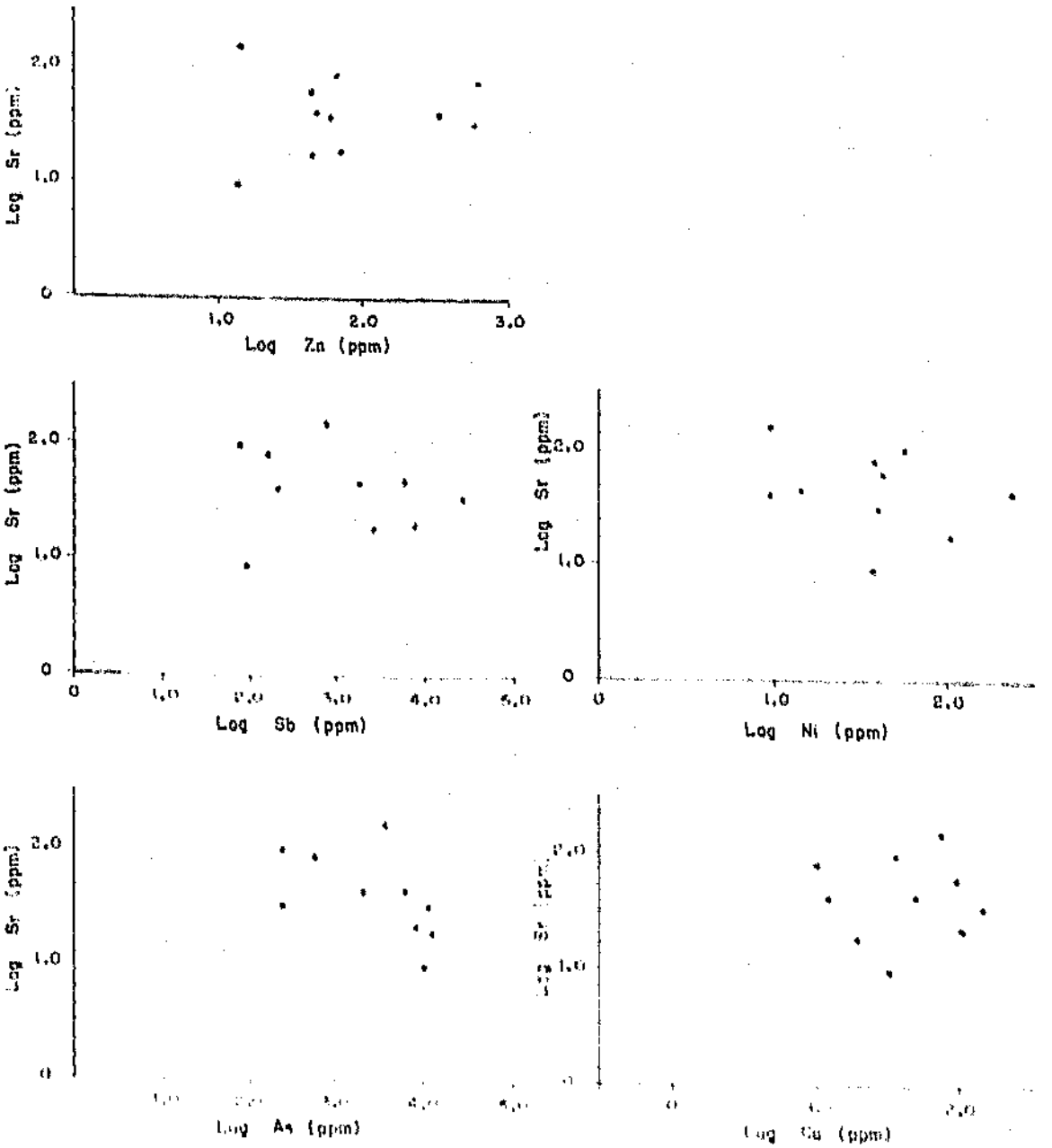


Figure 6.10: Variation diagrams for As, Sb, Zn, Ni and Cu with Sr, samples are listed in Appendix IV.

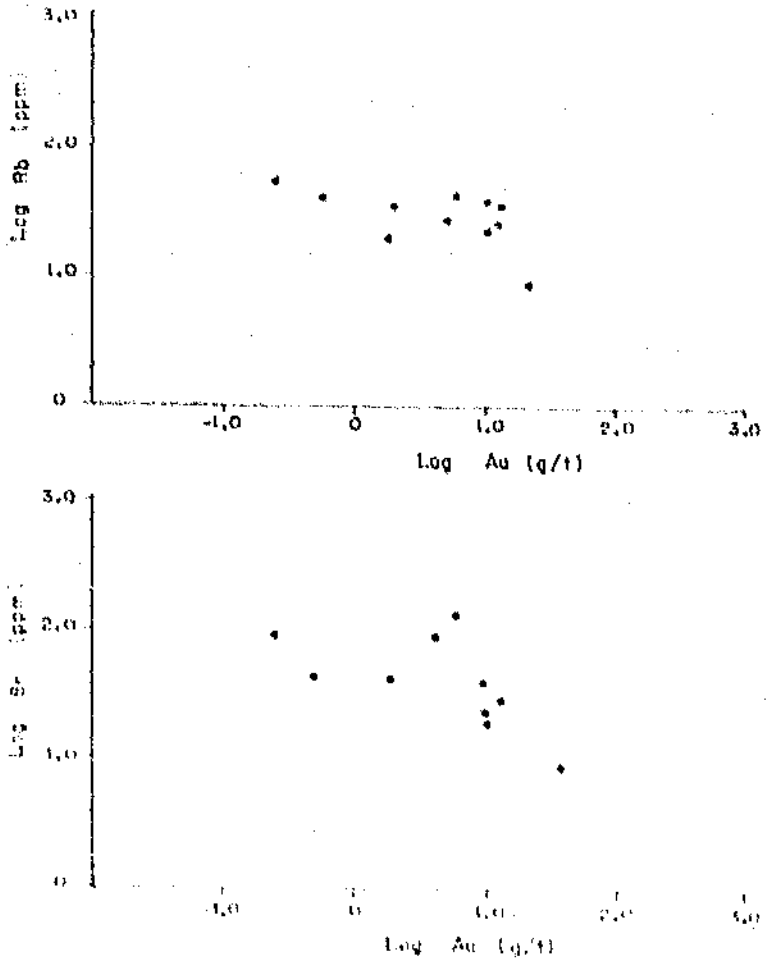


Figure 6.9: Variation diagrams for Au with Sr and Rb, samples are listed in Appendix IV.

syngenetic, and probably endogenous, hydrothermal theory provides the most satisfactory answer to explain the genesis of the early Sb mineralization.

Following and superimposed on the early antimony mineralization of the "A" Zone, a second phase of hydrothermal activity took place precipitating gold along the interface between the Fat Boy package and the underlying quartz wacke facies. This second hydrothermal event is thought to be intimately related to the end of the thrusting event (D1), the "E" Zone structure and probably to the regional greenschist metamorphism. All of these events postdate the consolidation of the Last Hope Formation sediments. Subsidiary thrusts and/or shears in the footwall of the Main Thrust Front (Fig. 7.3) and related to the "E" Zone structure, are considered to have acted as channels for the gold and arsenic-rich fluids and controlled their final precipitation. These thrusts and/or shears are preferentially developed along lithological contacts.

The syngenetic Fe-dolomitization and the early antimony mineralization, probably prepared the "ground" by establishing a favourable physico-chemical environment, necessary for the subsequent gold precipitation.

indicated that the concentration of Sb and Hg-sulphides in sodium sulphide solutions, depends on the pressure, temperature, pH, concentration of the solution, and/or the oxidation state of the transporting agent. The deposition of Sb and Hg-sulphides is controlled by changes in temperature, oxidation state and pH. [illegible] temperature. Increasing pressure, acidic conditions, oxidation and dilution of the fluids by groundwaters will decrease the solubility of Sb and Hg-sulphides.

Abbot et al. (1986), considered that fumarolic and late stage volcanic exhalations provide the material responsible for an early antimony enrichment in unconsolidated, epiclastic sediments and tuffs, accompanied by carbonatization and silicification, at the Alpha-Gravelotte antimony ore body, Murchison greenstone belt.

Similar early mineralization can be explained by the "Halo mineralization model" (Marqolin, 1986). According to this model the mineralization system is considered to be a centre of intense hydrothermal activity from nearby volcanism expressed as hot springs or fumaroles at the time of the deposition of enclosing debris flow conglomerates and tuffaceous sediments. Similar aquifers at the Cannon mine, U.S.A (Marqolin, 1986) gave rise to a Au-Ag mineralized zone of up to [illegible] in strike length.

Considering the various possible environments favourable for [illegible] antimony ore at Signal Hill remains uncertain. However, it is the writer's opinion, because of the similarities discussed above, that the

2) an epigenetic infiltration of a low temperature hydrothermal fluid at a later stage, which post-dates the deposition of the Last Hope sediments and the early pervasive carbonatization.

3) remobilination of pre-existing epigenetic or syngenetic antimony. This event would therefore post-date the deposition of the Last Hope sediments as well as the pervasive carbonatization but predated the Au-Ag mineralization.

Several comparisons can be drawn between the Au-Ag-Sb mineralization of Signal Hill and other antimony-gold occurrences, especially at the "Antimony-Line" of the Murchison greenstone belt, South Africa.

In his study of the Antimony deposits in the Murchison range, Muff (1978) states that the antimony-mercury association was initially introduced by submarine, synsedimentary or syngenetic-hydrothermal activities. Boyle (1979) mentioned several localities around the world where antimony and mercury deposition from hot springs are known: e.g. Sulfur Springs, Cal., Wilbur Springs District, Cal., Beaver Creek district, Cal., and several others. Furthermore, Hg and/or Sb minerals also precipitate from hot springs in the USSR, and on Hokkaido in Japan (Boyle 1979).

Ramdohr (1980), considered that the mercury-bearing sulphide in a stibnite-mercury ore appears late and as a replacement phase

Based on the research of Kraushopf (1956), Tunell (1964), Barnes and Czamanske (1967), White (1967), Dickson and Tunell (1968) and Brookins (1972), Muff (1978) mentioned that cinnabar and stibnite are not precipitated simultaneously from Sb and Hg-carrying solutions, and in the case of antimony and mercury sulphide deposition, their precipitation overlaps. Muff (1978)

zones have been identified, namely the Contact mineralization and the Footwall mineralization.

The Contact mineralization occurs at the basal contact between the Fat Boy diamictite package and the underlying quartz wacke. The host rocks are sheared and weakly silicified.

The Footwall mineralization is present in silicified quartz wacke of the "A" Zone at its western extremity. It consists of lenses of sheared, silicified and sericitized material associated with antimony-rich Footwall veins.

2) antimony ore (stibnite, berthierite, sphalerite and chalcopyrite) is related to an early phase of mineralization which predates the Au-As mineralization.

3) it is believed that the mercury is intimately associated with the early antimony mineralization. Mercury is present within metacinnabarite or [illegible] which replaces stibnite, native antimony, berthierite and the chalcostibite.

4) three distinct gangue generations have been identified. A quartz and carbonate rich gangue is related to the early antimony phase. A second generation is associated with the Au-As mineralization, and a third barren siliceous gangue formed during the late ductile deformation of the host.

5) the antimony ore was locally remobilized as it can be seen filling later fractures.

6) gold was the last phase to precipitate at the "A" Zone.

7) observations 2 to 6, can be extrapolated to the "B" Zone. It is considered that the same structure responsible for the Au-As mineralization of the "A" Zone is also responsible for the Au-As mineralization of the "B" Zone.

Regarding the source of the early antimony, no firm conclusion can be reached. At least three possible scenarios could be considered:

1) the mineralizing fluids were contemporaneous with the deposition of the last Hope sediments and with the pervasive carbonatization produced by nearby volcanic acti-

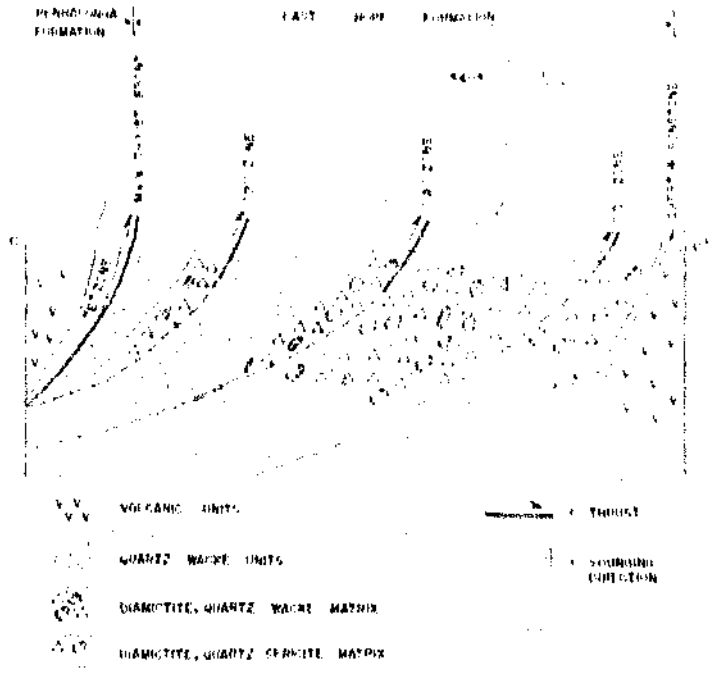


Figure 7.3: Cross section through the Last Hope Formation from the overturned Penhalonga Formation to the right way-up Penhalonga Formation (location of the cross section in Appendix IX).

7.4.3 Ore chemistry, mineralogy and emplacement

The "A" Zone mineralization is chemically characterized by an association of Au, As, Sb and Hg. While a good correlation exists between Au and As, the Au does not show any direct correlation with Sb or Hg. However, it has been indicated that the Hg is intimately associated with the early antimony mineralization.

A summary of observations from microscopic and macroscopic studies are listed below:

1) In the "A" Zone, two distinct Au-As-Sb mineralization

[illegible] of the Fat Boy Formation.

It is proposed that the combination of the large scale folding the granitoid batholith intrusions and the metamorphism resulting from these deformation events could have played a critical role in the mobilization and the subsequent canalization of the Au-As rich hydrothermal fluid along the "E" Zone structure associated with the main thrusting event. The development of the regional schistosity followed the increased folding and compressional effects in the schist belt possibly due to the intrusion of granitic plutons at higher levels in the crust. The third and fourth deformational events created a series of conjugated normal and reverse faults followed by the development of crenulation cleavage widely observed throughout the whole Tati schist belt.

An apparent angular unconformity exists between the Fat Boy package and the underlying quartz wacke facies. Contacts examined in core intersections are highly sheared and brecciated. No undeformed contact between these two host rocks was observed. Furthermore, it has been observed that Footwall veins belonging to footwall silicified quartz wackes do not cross into the Fat boy package. These observations indicate that the origin of the angular contact between the Fat Boy package and the underlying quartz wacke assemblage is of tectonic nature. However, the amount of displacement is unknown.

[illegible] Hope [illegible] [illegible] [illegible]

associated with felsic volcanic activities responsible for the sediment accumulation in the Chance area (Taylor et al (1980)). The antimony mineralisation at Signal Hill deposit is believed to be syngenetic with the felsic volcanism contemporaneous to the Last Hope Formation.

7.4 Geology of the Signal Hill area

7.4.1 Sedimentological Setting and lithogeochemistry.

There is evidence that the Last Hope Formation was deposited following an uplift of the underlying formation at the end of the Penhalonga era. This uplift together with synchronous volcanic activity , could have been responsible for the development of an alluvial fan which debouched rapidly into a water body.

A stratiform and occasionally discordant pervasive carbonatization affected the non-consolidated sediments of the Last Hope Formation as well as the volcanic units of the upper Penhalonga Formation. This suggests that these fluids were synchronous with the deposition of the Last Hope Formation and migrated through favourable beds especially porous quartz wackes, diamictites, tuffaceous units, and lithological contacts. These fluids could have been generated by nearby contemporaneous volcanic activity.

The geochemistry of the upper members of the Penhalonga Formation suggests an association of homogenic units of andesitic affinity with minor members of basaltic composition terminated by

associated with felsic volcanic centres responsible for the sediment accumulation in the Shaws area (Foster et al (1986)). The antimony mineralization at Signal Hill deposit is believed to be synchronous with the felsic volcanics contemporaneous to the Last Hope Formation.

7.4 Geology of the Signal Hill area

7.4.1 Sedimentological setting and lithogeochemistry.

There is evidence that the Last Hope Formation was deposited following an uplift of the underlying formation at the end of the Penhalonga era. This uplift together with synchronous volcanic activity , could have been responsible for the development of an alluvial fan which debouched rapidly into a water body.

A stratiform and occasionally discordant pervasive carbonatization affected the non-consolidated sediments of the Last Hope Formation as well as the volcanic units of the upper Penhalonga Formation. This suggests that these fluids were synchronous with the deposition of the Last Hope Formation and migrated through favourable units especially porous quartz wackes, diamictites, turbiditic units, and lithological contacts. These fluids could have been generated by nearby contemporaneous volcanic activity.

The geochemistry of the upper members of the Penhalonga Formation suggests an assemblage of volcanogenic units of andesitic affinity with minor members of basaltic composition terminated by

Major tectonism followed the deposition of the rocks of the Shamvaian Group. This was accompanied by low to medium grade metamorphism and eventually culminated in the intrusion of the 2.7 Ga Sesombi and 2.6 Ga Chilimanzi suite of late granites, especially in the western part of the Zimbabwe craton (Foster et al (1986a)).

Table 7.1: Zimbabwean Archaean greenstone succession compared to the Tati schist belt stratigraphy (Foster et al (1986a) and this study).

ZIMBABWEAN ARCHAEAN GREENSTONE SUCCESSION compared to THE TATI SCHIST BELT

ZIMBABWEAN ARCHAEAN GREENSTONE			TATI SCHIST BELT
Ga	Group/Suite	Details	
2.6	CHILIMANZI	Tonalite, Granodiorite	Northern Batholith
2.7	SESOMBI	Trondhjemite	Hill View pluton
			Other Batholiths ?
2.7	SHAMVAIAN	Clastic sediments with volcanism felsic	LAST HOPE Fm
		UNCONFORMITY	
2.7	UPPER		PENHALONGA Fm
2.9	GREENSTONE	UPPER BULAWAYO Fm	LADY MARY Fm
			OLD TATI Fm
2.9 ?	LOWER GREENSTONE	LOWER BULAWAYO Fm	LOWER OLD TATI Fm
			MATSILOJE Fm
		UPPER BELINGWE Fm	
		LOWER BELINGWE Fm	
		UNCONFORMITY	
3.5	SEBAKWIAN		The equivalent was not observed

Table 7.1 shows the Zimbabwean Archaean greenstone succession compared to the Tati schist belt stratigraphy. Similarities between the Last Hope Formation and the Shamvaian Group can be outlined. While stratabound gold mineralisation is reported to be

greenstone succession (e.g. [illegible]). The [illegible] Upper Greenstones comprise an import suite of [illegible], [illegible] basalt, and [illegible], which were [illegible] [illegible] and [illegible] pyroclastic units and flows.

The lower Greenstones were the result of [illegible] continental crust containing remnants of [illegible] greenstones [illegible]. They were, in turn, deformed and eroded prior to the deposition of the Upper Greenstones.

The Upper Greenstones are marked by the deposition of the Basal Sedimentary Unit, a thin sequence dominated by sulphide facies iron formation. This initial sedimentation was followed by the ultramafic dominant flows of the Komatiitic Unit, which in turn, was succeeded by a thick pile of massive and pillowed tholeiitic and komatiitic flows of the Basaltic Unit. Volcanic activity culminated in the west of the area with the occurrence of andesitic-dominant assemblages which are lenticular faults, dacites, and rhyolites. Following the decline of the volcanic activity, transformation were deposited over the top of the volcanic pile.

The sediments of the Shamvaian Group were laid down unconformably on the Upper Greenstones, probably in isolated basins. Clastic sediments dominate in the preserved sequences but minor volcanism is also observed. The basic volcanic in the Shamva area (NE Zimbabwe) was accompanied by hydrothermal activity which generated important stratabound gold deposits within the pyroclastic and volcaniclastic rocks of [illegible] (Prendergast).

The pivot point where the northern limb broke away and then was pushed towards the southern limb by the intrusion of the Northern batholith, could be located at the position of the Hill View Tonalite. This small pluton could have intruded along the zone of weakness created by the pivot point.

Several other structural features suggest that a major tectonic event, younger than any tonalitic plutons, took place and also contributed to the deformation of the schist belt. This is demonstrated in the southeastern portion of the schist belt, where chert and ironstone members of the Matsiloje Formation together with the regional schistosity have been intensively folded (see Appendices VII and VIII). Considering that the regional foliation (S_2) occurred late in the deformational history of the schist belt, and that the development of the foliation was contemporaneous or slightly younger than the consolidation of the tonalitic batholiths and plutons (Chapter 4), then a younger event would have to be interpreted to explain the folding of the regional foliation.

7.3 Correlation of the Tati schist belt with Archaean greenstone belt within the Zimbabwe craton

Foster et al (1986a), provide a detailed description of the Archaean greenstone succession in Zimbabwe. They describe the succession as follows. Relics of metavolcanic rocks dominated by mafic and ultramafic types with minor felsic varieties, known as the Sebakwian Group, represent the oldest rocks of the Archaean

APPENDIX III

Major and trace elements analysis of sediments from the Last Hope Formation.

DESCRIPTION of SAMPLES

Sample

066A	Quartz wacke
067A	Slightly silicified quartz wacke
077A	Coarse grained quartz wacke
077B	Quartz wacke
077D	Silicified quartz wacke
077E	Silicified quartz wacke
081A	Unaltered quartz wacke
081B	Very coarse grained quartz wacke
081C	Coarse grained quartz wacke
081D	Coarse grained quartz wacke
081E	Coarse grained quartz wacke[*]
081F	Coarse grained quartz wacke[*]
081G	Coarse grained quartz wacke
081H	Coarse grained quartz wacke
081K	Very coarse grained quartz wacke
081M	Very coarse grained quartz wacke[*]
081N	Quartz wacke[*]
081P	Silicified quartz wacke
083A	Silicified quartz wacke
083B	Carbonated coarse grained quartz wacke[*]
083C	Silicified quartz wacke[*]
083D	Very coarse grained quartz wacke
083E	Grey, medium grained quartz wacke[*]
083F	Dark grey coarse grained quartz wacke[*]
083G	Very coarse grained quartz wacke
083H	Dark grey coarse grained quartz wacke
107A	very coarse grained quartz wacke
107B	Coarse grained quartz wacke
107C	Dark grey coarse grained quartz wacke
107D	Coarse grained quartz wacke
108A	Coarse grained quartz wacke[*]
108B	Carbonated quartz wacke
108C	Coarse grained quartz wacke
108D	Silicified quartz wacke
110A	Coarse grained quartz wacke[*]
110B	Coarse grained quartz wacke[*]
111A	Coarse grained quartz wacke
111B	Dark grey coarse grained quartz wacke
077C	Volcanic fragment from diamictite
077X	Volcanic fragment from diamictite
083Z	Volcanic fragment from diamictite

Analist:

[*] : Bergstrom And Bakker, Johannesburg

[**] : XRAL Assay Laboratories, Don Mills, Canada

9930E	9930E	Diamictite	2.66
STA032	10150E, 10045N	Diamictite	2.66
STA031	10205E, 10060N	Diamictite	
STA031	10205E, 10030N	Silicified quartz wacke	2.50
STA030	10318E, 10015N	Diamictite	2.67
STA029	10318E, 10035N	Quartz wacke	2.64

C) Samples from the borehole SPD.083.

Sample	Depth	Description	S.G.	Grade Au g/t
126	126	Coarse grained quartz wacke, unaltered	2.68	
148	148	Coarse grained quartz wacke, unaltered	2.69	
10415	175	Carbonated diamictite	2.79	0.01
186	186	Coarse grained quartz wacke, unaltered	2.69	
195	195	Coarse grained quartz wacke, unaltered	2.72	
204	204	Diamictite, unaltered	2.83	
10421	213	Diamictite, unaltered	2.56	0.15
10429	218	Coarse grained, quartz wacke, altered	2.69	0.17
10432	223	Coarse grained quartz wacke, altered	2.71	1.30
10437	229	Coarse grained quartz wacke, altered	2.68	0.05
245	245	Dark quartz wacke, unaltered	2.70	
258	258	Dark quartz wacke, unaltered	2.70	

APPENDIX II

Specific gravity determination

Specific gravity determinations were done using grab samples from trenches for weathered material and samples from borehole SPD 083 for unaltered, altered and mineralized samples. All samples were varnished with wood varnish (to seal the pores). A triple beam balance was used for weighting the sample in air and in water.

$$SG = \frac{W\ (air)}{W\ (air) - W\ (water)}$$

A) Weathered samples
Ore sample

Sample	Location	Description	S.G.	Grade Au g/t
15608	9600E, 10010N	Silicified quartz wacke	2.72	109.40
15577	9700E, 10003N	Silicified quartz wacke	2.55	0.84
113-C	9832E, 10064N	Limonitic silicified quartz wacke.	1.40	1.30
A-719	9863E, 10060N	Diamictite	2.57	2.05
STA-044	9878E, 10056N	Silicified quartz wacke	2.63	1.30
A-706	9930E, 10078N	Diamictite	2.44	14.00
15976	9931E, 10079N	Silicified quartz wacke	2.64	
A-362	9998E, 10086N	Footwall ore sample	2.64	2.50
10000E	10000E, 10072N	Silicified quartz wacke	2.65	4.00
160-1	10010E, 10072N	Silicified quartz wacke	2.48	
STA-032	10156E, 10057N	Sheared Diamictite	2.52	1.50
STA 029	10318E, 10035N	Sheared Diamictite	2.60	0.58

B) Weathered samples
Waste

Sample	Location	Description	S.G.
15602	9600E	Diamictite	2.65
15570	9700E	Silicified quartz wacke	2.61
088-C	9850E	Diamictite	2.52
035-C	9923E, 10074N	Silicified quartz wacke	2.60

APPENDIX I

Major and trace elements analysis of rocks from upper Pont - Longa Formation

Summer, R. (1969). Ancient mining in Rhodesia and adjacent areas. Memoir 3, National Museums of Rhodesia, Salisbury, p. 236.

Thatcher, R. (1990). Final report, Semi-detailed photogeological mapping and interpretation of Landsat 5 Thematic Mapper Imagery covering the Selnickel area near Francistown. Falconbridge Exploration Botswana, Bulletin 272.

Tucker, M. (1989). The field description of sedimentary rocks. Geological society of London, handbook series. Open University press, Milton Keynes, p. 112.

Turell, G. (1964). Chemical processes in formation of mercury ores and ores of mercury and antimony. Geochim. Cosmochim. Acta. v. 38, p. 1019-1047.

Von Spaeth, W. (1970). Quarterly Reports for 1970. Selope Botswana (Pty) Ltd.

White, D.E. (1967). Mercury and base-metal deposits with associated thermal and mineral waters. In Barnes, H.L., Editor, Geochemistry of Hydrothermal Ore Deposits. Holt, Rinehard, and Winston, New York, p. 670.

Winchester, L.A., and Max, M.D. (1984). Element mobility associated with syn-metamorphic shear zones near Scotchport, NW Mayo, Ireland. Journal of Metamorphic Geology, v. 2, p. 1-11

McClay, K. (1987). The mapping of geological structures. Geological Society of London handbook. Open University press. p. 160.

Molyneux, T.G. (1971). Gold section of Sedge (Botswana) Ltd, Prospecting in Tati Concession. Sedge Botswana, p. 70.

Mufi, R. (1978). The Antimony deposits in the Murchison range of the northeastern Transvaal, Republic of South Africa. in Gebrüder Borntraeger Editor, Monograph Series on Mineral Deposits, No 16, Berlin, p. 79.

Pearce, J.A., and Cann, J.R. (1973). Tectonic setting of basic volcanic rocks determined using trace element analyses. Earth and Planetary Science Letters, v. 19, p. 290-300.

Ramdohr, P. (1980). The Ore Minerals and their intergrowths. Pergamon press, second edition vol 1 and 2, p. 1269.

Ramsay, J.G., Huber, M.I. (1989). The techniques of Modern Structural Geology, volume 2: Folds and Fractures. Academic press limited. London. p. 700.

Reineck, H.E., Singh, I.B. (1982) Depositional Sedimentary Environments, with reference to terrigenous clastic. Springer-Verlag Editor, New York, p. 439.

Siegfried, P. (1990). Progress Report on Work Done in Prospecting Licence 2/87 (Sikukwe). During the period January 1990 to December 1990. Internal report Falconbridge Exploration Botswana, Bulletin 259.

Smith, R.E. (1968). Redistribution of major elements in the alteration of some basic lavas during burial metamorphism. Journal of Petrology, Vol. 9, p. 191-219.

Stowe, C.W., Morris, J. H. (1986). Gold mineralisation in Ordovician greywackes at Clontibret, Ireland. In Keppie, J.D., Boyle, R.W. and Haynes, S.J., Editors, Turbidite hosted gold deposits. Geological Association of Canada Special Paper 32, p. 67-86.

Foster, R.P., Furber, F.M.W., Gilligan, J.M. and Green, D. (1986b) Shamva Gold Mine, Zimbabwe: A product of calc-alkaline linked exhalative, volcaniclastic, and epiclastic sedimentation in the late Archean in Turbidite-hosted gold deposits, Editors: Keppie, J. Duncan, boule, R.W. and Haynes, S.J., Geological Association of Canada Special Paper 32, p. 41-66.

Harwood, A.C. (1986). A mineralogical and fluid inclusion investigation of a Falconbridge Exploration prospect, Botswana. Department Geology and Applied Geology, University of Natal, Durban. Falconbridge Exploration Botswana, internal report.

Kerrick, D.M. (1990). Review in Mineralogy, The Al2SiO5 Polymorphs. Ribbe, P.H. Editor. Mineralogical Society of America, V. 22 p. 311-352

Key, R.M. (1976). The Geology of the Area Around Francistown and Phikwe, Northeast and Central Districts, Botswana. Botswana Geological Survey, Memoir 3, p. 131.

Kranidiotis, P. and MacLean, W.H. (1987). Systematics of Chlorite Alteration at the Phelps Dodge Massive Sulfide Deposit, Matagami, Quebec. Economic Geology, Vol 82, p. 1898-1911.

Krauskopf, K.B. (1956). Factors controlling the concentrations of thirteen rare metals in sea water; Geochim. Cosmochim. Acta, v. 9, p. 1-32B

Litherland, M. (1976). The Eastern geotraverse-a field reconnaissance. Dept. Geol. Surv. Botswana, Mid, (unpublished).

Mangotin, J. (1989). Arkose-hosted, aquifer-controlled epithermal Au-Ag mineralisation, Wenatchee. Econ. Geol. V. 84, p. 1891-1902.

Martin, D.E. (1989). Geology of the "A" zone, Signal Hill Project, Tati Schist Belt, Botswana, Selbex-Falconbridge JV, BP Minerals Development Ltd. Newbury, Unpubl.

Mason, R. (1970). The Geology of the country between Francistown and Mmadinare, northeastern Botswana. Unpubl. Ph. D. Thesis, Univ. Witwatersrand, Johannesburg, p. 91.

Bull, W.R. (1972) Recognition of alluvial fan deposits. In J.K. Rigby and W.K. Hamblin, The stratigraphic record in Recognition of ancient sedimentary environments. Society of Economic Paleontologists and Mineralogists, Special Publication 16, p. 63-83.

Byron, C.L. (1983) Progress Report on the Last Hope Gold/Antimony Deposit. Prospecting Licence 1/78. Falconbridge Exploration Botswana, Bulletin 194

Cain, A.C. (1980). Geology and ore reserves of the Map-Nora gold mines: Prospecting licence 1/78, Tati schist belt. Falconbridge Exploration Limited, Bulletin 100.

Cann, J.R. (1970). Rb, Sr, Y, Zr, Nb in some ocean floor basaltic rocks. Earth and Planetary Science Letters, v. 10, p. 7-11.

Crockett, R.N. (1967). Summary of mining and prospecting records, Tati Concession. Dept. Geol. Surv. Bech., RNC 15 (unpublished)

Dickson, F.W. and Tunnell, G. (1968). Mercury and antimony deposits associated with active hot springs in the western United States, p 1673-1701. In Ridge, J.D. Editor. Ore Deposits in the United States, V. 2. A.I.M.E. New York.

Davies, J.F., Grant, R.W.E. and Whitehead, R.E.S. (1979). Immobile trace elements and Archean volcanic stratigraphy in the Timmins mining area, Ontario, Canada. Canadian Journal of Earth Science, Vol 16, p 305-311.

Flint, R.F., et al. (1960), Diamictite, a substitute term for symmictite. Geological Society of America, Bulletin, v.71 p. 1809.

Floyd, P.A., and Winchester, J.A. (1978). Identification and discrimination of altered and metamorphosed volcanic rocks using immobile elements. Chemical Geology, v. 21, p. 291-306.

Foster, R.P., Mann, A.G., Stowe, C.W., and Wilson J.F. (1986a) Archaean gold mineralisation in Zimbabwe, In Anhaeusser, C.R., and Maske, S. Editors, Mineral Deposits of Southern Africa Vols I and II, Geol. Soc. S. Afr., p. 43-123.

REFERENCE LIST

Abbot, J.E., Van Vuuren, C.J.J. and Viljoen, M.J. (1986) The Alpha-Gravelotte Antimony ore body, Murchison Greenstone Belt. In Anhaeussor, C.R., and Maske, S. Editors, Mineral Deposits of Southern Africa Vols I and II, Geol. Soc. S. Afr., p. 321-332

Audet, M.A. (1990). Signal Hill gold project, prospecting licence 24/84, northeast Botswana. Progress report on work undertaken on the Signal Hill prospect area from June 1986 to December 1990. Falconbridge Exploration Botswana, Bulletin B258

Barnes, H.L. and Czamanske, G.L. (1967). Solubilities and transport of ore minerals. In Barnes, H.L., Editor. Geochemistry of Hydrothermal Ore Deposits. Holt, Rinehard, and Winston, New York. p. 670.

Bates, R.L.and Jackson, J.A., (1984). Dictionary of geological terms. Bates, R.L. and Jackson, J.A. Editors. Third edition. p. 788.

Blaine, J.L. (1986). Progress report on the Signal Hill Project, Prospecting Licence PL 24/84, for the Period August 1984 to June 1986. Falconbridge Exploration Botswana, Bulletin B219

Blaine, J.L., Audet, M.A. and Haynes, D. (1990). Signal Hill gold project, Botswana, Review and feasibility study. Falconbridge Exploration Botswana, Bulletin B253.

Blatt, H., Middleton, G. and Murray, R. (1972). Origin of sedimentary rocks. Prentice-Hall, Englewood Cliffs, N.J, p. 800.

Boyle, R.W. (1979) The geochemistry of gold and its deposits. Canada Geol. Survey, Bull., V. 280, p. 584.

Brooking D.G. (1972). Stability of stibnite, metastibnite, and some probable dissolved antimony species at 298.15°K and 1 atmosphere. Econ. Geol. v. 67. p. 369-372.

vi) A third barren hydrothermal event locally brecciated the two previous phases.

Using the data from this dissertation, and incorporating previously published information, the sequence of events described above is believed to be the most satisfactory theory to explain the geology of the Signal Hill area and the associated Au-As-Sb deposits.

deposition of the Last Hope Formation.

iv) At least four stages of tectonic deformation affected the Signal Hill area.

It is proposed that the first stage was the combination of large scale folding, granitoid batholith intrusions and the resulting increase in metamorphism throughout the Tati schist belt. This deformation event together with the Main thrusting event and the associated "E" Zone structure, could have played a critical role in the mobilization and the subsequent canalization of the Au-As rich hydrothermal fluid.

The second distinct recognizable deformational event followed the end of the thrusting event. The development of the regional foliation followed the increased folding and compressional effects in the schist belt possibly due to the intrusion of the granitic plutons at higher levels in the crust. The third and fourth deformational events created normal and reverse faults followed by the development of the crenulation cleavage widely observed throughout the whole schist belt.

[illegible]

CHAPTER EIGHT

CONCLUSIONS

In the discussion of the geology of the Signal Hill area and of the genesis of the complex Au-As-Sb deposits, numerous conclusions can be made.

i) The Last Hope formation sediments [illegible] characteristic of an alluvial fan which debouches rapidly into a water body. The sediments were deposited [illegible] with volcanic activity and possibly were related to uplift of the underlying formations at the end of the Permian time.

ii) A stratiform and occasionally discordant pervasive carbonatization affected the non-consolidated sediments of the Last Hope Formation as well as the volcanic units of the upper Penhalonga Formation. This suggests that these fluids were emplaced before the final consolidation of the Last Hope Formation.

iii) The origin of the early antimony mineralization is still uncertain. However, the mineralogical study shows that the antimony ore predates the Au-As mineralization. The affinity between Sb and Hg suggests fumarolic or hot spring-type of mineralization related to nearby volcanism. It is suggested that the early antimony mineralization is related to a syngenetic, and [illegible]

APPENDIX VI

Major and trace elements analysis of rocks from the "E" Zone structure

	E-01	E-02
Major (%)		
SiO2	33.80	13.70
TiO2	0.04	0.02
Al2O3	0.50	0.40
Fe2O3	5.70	6.34
MnO	0.04	0.13
MgO	21.60	24.30
CaO	7.10	14.40
Na2O	nd	nd
K2O	nd	0.01
P2O5	0.02	0.01
L.O.I	30.00	39.70
Total	99.06	98.88
Trace (ppm)		
Rb	nd	nd
Sr	70	300
Y	nd	nd
Zr	1	2
Nb	nd	nd
As	1.44	1,964
Sb	1.03	4.10
Au	0.00	0.05

Analist: Bergestrom And Bakker, Johannesburg, R.S.A

APPENDIX V (Con't)

"A" Zone surface ore samples collected and assayed by Seltrust Botswana in 1983.

Element	G-142	G-143	G-144	G-145	G-146	G-147
Ba (ppm)	400	468	478	432	412	876
Cu (ppm)	165	107	90	58	22	62
Zn (ppm)	107	137	56	40	25	31
Hg (ppm)	560	220	100	60	60	60
As (%)	5.13	2.16	0.44	0.17	0.07	2.04
Sb (%)	1.45	0.12	12.33	1.14	0.06	0.26
Au (g/t)	0.86	0.30	5.40	17.10	0.03	19.00

APPENDIX V

"A" Zone surface ore samples collected and assayed by Seltrust Botswana in 1983.

"A" Zone

	G-106 Element	G-107	G-108	G-110	G-111	G-112	G-113	G-114	G-115
Ba (ppm)	650	437	361	220	80[illegible]	455	187	144	440
Cu (ppm)	46	46	21	92	36	71	40	41	28
Zn (ppm)	32	44	35	45	79	159	61	186	81
Hg (ppm)	230	250	100	540	140	660	490	290	430
As (%)	0.09	0.09	0.06	0.25	0.18	0.26	0.14	0.40	0.08
Sb (%)	0.34	0.18	0.03	1e-5	0.04	0.13	0.60	0.37	0.03
Au (g/t)	9.6	20.4	0.36	7.10	7.9	4.0	10.9	7.0	3.6

	G-116 Element	G-118	G-120	G-127	G-129	G-129	G-130	G-131	G-132
Ba (ppm)	348	394	53	501	67	201	154	441	67
Cu (ppm)	36	41	11	104	557	250	140	61	147
Zn (ppm)	63	78	29	44	102	43	187	64	77
Hg (ppm)	130	110	50	540	110	550	550	240	160
As (%)	0.05	0.27	0.10	1.68	0.68	0.60	0.79	1.86	0.41
Sb (%)	0.75	0.14	0.01	2.44	1e-5	1e-5	1e-5	1.14	0.03
Au (g/t)	2.9	1.44	0.18	2.10	0.76	1.64	2.0	2.29	0.39

	G-133 Element	G-134	G-135	G-136	G-137	G-141	G-142	G-143	G-144
Ba (ppm)	344	8[illegible]	490	499	143	530	39[illegible]	1e-5	3e-5
Cu (ppm)	100	8[illegible]	72	110	38	109	67	11.2	116
Zn (ppm)	108	140	48	92	144	107	78	92	142
Hg (ppm)	490	800	70	100	40	60	1e-5	110	2e-5
As (%)	4.21	1.16	3.84	2.64	2.20	1.20	8.1[illegible]	0.19	3e-5
Sb (%)	4.44	0.46	2.83	0.54	0.31	0.28	9.15	1e-5	1.14
Au (g/t)	1.69	0.[illegible]	2.40	1.44	1.18	0.24	3.11	0.[illegible]	2e-5

APPENDIX IV (Con't)

Major and trace elements analysis of the "A" Zone ore samples.

Major (%)				
[illegible]	[illegible]	[illegible]	[illegible]	[illegible]
TiO_2	0.24	[illegible]	0.17	nd
Al_2O_3	[illegible]	10.4	[illegible]	[illegible]
Fe_2O_3	[illegible]	[illegible]	[illegible]	[illegible]
MnO	0.01	0.03	0.03	0.01
MgO	nd	0.18	0.18	nd
CaO	[illegible]	[illegible]	[illegible]	[illegible]
$H_2O(+)$	nd	[illegible]	[illegible]	nd
K_2O	[illegible]	[illegible]	[illegible]	[illegible]
P_2O_5	nd	[illegible]	[illegible]	nd
LOI	[illegible]	[illegible]	[illegible]	[illegible]
Total	[illegible]	[illegible]	[illegible]	[illegible]
Trace (ppm)				
Sb	[illegible]	[illegible]	[illegible]	
Sr	[illegible]	[illegible]	44.3	
Ba	[illegible]	[illegible]	1.35	
Co	[illegible]	[illegible]	[illegible]	[illegible]
Ni	[illegible]	[illegible]	[illegible]	[illegible]
Cu	[illegible]	[illegible]	[illegible]	[illegible]
Zn	[illegible]	[illegible]	[illegible]	[illegible]
V	[illegible]	[illegible]	[illegible]	[illegible]
Cr	[illegible]	[illegible]	[illegible]	[illegible]
Y	[illegible]	[illegible]	[illegible]	[illegible]
Zr	[illegible]	[illegible]	[illegible]	
Nb	[illegible]	nd	nd	
Au		[illegible]	[illegible]	[illegible]
Ag		[illegible]	[illegible]	[illegible]
As		[illegible]	[illegible]	[illegible]

APPENDIX IV

Major and trace elements analysis of the "A" Zone ore samples.

	[illegible]	[illegible]	[illegible]	[illegible]	[illegible]	[illegible]	[illegible]	[illegible]	[illegible]
Major (%)									
SiO2	[illegible]	50.03	81.63	67.20	81.93	64.01	81.63	[illegible]	[illegible]
TiO2	1.03	0.50	0.29	0.34	1.14	1.08	0.95	1.30	0.69
Al2O3	[illegible]	12.85	8.50	[illegible]	[illegible]	[illegible]	[illegible]	[illegible]	[illegible]
Fe2O3	15.46	8.02	1.69	0.71	1.20	10.30	1.25	0.05	[illegible]
MnO	0.26	0.27	0.02	0.02	0.02	0.12	0.03	0.02	0.01
MgO	0.30	[illegible]	nd	nd	nd	0.22	0.06	nd	[illegible]
CaO	0.18	3.04	0.15	0.00	0.06	[illegible]	0.31	[illegible]	[illegible]
Na2O	nd	0.02	0.01	nd	nd	nd	nd	nd	0.14
K2O	0.57	1.71	1.05	0.40	1.02	1.50	1.45	0.31	1.37
P2O5	nd	0.11	0.02	0.07	nd	0.05	0.01	nd	0.01
L.O.I	[illegible]	[illegible]	[illegible]	[illegible]	[illegible]	[illegible]	[illegible]	[illegible]	[illegible]
Total	[illegible]	[illegible]	[illegible]	[illegible]	[illegible]	[illegible]	[illegible]	[illegible]	[illegible]
Trace (ppm)									
Rb	[illegible]	[illegible]	[illegible]	[illegible]	[illegible]	[illegible]	[illegible]	[illegible]	[illegible]
Sr	[illegible]	[illegible]	[illegible]	nd	[illegible]	[illegible]	[illegible]	[illegible]	[illegible]
Ba	[illegible]	[illegible]	[illegible]	na	[illegible]	[illegible]	[illegible]	[illegible]	[illegible]
Co	[illegible]	[illegible]	[illegible]	[illegible]	[illegible]	[illegible]	[illegible]	[illegible]	[illegible]
Ni	[illegible]	[illegible]	[illegible]	[illegible]	[illegible]	nd	[illegible]	[illegible]	[illegible]
Cu	[illegible]	[illegible]	[illegible]	[illegible]	[illegible]	[illegible]	nd	[illegible]	[illegible]
Zn	[illegible]	[illegible]	[illegible]	[illegible]	[illegible]	[illegible]	[illegible]	[illegible]	[illegible]
V	[illegible]	[illegible]	[illegible]	[illegible]	[illegible]	[illegible]	[illegible]	[illegible]	[illegible]
Cr	[illegible]	[illegible]	[illegible]	[illegible]	[illegible]	[illegible]	[illegible]	nd	[illegible]
Y	[illegible]	[illegible]	[illegible]	[illegible]	[illegible]	[illegible]	[illegible]	[illegible]	[illegible]
Zr	[illegible]	[illegible]	[illegible]	nd	[illegible]	nd	[illegible]	[illegible]	[illegible]
Th	nd	[illegible]	nd	nd	nd	nd	[illegible]	[illegible]	[illegible]
As	[illegible]	[illegible]	[illegible]	[illegible]	[illegible]	[illegible]	[illegible]	[illegible]	[illegible]
Sb	[illegible]	[illegible]	[illegible]	[illegible]	[illegible]	[illegible]	[illegible]	[illegible]	[illegible]
Au	[illegible]	[illegible]	[illegible]	[illegible]	[illegible]	[illegible]	[illegible]	[illegible]	[illegible]

APPENDIX III (Con't)

Major and trace elements analysis of sediments from the Last Hope Formation.

Major (%)					
Total					
Trace (ppm)					

APPENDIX III (Con't)

Major and trace elements analysis of sediments from the Last Hope Formation.

Major (%)									
Trace (ppm)									

APPENDIX III (Con't)

Major and trace elements analysis of sediments from the Last Hope Formation.

Major (%)									
SiO_2									
TiO_2									
Al_2O_3									
Fe_2O_3									
MnO									
MgO									
CaO									
Na_2O									
K_2O									
P_2O_5									
L.O.I									
Total									
Trace (ppm)									
Rb									
Sr									
Ba									
Ce									
Ni									
Cu									
Zn									
V									
Cr									
Y									
Zr									
Th									

APPENDIX III (Con't)

Major and trace elements analysis of sediments from the Last Hope Formation.

	0810	081E	081F	081G	081H	081K	081M	081N	081P
Major (%)									
SiO2	56.39	59.00	66.40	61.70	59.40	59.27	58.60	61.30	63.10
TiO2	0.29	0.27	0.20	0.28	0.29	0.32	0.27	0.16	0.20
Al2O3	9.50	12.0	8.64	11.00	13.30	9.01	9.40	8.97	10.20
Fe2O3	0.77	0.90	0.77	1.24	0.90	1.40	1.11	1.21	1.30
MnO	nd	0.04	0.04	0.01	0.01	0.01	0.06	0.02	0.02
MgO	nd	0.21	0.13	0.01	nd	nd	0.13	0.42	nd
CaO	0.09	0.44	0.28	0.21	0.11	0.09	0.23	0.33	0.11
Na2O	nd	0.79	0.57	nd	0.67	nd	0.47	0.49	0.15
K2O	1.60	2.28	1.60	2.00	2.58	1.40	1.67	1.51	1.70
P2O5	nd	0.06	0.04	0.02	0.02	0.01	0.03	0.05	0.03
LOI	1.20	1.80	1.30	1.75	1.87	1.57	1.50	1.40	1.50
Total	69.75	99.70	99.60	98.36	99.70	99.00	99.70	99.00	99.62
Trace (ppm)									
Rb	43.2	66.0	42.2	62.5	68.6	53.5	45.2	40.7	51.7
Sr	61.8	68.1	54.2	75.9	120	49.4	61.7	100	64.6
Ba	305	491	293	417	470	302	308	439	417
Co	8.27	8.44	9.00	9.87	7.98	7.07	9.50	7.06	7.31
Ni	16.0	16.5	13.8	22.3	17.5	15.8	15.0	9.50	13.9
Cu	8.30	6.23	6.61	10.1	9.35	14.0	7.79	6.20	14.4
Zn	11.4	8.39	9.05	9.00	4.76	41.1	32.0	7.08	11.6
V	37.8	44.0	38.7	48.2	53.1	45.8	31.6	29.2	42.5
Cr	90.9	5.83	7.64	1.41	6.60	49.2	39.4	5.70	5.62
Y	9.03	11.4	10.7	11.2	10.2	9.64	7.04	7.81	9.48
Zr	67.3	92.0	65.2	101	124	76.4	72.1	58.6	74.1
Nb	4.97	4.85	4.36	5.96	7.43	5.45	5.37	4.26	4.91

APPENDIX III

Major and trace elements analysis of sediments from the Last Hope Formation.

	066A	067A	077A	077B	077C	077E	094A	143B	082C
Major (%)									
SiO2	83.84	77.34	82.68	82.70	85.16	85.17	84.35	84.79	86.54
TiO2	0.21	0.37	0.13	0.21	0.16	0.12	0.25	0.15	0.14
Al2O3	9.55	14.12	9.69	10.26	6.45	8.34	10.19	9.61	6.11
Fe2O3	0.89	0.80	0.96	0.94	1.57	1.29	0.75	0.85	1.19
MnO	0.03	0.01	0.01	0.02	0.02	0.02	0.02	nd	0.03
MgO	nd	0.04	0.19	nd	1.37	0.50	nd	nd	0.10
CaO	0.09	0.40	0.06	x	0.51	0.17	0.08	0.19	0.10
Na2O	1.07	0.86	nd	0.03	nd	nd	0.07	0.12	nd
K2O	1.71	2.43	1.91	1.86	1.47	1.69	1.52	1.71	1.24
P2O5	0.02	nd	nd	nd	0.03	0.04	0.02	0.01	0.02
LOI	1.70	2.36	3.39	2.20	1.90	1.68	1.25	1.24	1.31
Total	99.10	98.82	99.26	98.20	100.64	99.17	98.70	98.69	98.78
Trace (ppm)									
Rb	170	205	208	196	81.4	96.5	144.0	167.0	135.5
Sr	65.9	106	60.4	74.6	89.0	107.5	56.0	87.0	81.5
Ba	361	494	327	359	330	359	306	324	301
Co	7.77	10.4	9.89	9.80	8.15	9.70	16.0	9.15	9.15
Ni	14.0	21.9	10.3	22.5	14.0	14.0	11.0	11.0	12.5
Cu	5.96	5.13	7.15	2.66	13.4	8.01	11.0	4.61	9.15
Zn	12.1	10.4	32.9	13.6	9.63	8.70	10.4	8.40	7.70
V	46.8	75.2	28.1	46.4	90.1	89.9	57.0	87.0	57.0
Cr	11.5	10.2	45.0	19.2	99.0	43.1	11.0	10.0	32.0
Y	9.00	12.1	2.31	11.5	5.11	11.41	11.5	5.15	11.91
Zr	25.7	53.7	25.0	13.5	11.0	11.0	25.0	5.13	11.0
Pb	4.78	11.04	4.81	4.57	4.19	4.30	4.57	4.01	4.41

Author: Audet M.A
Name of thesis: Geological study of the signal hill au-as-sb deposits archaean tati schist belt northeast botswana

PUBLISHER:
University of the Witwatersrand, Johannesburg
©2015

LEGALNOTICES:

Copyright Notice: All materials on the University of the Witwatersrand, Johannesburg Library website are protected by South African copyright law and may not be distributed, transmitted, displayed or otherwise published in any format, without the prior written permission of the copyright owner.

Disclaimer and Terms of Use: Provided that you maintain all copyright and other notices contained therein, you may download material (one machine readable copy and one print copy per page)for your personal and/or educational non-commercial use only.

The University of the Witwatersrand, Johannesburg, is not responsible for any errors or omissions and excludes any and all liability for any errors in or omissions from the information on the Library website.